

Magnus Moen Sydtangen

Optimization of offset in the workability function

An optimization of the equation to calculate the flow resistance ratio, and the offset in the workability function

Master's thesis in Master of Science in Civil and Environmental Engineering

Supervisor: Stefan Jacobsen

Co-supervisor: Rolands Cepuritis

June 2023

Magnus Moen Sydtangen

Optimization of offset in the workability function

An optimization of the equation to calculate the flow resistance ratio, and the offset in the workability function

Master's thesis in Master of Science in Civil and Environmental Engineering

Supervisor: Stefan Jacobsen

Co-supervisor: Rolands Cepuritis

June 2023

Norwegian University of Science and Technology

Faculty of Engineering

Department of Structural Engineering




Norwegian University of
Science and Technology



MASTER THESIS 2023

SUBJECT AREA: Concrete technology	DATE: 09.06.2022	NO. OF PAGES: 58 + 53
--------------------------------------	---------------------	--------------------------

TITLE: Optimization of offset in the workability function Optimalisering av offset i støpelighetsfunksjonen	
BY: Magnus Moen Sydtangen	

SUMMARY: This master's thesis investigates the relationship between the flow resistance ratio and the superplasticizers to cement content ratio (sp/c). Additionally, it examines the suitability of the workability function in relation to the observed variables. It explores the possibility of adjusting the offset variable to improve the fit of the workability function. Analyzing the focus of the master thesis is performed by using data from existing reports and experiments conducted for this master thesis. To determine the flow resistance ratio of the matrixes, the constants are adjusted to account for the sp/c. These constants reduce the difference between the calculated values and the observed variables from 5.9% to 8.6% with the data from the reports and the experiments, respectively. This is a significant improvement from the previous coefficients. Linear optimization of the offset in the workability function is used to reduce the difference between the workability function and the observed values. The optimized offset for one equation reduces the difference between the observed values and the workability function by 21.8%, but the difference is still significant.

SUPERVISOR(S): Stefan Jacobsen and Rolands Cepuritis CARRIED OUT AT: Norwegian University of Science and Technology (NTNU)

Abstract

This master's thesis investigates the relationship between the flow resistance ratio and the superplasticizers to cement content ratio (sp/c). Additionally, it examines the suitability of the workability function in relation to the observed variables. It explores the possibility of adjusting the offset variable to improve the fit of the workability function.

Analyzing the focus of the master thesis is performed by using data from existing reports and experiments conducted for this master thesis. To determine the flow resistance ratio of the matrixes, the constants are adjusted to account for the sp/c. These constants reduce the difference between the calculated values and the observed variables from 5.9% to 8.6% with the data from the reports and the experiments, respectively. This is a significant improvement from the previous coefficients. Linear optimization of the offset in the workability function is used to reduce the difference between the workability function and the observed values. The optimized offset for one equation reduces the difference between the observed values and the workability function by 21.8%, but the difference is still significant.

Sammendrag

Denne masteroppgaven undersøker forholdet mellom strømningsmotstandsforholdet og forholdet mellom superplastiserende stoffer og sementinnhold (sp/c). I tillegg undersøker den passformen til støplighetsfunksjonen i forhold til de observerte variablene og utforsker muligheten for å justere offset-variabelen for å forbedre tilpasningen til støplighetsfunksjonen.

Analyse av problemstillingen i masteroppgaven utføres ved å bruke data fra eksisterende rapporter og eksperimenter utført for denne masteroppgaven. For å beregne strømningsmotstandsforholdet til matriksene er konstantene justert for sp/c . De justerte konstantene reduserer forskjellen mellom de beregnede verdiene og de observerte variablene til henholdsvis 5,9% og 8,6% med dataene fra rapportene og eksperimentene. Dette er en betydelig forbedring fra de tidligere koeffisientene. Lineær optimalisering av offseten i støplighetsfunksjonen brukes for å redusere forskjellen mellom støplighetsfunksjonen og de observerte verdiene. Den optimaliserte offseten reduserer forskjellen mellom de observerte verdiene og støplighetsfunksjonen med 21,8%, men forskjellen er fortsatt betydelig.

Preface

This master's thesis is a part of the Master of Science in Civil and Environmental Engineering at the Norwegian University of Science and Technology (NTNU).

This study focuses on investigating the impact of the solid content to cement content ratio (sp/c) on the flow resistance ratio. Additionally, it aims to enhance the workability function by examining its offset variable. Machine learning techniques are employed to develop an optimized equation for the offset variable.

Engaging in this study has been challenging and educational. The process has increased my knowledge about the rheological properties of fresh concrete through literature study and performing experiments. Throughout this study, my skills in data processing have increased, and I have learned the basic of machine learning while deepening my understanding of the theories governing the rheological properties of concrete.

I want to express my gratitude to Stefan Jacobsen and Rolands Cepuritis, who have been my supervisor and co-supervisor, respectively. Their knowledge, insights into theories, data sets, and practical reasoning have been invaluable contributions to this research. I also want to thank Svein Meland at Norstone for providing the filler used in this thesis, and Kåre Olsby and Thomas Uhlving for good help in the laboratory.

Trondheim, June 2023

Magnus Moen Sydtangen

Magnus Moen Sydtangen

Table of contents

- Abstract i
- Sammendrag ii
- Preface iii
- Table of contents iv
- List of explanation and symbols vii

- 1 Introduction 1**

- 2 Literature review, data and method 3**

 - 2.1 Literature review 3
 - 2.1.1 Particle matrix model 3
 - 2.1.2 The workability function 5
 - 2.1.3 Bingham model 7
 - 2.1.4 Viscosity 9
 - 2.1.5 Calculation of flow resistance ratio 12
 - 2.1.6 Void space measurements 13
 - 2.1.7 The materials' effect on fresh concrete 14
 - 2.2 Data from other sources 16
 - 2.3 Own experiments 17
 - 2.3.1 Materials 17
 - 2.3.2 Mixing procedures 19
 - 2.3.3 Laboratory methods 20
 - 2.4 Data analysis 22
 - 2.4.1 Data analysis 23
 - 2.4.2 Workability function and assumptions and explanations 23
 - 2.4.3 Machine learning 24

- 3 Results 27**

 - 3.1 Results from existing data 27
 - 3.1.1 Matrix 27
 - 3.1.2 Concrete 30
 - 3.2 Results from own experiments 31

3.2.1	Matrix	31
3.2.2	Concrete	32
4	Analysis	36
4.1	Analyzing the matrix	36
4.1.1	Calculated flow resistance ratio data existing data	36
4.2	Modification of the offset in the workability function	40
4.2.1	The training data	41
4.2.2	Comparing data	45
4.3	Modifying the void space	46
4.3.1	Increase the void space by 3.5%	47
4.3.2	Reduce the void space by 3.5%	48
5	Discussion	50
5.1	Calculating the flow resistance ratio	50
5.2	The workability function	51
5.2.1	The optimized workability function with machine learning	51
5.2.2	Modified the void space	51
5.3	Limitations	51
5.3.1	Data collected	52
5.3.2	Coefficients for the flow resistance ratio	52
5.3.3	Linear optimization of offset	52
5.3.4	Workability function	53
5.4	Further work	53
6	Conclusion	54
	References	55
	Appendix	59
A	Manual of laboratory tests	59
A.1	FlowCyl	59
B	Aggregate size distribution	60
C	Matrix calculations	63
D	Concrete from data set	66
E	The mixes and results from the experiments	74
E.1	Matrix mixes and calculations	74

E.1.1	Pictures for the slump flow of the matrix	75
E.2	Concrete mixes	80
E.3	Pictures of the slump flow of the concrete mixes	81
F	Workability function with original offset	87
G	Workability function with offset from linear optimization	94
G.1	Linear optimization training	94
G.2	Comparing data	101
H	Workability function with changed void space	105
H.1	Increased void space	105
H.2	Reduced void space	108

List of abbreviations

Explanations

- CVC Conventional compacted concrete
- FM The fines module of the aggregate
- Fm The finess module of the sand
- Fp The amount of filler in modified pasta
- Hp The rocks voids space in volume percentage
- HS Measured void space in volume percentage of dry sand
- PMM Particle matrix model
- PSD Particle size distribution
- SCC Self compacting concrete
- Slump The heigth of the concrete after the cone test
- Slumpflow The diameter of the concrete after the cone test
- TS The sands aggregate parameter
- w/c Water cement ratio

List of symbols

- μ_a Apparent viscosity

ρ	Volumetric weight
α	The gradient of the tangent
β	An equation in the new consistency function
$\dot{\gamma}$	Shear rate
λ_Q	Flow resistance ratio
μ	Plastic viscosity
ϕ	Solid fraction
τ	Shear stress
τ_0	Yield stress
Fp_m^S	The gradient's point of interaction with the lower asymptotic for slump
Fp_m^U	The gradient's point of interaction with the lower asymptotic for slump
b	Binder
bio	Biotite
c	Cement content
FA	Fly ash
fi	Filler
g	Gravitational acceleration
H	Void space
h	Initial height of the cement
Hm	The aggregates void space module

Kp	Workability function
m	The lower asymptotic of the slump
Mv	Matrix volume in percentage of total volume
n	The upper asymptotic of the slump
O	Offset of the matrix surplus
p	Powder
p	Pressure distribution
R	Radius of the measured flow
r	Initial radius of the cone shaped cement based material
SF	Silica fume
SP	Superplasticizers
V	Volume of the test sample
VSSA	Volume specific surface area
w	Water content

Chapter 1

Introduction

Concrete is the world's second most consumed material, with almost three tonnes for each person every year [7]. Most of the CO₂ emissions from concrete come from the production of cement [11]. Reduce the emissions from concrete, one possible solution is to reduce the amount of cement in the concrete. When casting concrete, there is a desired slump flow requirement, and one important factor in getting the desired slump flow without separation is necessary to have a sufficient amount of cement. To reduce the cement, and thereby reducing the emissions, it is important to have a tool to estimate the slump flow of the concrete. This would also reduce the cost of concrete production because it reduces the need to test the performance of the concrete.

In 1996 Ernst Mørtzell created a model which estimates the slump flow of concrete dependent on certain parameters in the concrete and the materials added to the concrete, this model is called the workability function. Cepuritis, Smeplass, and Mørtzell updated the workability of the current model with the goal of simplifying and increasing the fit of the model. The main parameters that are believed to be affecting the slump flow of the concrete are assumed to be void space, amount of superplasticizer, matrix volume, and matrix properties, which are mainly the flow resistance ratio.

The scope of this master thesis is to investigate the effect of superplasticizers on flow resistance ratio through a literature review and own experiments. Additionally, the aim is to improve the accuracy of the workability function by changing the offset equation and deviation within the void space.

This master's thesis builds upon the specialization project in TKT4550, written by

Magnus Moen Sydtangen in the autumn of 2022. The research background consists of a comprehensive literature review, analyzing relevant sources. Additionally, the thesis includes data analysis of external sources and conducting original experiments.

First, the literature review is used to understand the problem presented for this master thesis. This includes studying various concepts such as the particle-matrix model, workability function, Bingham model, viscosity yield stress, calculation of flow resistance ratio, void space measurements, and the influence of materials on fresh concrete. Further, data from existing reports and data from experiments are presented, with the following experimental methods for the experiments performed for this master thesis. Finally, the Chapter provides information about the data analysis used to analyze the data. Chapter 3 presents the results from the existing data and the data presented for this master thesis, analyzing the effect on matrix and concrete and the workability function. Chapter 4 compares the observed variables with the function for flow resistance ratio and workability function. In Chapter 5, the results from Chapter 4 and compared with the limitations based on the analyzes which are performed before the conclusion is performed in Chapter 6.

Chapter 2

Literature review, data and method

This chapter starts with an extensive review of prior research, focusing on the literature about the particle-matrix model. The particle-matrix model is introduced, along with the accompanying workability function derived from it. Further, this chapter examines the parameters influencing the workability function, providing insights for future analyzes.

Following the theoretical discussion, the subsequent section deepens into the data utilized within this thesis. In addition to the data collected from previous papers and reports, specific experiments were conducted specifically for this research. The experiments undertaken for this thesis encompassed matrix quality variations, namely B35 M60 and B55 M40, employing aggregates of Årdal 0/8 mm and Årdal 8/16 mm.

2.1 Literature review

This section presents the literature review for this master thesis. It begins with introducing the particle-matrix model, followed by presenting the workability function derived from the particle-matrix model. Additionally, the Bingham model, viscosity, and calculation of the flow resistance ratio Finally, the differences in void space measurements, and the influence of materials on fresh concrete are discussed.

2.1.1 Particle matrix model

The particle-matrix model, developed by Ernst Mørtzell [17], proposes that three parameters in concrete determine its rheological properties:

- Volume ratio matrix/particles

- Properties of the matrix
- Properties of the particles

These parameters are illustrated in Figure 2.1.

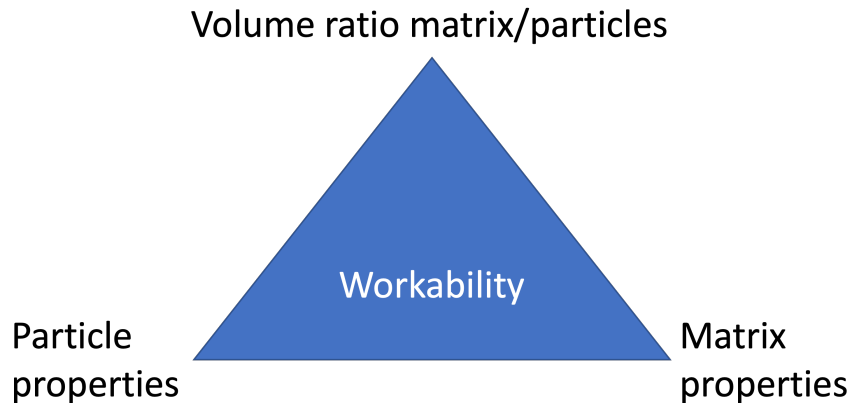


Figure 2.1: Particle matrix model, similar to Figure 4.1 in Concrete Technology [11]

The matrix consists of free water, additives, and solid materials smaller than 0.125 mm in diameter. Typical materials included in the matrix are cement, silica fume, fly ash, slag, and filler. The particles are all solid material with a particle size larger than 0.125 mm. Typical particles are aggregate.

The matrix's rheological properties are characterized by utilizing FlowCyl, which quantifies the properties of flow resistance ratio, denoted λ_Q .

Matrix phase

Matrix has two main ingredients, which are filler and cement paste. The filler is part of the aggregate smaller than 0.125 mm. The cement paste is the mixture of cement, pozzolans, admixtures, and water [11].

The matrix volume and the water/binder ratio will affect the workability of the concrete. Concrete with high strength has a low water/binder ratio, which gives low workability of the concrete. Low void space reduces the amount of matrix needed to get the wanted workability, reducing the amount of cement needed.

Concrete workability can be either "particle-dominated" or "matrix dominated". When the workability is "particle-dominated", the impact between particles is the dominating effect. A matrix-dominated concrete will have viscous flow due to the matrix increasing the space between the aggregate, so the property of the matrix will govern concrete flow properties. When the slump is below 150 mm, the concrete is particle dominated, above 150 mm, the concrete is matrix dominated.

Particle phase

The most important characteristics of the particle phase are the void space between the particles [11]. The particle size distribution (PSD) influences the particle's ability to compact and close the void space. A fine particle size distribution has a higher specific surface and, therefore, less void space the matrix has to fill compared to a coarse PSD. The fine PSD creates a matrix with better workability, given that other things are held constant.

The particles' shape also affects the void space [11]. Round particles give a higher degree of packing between the particles and a lower void space. Glacial deposits are a common source of round particles, however, due to their limited availability, aggregates are also produced by crushing stones. The crushed stone is usually more angular shaped unless the shape is improved using a vertical shaft impact (VSI) or similar equipment. An angular shape will reduce the ability of the particles to compact and increase the void space.

The offset is the difference between the void space (H) and the matrix volume (F_p). The concrete will have low workability when the void space exceeds the matrix volume. When the matrix surplus is positive, there is more matrix than void space in the concrete, the concrete will flow. One possible method to increase the workability of the concrete is to increase the matrix volume, i.e., increase the offset.

2.1.2 The workability function

The particle-matrix model is the basis for creating the workability function, also created by Mørtzell [17]. The fundamental idea behind the workability function is that the workability of concrete can be described by the amount of filler in the matrix, subtracted by the

aggregate void space module and flow resistance ratio. The original function is given in Equation 2.1:

$$Kp = \frac{n - m}{2} \cdot (\text{Tanh}(2 \cdot \alpha \cdot \frac{Fp - Hm}{100} - 1) + 1) + m \quad (2.1)$$

The lower and upper asymptotes are represented by m and n, respectively. The gradient tangent is denoted by α . Additionally, the void space modulus is Hm, and the matrix volume filler modified paste is represented by Fp. It is important to note that both Hm and Fp are expressed in volume fractions.

The value of α depend on λ_Q and can be calculated using the following equation:

$$\alpha = 19 \cdot e^{-2,45 \cdot \lambda_Q} \quad (2.2)$$

The void space module is based on modifying the aggregate void space by trying to account for the degree of particle contact [17]. Equation 2.1 does not account for the properties of the matrix, which are discussed in section 2.1.1.

New workability function

Cepuritis, Smeplass, and Mørtzell reviced the original workability function presented above, to include the properties of the matrix more than before. This is in this thesis called the new workability function. The new workability function includes the void space in the concrete and an offset variable.

$$Kp = \frac{n - m}{2} \cdot (\text{Tanh}(\alpha \cdot (2 \cdot Mv - 1 - (2 \cdot (H + O) - 1 + 1/\alpha))) + 1) + m \quad (2.3)$$

Mv is the matrix volume in the percentage of the total volume of the concrete, H is the measured void space in the aggregate, and O is the offset. O is the necessary surplus of the matrix to go from zero slumps in the cone test to get concrete that flows. The sum of the void space and the offset is all the matrix in the concrete.

Also, α have been updated after the original equation and are now given by

$$\alpha = (H + O) \cdot e^{-4/3 \cdot \lambda_Q} \quad (2.4)$$

The offset is calculated according to the following equation:

$$O = O_{min} + \frac{O_{max} - O_{min}}{\lambda_{Q,max} - \lambda_{Q,min}} * \lambda_Q \quad (2.5)$$

Two different names are used for the offset in the compendium for the subject TKT4215 [11]. The names are matrix surplus and the excess matrix, but they are the same as the offset. Offset is the matrix volume added after the void space is filled with matrix. This extra matrix ensures that the particles are no longer in contact with each other.

n is determined by the following equation:

$$n(sp/c) = \begin{cases} 600, & \text{if } SP \leq 1\% \\ 300 * sp/c + 300, & \text{if } 1\% < SP < 1.5\% \\ 750, & \text{if } SP \geq 1.5\% \end{cases} \quad (2.6)$$

2.1.3 Bingham model

The flow properties of the concrete can be modeled as a Bingham fluid [24]. A Bingham fluid is a viscous fluid that can flow if the yield strength is exceeded [20]. For low shear stresses is a concrete behaving like a Bingham fluid [29]:

$$\tau = \tau_0 + \mu \cdot \dot{\gamma} \quad (2.7)$$

τ is the shear stress [Pa], τ_0 is the yield stress, μ is the plastic viscosity [Pa · s] and $\dot{\gamma}$ is the shear rate [s^{-1}]. An illustration of Equation 2.7 is illustrated in Figure 2.2.

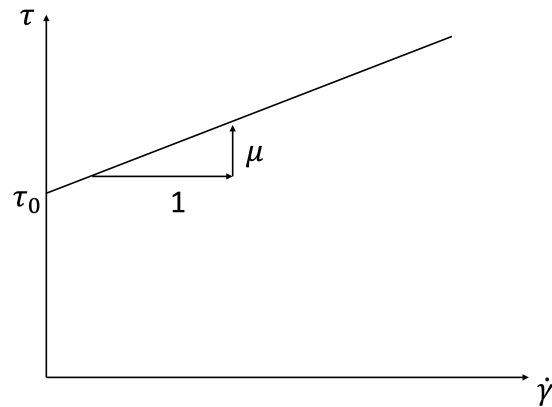


Figure 2.2: Bingham model

A BML-test can be utilized to find the parameters presented in Equation 2.7 and Figure 2.2. For more information about the BML Viscometer test, read section 2.3.3.

Cepuritis showed in [4] in Figure 4 in paper 6, that there is no clear relationship between the yield stress and plastic viscosity. Figure 4 shows that the w/c ratio will affect the plastic viscosity of the concrete. As the the w/c ratio decreases, the plastic viscosity increases.

Yield stress

The yield stress is the stress that has to be applied to the fresh concrete to make it go from solid to liquid form or between the liquid phases with different viscosity [16]. The reduction in yield stress can be attributed to a decrease in particle-particle attraction, as discussed in Banfill’s study on additivity [3]. The Bingham model explained in section 2.1.4 is the simplest way to model the fluid flow. As illustrated by Equation 2.11, the yield stress is essential when analyzing the flow of the fluid.

During the slump test, the concrete transitions from stationary to flowing as the cone is lifted. The point where the substance goes changes forms it the yield stress. The pressure by the fresh concrete in the slump cone can be written by Equation 2.8:

$$p = \rho \cdot g \cdot (h(r) - z) \tag{2.8}$$

Where p is the pressure distribution, ρ is the volumetric weight of the cement-based

material, g is gravitational acceleration, r is the initial radius of the cone-shaped cement-based material, h is the initial height of the cone-shaped cement-based material as the function of radius, and z is the pressure reference point. Roussel, Stafani, and Leroy [22] developed Equation 2.9 to estimate the yield stress from a slump test.

$$\tau_0 = \frac{225 \cdot \rho \cdot g \cdot V^2}{128 \cdot \pi^2 \cdot R^5} - \lambda \frac{R^2}{V} \quad (2.9)$$

Where V [mm³] is the test sample's volume, R [mm] is the radius of the measured flow, and λ is a coefficient which is a function of the tested fluid's surface tension and contact angle between the fluid and test surface.

2.1.4 Viscosity

Viscosity is a measure of the ability of the fluid to resist movement [9]. A fluid characterized by high viscosity requires greater force to induce motion compared to a fluid with lower viscosity. This section presents the basic understanding of viscosity and the most relevant viscosities.

Newtonian viscosity

A Newtonian fluid has constant viscosity with zero shear rates when the shear stress is zero [12]. The relationship between shear rate and shear stress is proportional, as illustrated in Figure 2.3.

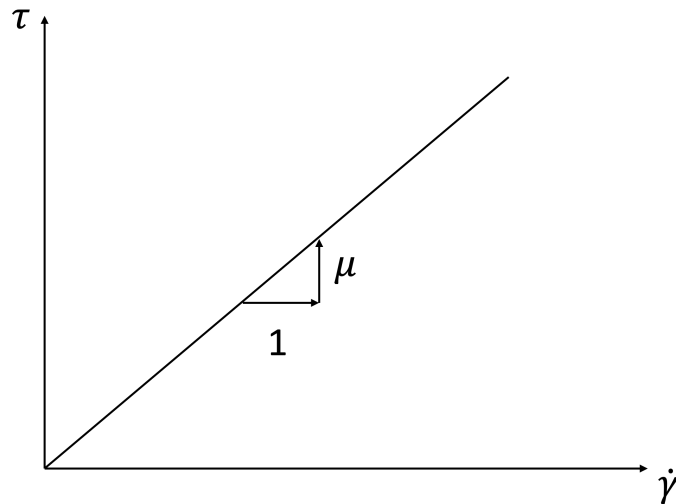


Figure 2.3: Newtonian fluid: $\tau = \mu \cdot \dot{\gamma}$

The mathematical for a Newtonian liquid is described by the Equation 2.10:

$$\tau = \eta \cdot \dot{\gamma} \quad (2.10)$$

τ is the shear stress [Pa], η describes the relationship between the shear rate and shear stress, and $\dot{\gamma}$ [s⁻¹] is the shear stress [29]. The value of the viscosity coefficient is dependent on the temperature of the liquid. The linear relationship between the shear rate and shear stress is passing through the origin, there would only be necessary to have one observation to determine η .

Plastic viscosity

A Newtonian fluid is the simplest model to model fluid behavior. For all materials except for a Newtonian fluid, the relationship between shear stress and shear rate is not constant [29]. Unlike the Newtonian fluid, the plastic viscosity also considers the "shear history". Unlike Newtonian viscosity, there is no linear relationship between the shear stress and shear rate, and the line will not pass through the origin. The model for plastic viscosity is also called the Bingham model, and the Bingham model is the simplest of all flow behaviors other than the Newtonian flow model [29].

The equation for plastic viscosity can be written as:

$$\tau = \tau_0 + \mu \cdot \dot{\gamma} \tag{2.11}$$

where τ_0 [Pa] is the yield stress and μ [Pa · s] is the plastic viscosity. A convex curve is said to be shear thinning. Meanwhile, a concave curve is said to be shear thickening [29]. It is called shear thickening since the shear stress increases more rapidly than the shear rate. Shear thickening implies that the increased shear stress makes it harder to move the fluid.

Apparent viscosity

Apparent viscosity is defined as the acting shear stress divided by the shear rate, $\mu_a = \frac{\tau}{\dot{\gamma}}$ [16]. Concrete is a non-Newtonian material [21], which means that the material needs a certain amount of shear force to start moving. That means Figure 2.4 will not start from the origin of $\dot{\gamma}$ and τ .

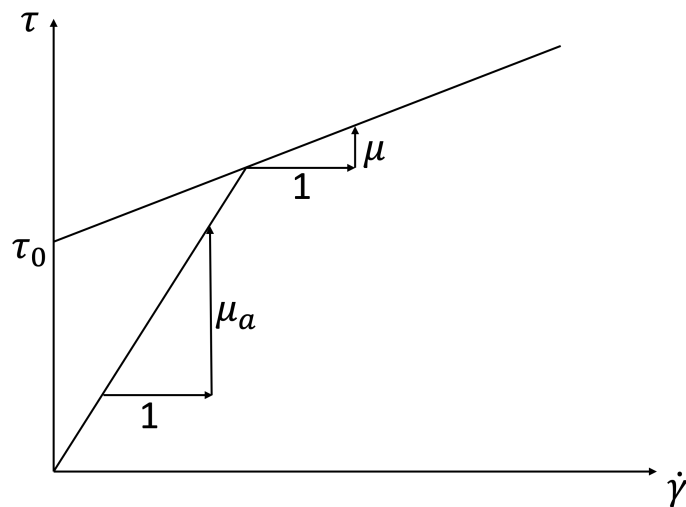


Figure 2.4: Geometric considerations to apparent viscosity

$\dot{\gamma}$ is the shear rate of the fluid. The apparent viscosity is the slope from the origin to the point $(\dot{\gamma}, \tau)$. The plastic viscosity is the slope from $(0, \tau_0)$ to $(\dot{\gamma}, \tau)$. By using the geometric considerations from Figure 2.4 it is possible to express μ_a with τ_0 :

$$\mu_a = \frac{\tau}{\dot{\gamma}} = \frac{\tau_0 + \mu \cdot \dot{\gamma}}{\dot{\gamma}} + \mu = \frac{\tau_0}{\dot{\gamma}} + \mu \tag{2.12}$$

When an external shear stress is applied on a fluid, the plastic viscosity represents the internal resistance of the fluid as it begins to flow. The apparent viscosity can be said to be the viscosity felt by the fluid at $\dot{\gamma}$.

Both Figure 2.4 and Equation 2.12 illustrate that the effect of τ_0 depends on the size of $\dot{\gamma}$. If $\dot{\gamma}$ is large, the effect from τ_0 is small, but if $\dot{\gamma}$ is small, the effect from τ_0 is small. In Cepuritis et al. [5] they present an example with three different values:

No.	τ_0 [Pa]	μ [Pas]	$\dot{\gamma}$ [s ⁻¹]	μ_a [Pas]
1	4.58	0.38	150	0.412
2	7.28	0.38	150	0.429
3	4.85	0.57	150	0.602
4	4.58	0.38	75	0.411
5	7.28	0.38	75	0.477
6	4.85	0.57	75	0.631

Table 2.1: Calculation of μ_a from [5]

From Table 2.1, the difference between 1 and 2 is an increase in τ_0 with 50%, which increases μ_a with 4%. The disparity between numbers 1 and 3 lies in the fact that μ is augmented by 50. The increase in the percentage of μ_a described by τ_0 is larger for numbers 4 and 5 than for numbers 1 and 2.

2.1.5 Calculation of flow resistance ratio

Skare et al. [24] presented an empirical equation to calculate the matrix's flow resistance ratio (λ_Q). The equation is based on mixed design parameters:

$$\lambda_Q = k_1 \cdot \frac{VSSA}{100} - k_2 \cdot \phi - k_3 \cdot \frac{w}{p} - k_{4,i} \cdot \frac{SP}{c} + k_{5,i} \cdot \frac{c}{w} + k_6 \cdot \frac{bio}{fi} + k_7 \cdot \frac{FA}{b} + k_8 \cdot \frac{SF}{b} + k_{9,j} \cdot \frac{fi}{b} \quad (2.13)$$

Where ϕ is the solid fraction of the matrix and w, p, SP, c, fi, b, FA, SF, and bio represent the mass of water, powder, superplasticizer, cement, filler, binder, fly ash, silica fume, and biotite, respectively. VSSA is the surface area of the volume for all dry materials except for SF. There have been performed several studies of the coefficients of Equation 2.13, the different coefficients are presented in Table 2.2:

Table 2.2: Adjusted constants to equation 2.13

	k_1	k_2	k_3	k_4	k_5	k_6	k_7	k_8	k_9
Skare et al.	0.42	2.72	1.47	0.06	0.31	1.41	0.31	2.15	0.58
Adamski and Grefstad	0.38	1.07	1.44	0.07	0.13	0.17	-0.1	1.6	0.226
Adjusted values	0.42	1.07	1.44	60	0.13	0.17	-0.1	1.6	0.58

Skare et al. is the original coefficient [24]. Adamski and Grefstad presented in their master thesis some alternative coefficients [1]. Furthermore, Sydtangen et al. did also a study based on the data from Skare, a way to fit the calculated flow resistance to the observed observations for changing SP, and ended up with the coefficients in Table 2.2.

The VSSA can be calculated by:

$$VSSA = \sum_i VSSA_i \cdot \phi_i \tag{2.14}$$

$VSSA_i$ for each material, and ϕ_i is the volume fraction of powder material i in the matrix.

The surface area of the volume for each material is presented in Table 2.3.

Table 2.3: VSSA for all dry material, except silika fume from Leite Skare et al. [24]

Material	Volumetric specific surface area [mm ² /mm ³]
Fine filler	728
Intermediate filler	367
Coarse filler	522
VSI filler	260
Biotite	1122
Standard FA cement	829
Industry cement	1302
Fly Ash	970

2.1.6 Void space measurements

The void space measurements of the aggregate will vary depending on what type of measurement method is used [15]. In the report for Martius-Hammer et al. [15], there are four methods to measure void space:

- NZFC
- EPP 4C

- EN 1097-3
- NorBet

The four different measuring methods give stable results relative to each other. However, there can be significant variations of up to 7% between the measuring method that provides the highest void space, NZFC, and the one that yields the lowest void space, EPP 4C method. The difference between NZFC and EPP 4C varies between 6 and 7%. The EN 1097-3 measurements method is 2.2% lower than NZFC and, on average, 4.5% larger than EPP 4C.

2.1.7 The materials' effect on fresh concrete

Three materials' properties are mainly affecting the mobility of the concrete [11]:

- Friction between particles.
- Internal cohesion/stickiness to a solid surface.
- Resistance to internal flow of the liquid phase.

Concrete with large mobility can be created with a high water content and a low amount of coarse aggregate. Such concrete will be costly to create due to the high content of cement in order to keep the desired level of strength. To enhance the mobility of the concrete without incurring a significant increase in costs, adding a superplasticizer offers a viable solution. Figure 2.5 illustrates the effect that increased content of SP gives the concrete.

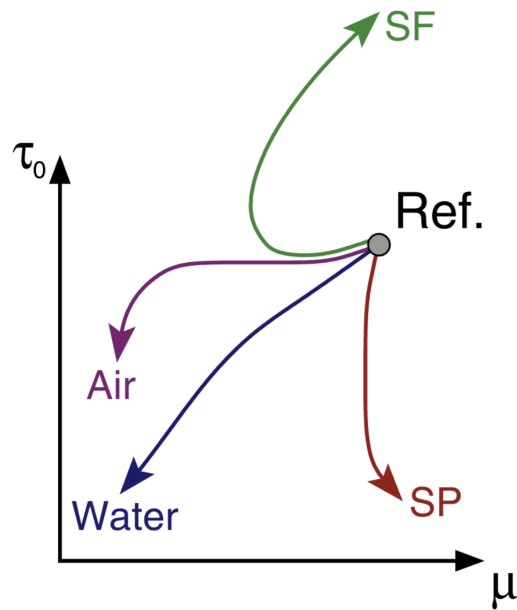


Figure 2.5: SP effect on τ_0 and μ from [31]

Plastic viscosity and yield stress are discussed in section 2.1.3 and 2.1.4, respectively. Figure 2.5 illustrates that the yield stress is reduced, but the viscosity is increased with increased content of SP. The assumption is that SP mainly affects the yield stress, not the plastic viscosity, and the Figure from Wallevik and Wallevik [31] supports this theory. In practice, this means that a higher content of SP will reduce the force applied to get the concrete to flow, also called plastic viscosity, but that the force needed to keep the concrete flowing will be the same.

Figure 2.5 illustrates other materials' effects on fresh concrete. Some of the materials have a more significant effect on the performance of hardened concrete. For example, water are reducing the strength, and increased air voids are increasing the concrete's better durability against frost deterioration [11]. Water also reduces the yield stress, but at the same time, it reduces the viscosity. Increased air voids will primarily affect the viscosity.

The amount and type of aggregate will also affect the mobility, as discussed in section 2.1.1. The effect on the yield stress and viscosity is illustrated in Figure 2.6.

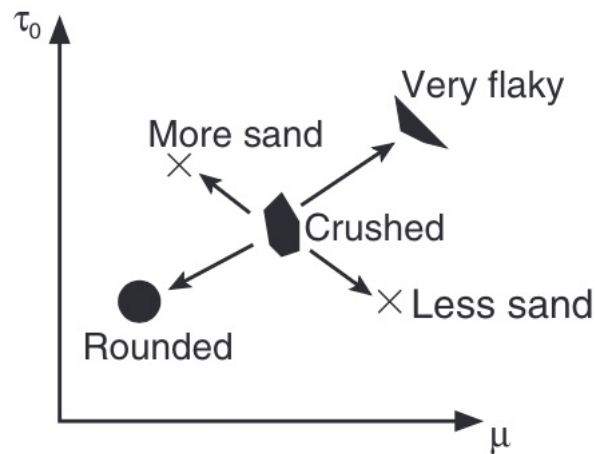


Figure 2.6: The aggregates effect on τ_0 and μ from [31]

The round aggregate reduces yield stress and viscosity, and more sand reduces viscosity and increases yield stress. Figure 2.6 are not saying anything about the size distribution of the aggregate.

2.2 Data from other sources

The data collected for concrete from previous studies are from 2 Sintef reports: Rheology of concrete with crushed aggregate [14] and Rheology of mortars with manufactured sand [15]. Miks project at NTNU, and the master thesis of Adamski and Grefstad [1]. Note that the methods utilized in these researches are outlined in their original papers and will not be elaborated upon here.

There is a total of 108 observations for concrete which are presented in Appendix D in Table D.1. The previous studies contain different measured variables due to different goals for the studies. Therefore there are not a total of 108 observations that can be used for the data analysis. There is a total of 57 observations utilized to analyze the data in Chapter 4.

The data collected for the matrix is collected from the doctoral thesis of Leite Skare [23], which is presented in Appendix C together with the analysis results. In total, there are 51 observations for the matrix.

2.3 Own experiments

This section presents information about the materials used, the mixing procedure utilized, and the laboratory methods used to find the parameters of the matrix and the concrete.

2.3.1 Materials

This section provides an overview of the materials and their specifications used in the concrete mixture. The presentation contains details about the cement, aggregates, and superplasticizers employed. The concrete mixes are a model test.

Cement and paste

The cement used in the laboratory is Norcem Standard FA CEM II/A-V 6-20% fly ash. Information about the product can be found on this reference [18].

Two types of concrete are tested, C35 M60 and C55 M40. The strength class are "C35", where the number is the strength in MPa, and "M60" is the durability class. "C35" is the strength class, where "C" is a prefix and the following number is defining the compressive strength in MPa. "M60" denotes the durability class, where "M" is a prefix and the number is the durability class. The lowest durability class is M90 while the highest durability class is MF40. Both the strength and durability classes have a water/binder ratio (w/b). The smallest w/c for the strength and durability classes will decide the w/b in the concrete. Figure 4.8 in [11] is the decisive factor for the compressive strength of the concrete. The water binder ratio for C35 and C55 concrete is about 0.7 w/c and 0.47 w/c, respectively. The M60 and M40 have a w/c of 0.6 and 0.4 w/c, respectively. Therefore, the w/c for the concrete is 0.6 for the B35 M60 concrete and 0.4 for the B55 M40 concrete.

Aggregates

The aggregate used in the test is Årdal 0/8 mm and 8/16 mm, with the following size distribution presented in Appendix B. The aggregate from Årdal is a natural deposit [2], which means that the glaciers create the particles and are, therefore, fairly round and, followingly, low void space volume [11]. For the given aggregate, the matrix volume

distribution will be:

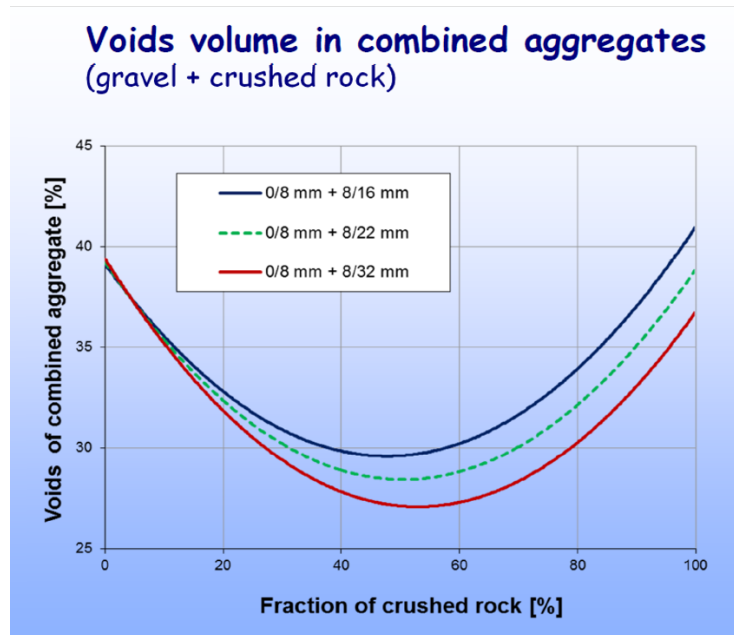


Figure 2.7: Void space with the aggregate

According to the recommendations in [11] and Figure 2.7 are chosen to use 60% of the aggregate with a size from 0-8 mm, and 40% of the aggregate with a size from 8-16 mm. The aggregate weights are chosen due to reducing the chance of segregation. The void space calculated by the excel-sheet developed by Cepuritis will be 26.16%. Then the void space is close to the lowest possible, but also with that distribution between the coarse and fine aggregate, there will contribute to the stability of the concrete.

The amount of each aggregate that will be used in the mixes will vary after the volume of concrete that is going to be produced.

The filler used in the matrix and sedigraph in the laboratory is sieved from Årdal with a size from 0 mm to 0.125 mm.

Superplasticizers

Mapei SX-23 is used as a superplasticizer [13]. For the mix with B35 M60, there will be used 0.3% of SX-23, and for the mix with B55 M40, there will be used 1.2% of SX-23.

For the last test, one will vary from 0.5% to 1.7% with 0.9%, 1.2%, and 1.5% in between.

2.3.2 Mixing procedures

The mixing procedures used to create the matrix and concrete with the materials from section 2.3.1 to perform the experiments described in section 2.3.3.

Mixing procedure matrix

The mixing procedure for the matrix is presented in the Appendix A.1. The equipment which is used to mix the matrix is presented in Figure 2.8:



Figure 2.8: The equipment which is used for mixing the matrix for the FlowCyl

Concrete mixing

Before mixing the concrete, it is essential to know the water content of the components of the concrete. Therefore, one kilogram of the aggregate is heated in about 20 minutes to most of the water is boiled out, and compare the weight before and after the heating. Then it is possible to correct the added water such that the water content is correct.

1. Adding the aggregates to the mixer.
2. Add cement to the mixer.
3. Dry mix the aggregates and the cement for one minute.
4. Add the water and superplasticizer for 30 seconds; then, keep mixing for one and a half minutes.

5. The mix rest for 2 minutes.
6. Mix for an additional one minute.

The mixes created in this master thesis are presented in Appendix E.2. There created two different strength classes, C55 and C35, with the durability classes M40 and M60, respectively. For the concrete C55 M40, the range of SP will be varied for the matrix volume 325 l/m^3 .

2.3.3 Laboratory methods

The laboratory work performed for this master's thesis will be presented in this section. Experiments are performed to quantify the parameters for the matrix and the concrete. The experiments performed to test the properties of the matrix are the FlowCyl test and mini-slump flow which are presented together with the slump test of the concrete. The experiments used to specify the concrete parameters are presented, which are the slump test, density test, air content, and BML test.

FlowCyl

FlowCyl is one method to measure the flow resistance ratio of the matrix, which is an important variable in the particle-matrix model.

The FlowCyl measurement in this thesis is performed with the following method:

- Weigh all of the dry materials with 0.1-gram certainty. Water is weighed in the yellow container shown in Figure 2.8, and SP-dosage is inserted in a syringe.
- The mixing are performed according to Table A.1 in Appendix A.
- The mix is filled in the FlowCyl in the opening of the container to the matrix reached the opening.
- The FlowCyl container is sealed until the computer program has started. First, the container will be unsealed when the computer program has started, and there is a scale which measure the weight of the matrix which have left the FlowCyl which are logged by the computer program. The

experiment stops when the matrix is no longer dripping through the bottom opening of the FlowCyl container.

After the FlowCyl is performed the data are inserted in the excel-sheet "FlowCyl calculation.xlsx" and the flow resistance ratio is the output.

Slump test

The slump test is performed according to NS-EN12350-2 [25].

The cone and base plate are dampened, and any excess moisture is removed with a cloth. While the cone is filled, it has to be held against the base plate. The cone is filled with three layers of concrete with equal height. Each layer has to be compressed with 25 strokes of the compacting rod before going to the next layer. The first layer is compacted through the total debt of the layer but without hitting the base plate. The second and third layers are also compacted through the total debt of the layer. If the compacting of the last layer of concrete results in the cone not filling to the edge with concrete, more concrete must be added, so there always is an excess of concrete. The excess concrete was removed, and the compacting rod was used with a rolling movement. The spilled concrete for the base plate is removed. The cone is lifted vertically in slow motion and is between 2 and 5 seconds. The cone was lifted vertically without any sideways or torsional movement. The whole procedure from the cone is filled with the first layer until the cone is removed shall be performed continuously and within 150 seconds.

The mini-slump flow is performed in the same way, the only difference is that the cone size for the mini-slump test is considerably smaller. The mini-slump cone has the dimensions [28]: top diameter = 19 mm, bottom diameter = 38 mm, height = 57 mm.

Air content

To test the air content of the concrete, the water column method according to NS-EN 12350-7 [26]. The air testing container is damped with a wet cloth before the testing, after this, fill the concrete in layers, as described for the slump flow. A compacting rod is used to compact each layer of the concrete with 25 strokes. This removes air pockets

in the concrete. The rod should never hit the bottom of the container or penetrate the previous layer. A rubber mallet is used to hit the side of the container to remove air bubbles or recesses of the surface of the concrete. The material in the last layer should be enough to fill the container without removing any excess concrete. If the previous layer did not fill the container, one more layer could be added. Seal the container, and water is added to the top of the lid to a specific level. The reduction in water level measures the volume reduction due to the added air. The water column is calibrated in the concrete specimen's air percentage.

Density test

The density test is performed in the container of the air content, which is presented above. The container has a known weight and volume. The container is filled with the air content test procedure and weighted after that. To find the density, subtract the weight of the container from the total weight and thereafter divide by the volume.

BML-test

The BML-Viscometer type WO-3 consists of two units, one test unit, and a computer registering the data. The test unit has two cylinders, the outer cylinder, which rotates, and the inner cylinder, which measures the torque and is logged by the computer. In this thesis, the BML Viscometer test is performed for concrete. The speed range of the outer cylinder is 0.001-0.9 rotations per second.

The BML viscometer test was constructed to measure concrete with a slump of 120 mm or higher. When there are no admixtures, getting good measurements of mixes with slump between 50-60 mm is possible. With admixtures, there is possible to have an even lower slump.

2.4 Data analysis

This section presents the methods used to analyze the data presented in section 2.2 and 2.3, which is performed in Chapter 4.

2.4.1 Data analysis

The data analysis for the matrix is performed by comparing the observed variables with the data from Equation 2.13 in section 2.1.5. The error is the differences between the results from the Equation 2.13 and the observed variables, which are used to measure the model's fit. The coefficients presented in 2.1.5 are adjusted to increase the model's fit.

The data analysis for the concrete is performed by utilizing linear optimization. Linear optimization is used to find the minimized error using an offset that minimizes the error in the workability function defined in section 2.1.2. More about the data analysis using the workability function is presented in section 2.4.2. The analysis is performed by comparing the workability function and the observed values. The deviation between those is calculated and presented as the error for each workability function, and the belonging observed variables. The error is used as a measurement of the fit of the workability function.

To perform the data analysis, Python is used. The package used is Pandas to simplify the data structure and, therefore, also the data analysis. Matplotlib and Seaborn are used to illustrate the figures. Numpy is used to perform numerical operations. PyTorch is used to perform machine learning which optimization the offset variable, which is discussed comprehensively in section 2.4.3.

2.4.2 Workability function and assumptions and explanations

The workability function used in the data analysis is presented in Equation 2.3. There are mainly four factors that influence the curve of the workability function:

- Flow resistance ratio, λ_Q
- Upper asymptote, n
- Void space, H
- Offset, O

As illustrated by Equation 2.13 λ_Q is affected by numerous factors but also by SP. The

effect of sp/c on flow resistance is investigated further in sections 3.1.1 and 4.1.

The lower asymptote is argued to be fixed at all times, which is 200 mm. The dosage of SP decides the higher asymptote. The equation which determines the n is defined in Equation 2.6. sp/c decides n because sp/c mainly affects the yield stress as presented in section 2.1.3 and 2.1.7. The yield stress is the main influence on the upper asymptote since the yield stress is where the substance goes from fluid to solid and vice versa. Therefore, also the decisive for when the substance will stop flowing. Since sp/c is assumed to have the main effect on yield stress, the sp/c is deciding the upper asymptotic.

The void space is the space between the particles in the aggregate, and the matrix needs to fill the voids created from the aggregate. The void space can be calculated from an Excel sheet, called "09-06-22 (AEG) Åpen versjon Proporsjonering 2021 MiKS utvikling.xlsm" developed by Rolands Cepuritis in 2022. As explained in section 2.1.2, the offset is the necessary surplus of the matrix to go from zero slumps to something that has flow. To calculate the offset, look at the equation. The offset considers the amount of matrix needed to push the particles away from each other after the void space is filled. This is generally in the 1.5 to 3-volume percentage of the mix. With a stiff matrix, i.e., a high flow resistance ratio, the offset must be larger than for matrixes with a lower flow resistance ratio. When linear optimization is utilized to find the optimized offset, it is assumed that the offset is linearly dependent on the flow resistance.

$$offset = a \cdot \lambda_Q + b \quad (2.15)$$

Where a is the slope of the offset and b is the intercept. The coefficients are decided by machine learning. Equation 2.15 is the general equation used to find the optimal offset variable according to the assumption of how the offset is affected.

2.4.3 Machine learning

Machine learning is a broad concept that can be utilized to perform many tasks [19]. This thesis uses linear optimization to improve the offset variable based on the data set. The Python package PyTorch is utilized to perform the linear optimization, a neural network

specialized [10]. To create the structure of the machine learning, which are described below with the functions and the basis of what the equations contains, is created by Chat GPT [6].

To perform the optimization with machine learning, linear minimization is used to calculate the model's fitness. There are defined four functions in Python, one of which calculates the workability function. A function called "init" is used to test the model's parameters which in this case is the slope and the intercept of the offset function, constant a and b in Equation 2.15. A function called "forward" used the input value, the flow resistance, and the parameters defined in "init". In this case, the input value is the flow resistance and calculates a new offset value. Last is the "optimize_offset" function, which is the one that optimizes the offset variable. The basis of how this function works is that it takes in random defined variables from the function "init", which are calculated with the workability function. Then it is calculated as an error which is the deviation between the workability function and the observed points. In the next iteration, there are testing a new random variable in "init", and the error is calculated. This way, the function aims to minimize the error. This is performed 20 000 times, and it is observed that all the variables are converging.

More advanced, the function "optimize_offset" calls the previously defined function, workability function, "init" and "forward", and uses the Adam optimizer to minimize the deviation between the observed variables and the workability function. The learning rate in the Adam optimizer is set to 0.1. The learning rate determines the step size, and the optimizer updates the step size during optimization. In addition, a scheduler is used to adjust the model's learning rate to increase as the learning process continues. For every 1000 iterations, the learning rate increases. In the "optimize_offset" function, the parameters a and b defined in Equation 2.15 are determined to be between -2 and 6 to reduce the training time and to make sure that the values are between these values. These values are decided by consideration based on the theory presented above. To calculate the error or loss, which it is called in machine learning, regularization is utilized to prevent overfitting [8]. There are used two types of regularization. The first regularization, L1, is also called Lasso Regularization. The second regularization, L2, is called Ridge

Regression. The regularization is used to reduce the variance of the model without increasing the bias. They have utilized two functions in the PyTorch library, which are called "loss.backward()" and "optimizer.step()", which are used to calculate a new iteration.

Due to only looking at optimizing Equation 2.15 in the Equation 2.3, which is the new workability function, the workability function is linearly optimized. This is oversimplifying the problem, and therefore not properly machine learning. To perform machine learning on the workability function it should be performed with a more general equation defined where the forward defines the entire workability function. This is more advanced and will not be performed in this thesis.

Chapter 3

Results

This chapter investigates the appearance of the data from the sources presented in section 2.2 and 2.3. The focus is on the sp/c effect on the flow resistance ratio, the matrix volume effect on slump flow, and the workability function. First, the results from the existing data are presented. Further, the data from experiments performed for this master thesis are presented.

3.1 Results from existing data

In this section, the results from the existing data are presented in section 2.2 is presented.

3.1.1 Matrix

Figure 3.1 illustrates the effect of sp/c on flow resistance ratio. To take a closer look at how the sp/c affects the matrix's flow resistance ratio, Figure 3.1 is included.

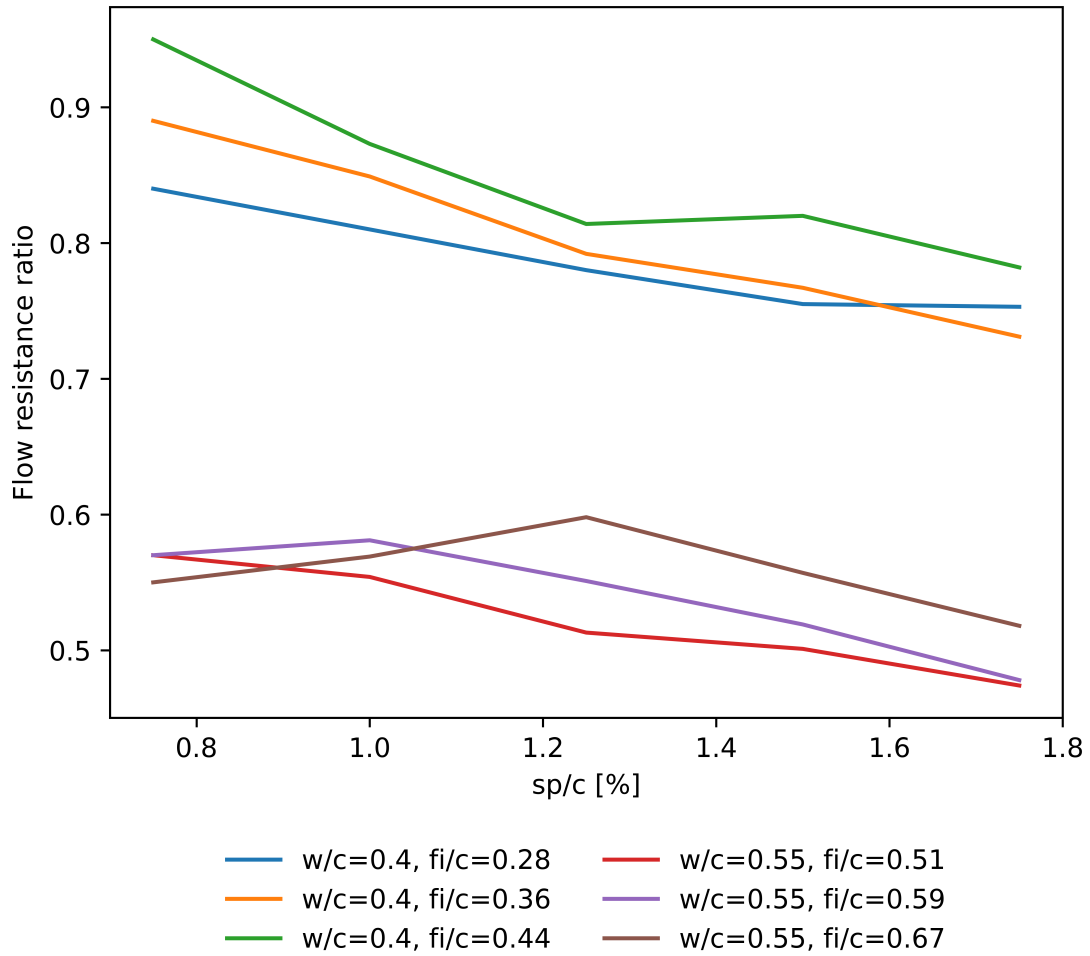


Figure 3.1: Flow resistance ratio given by sp/c , this figure is also presented in Sydtangen et al. [27].

The only varying parameter in Figure 3.1 is the sp/c . This figure illustrates that for all w/c and fi/c equal, the flow resistance ratio has a deviation in the area of 0.15 when the sp/c is varied between 0.75 and 1.75%. Figure 3.1 illustrates the sensitivity of the flow resistance on the changing levels of sp/c .

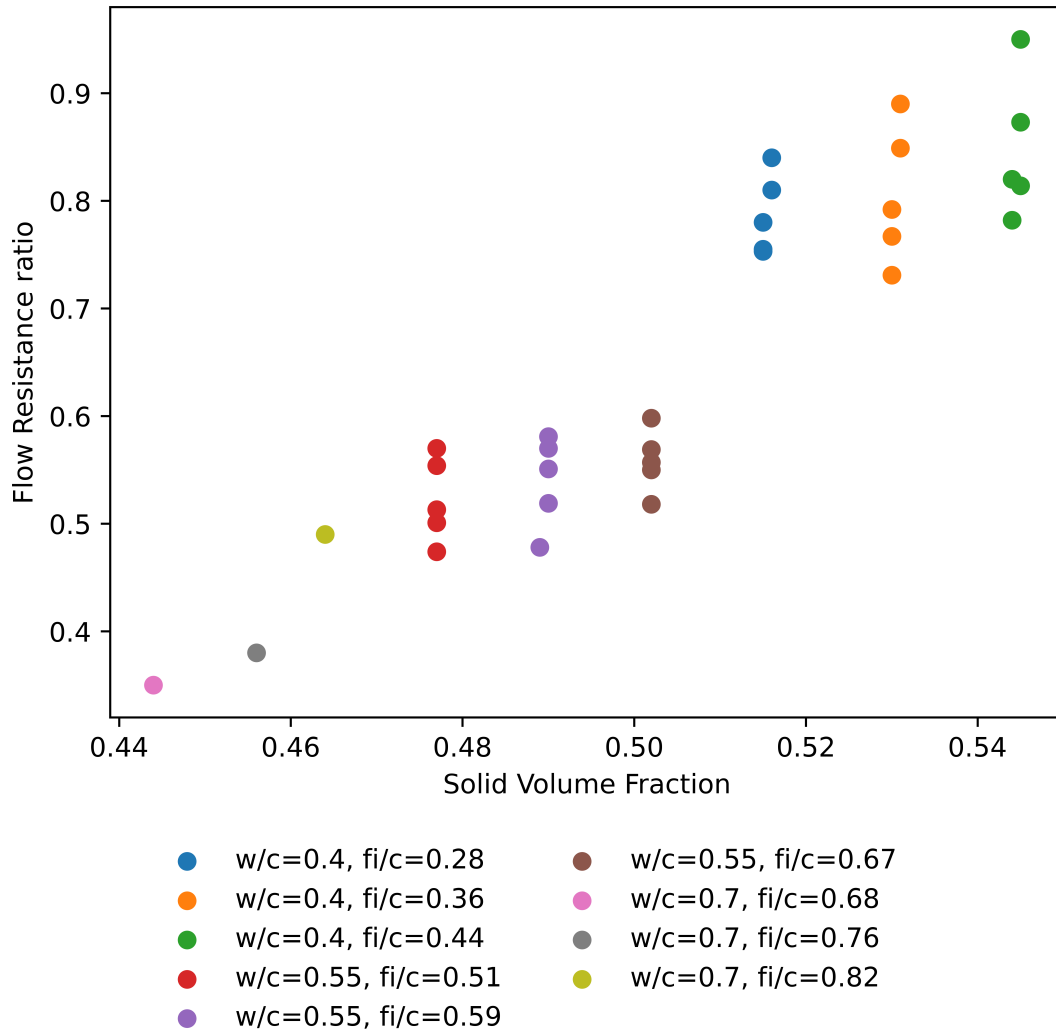


Figure 3.2: Plotted values for flow resistance and solid volume fraction grouped for w/c and fi/c . This figure is presented in Sydtangen et al. [27].

Figure 3.2 have nine different w/c with a corresponding fi/c . The only variable that varies between the labels' color is the sp/c . All the sp/c dosages vary from 0.75% to 1.75%. The difference within the labels varies from 0.087. The data's most significant difference is $w/c=0.55$ and $fi/c=0.67$, with a range in λ_Q from 0.55 to 0.35 when the sp/c varies from 0.75% to 1.75%.

The Figures 3.1 and 3.2 illustrate the same effect, that sp/c significantly affects λ_Q . The most significant impact of all other equals gives a difference in the flow resistance of 0.2 when there is an increase in the sp/c with 1%.

3.1.2 Concrete

The results for the calculation of the concrete are given in this section.

Workability function

The first four observations of void space in Rheology of Concrete with crushed aggregate [14] are measured. The rest of the observations are calculated with the Excel tool created by Cepuritis. The observations which are calculated with the Excel sheet is given in Table D.1 in Appendix D with a * in the void space column. The aggregate from Velde, used in the Sintef report, Rheology of concrete with crushed aggregate, is crushed [30]. To calculate the void space, the following inputs were used:

Void space	
D_{\max}	16 mm
Shape of the sand (0-8 mm)	Crushed
Shape of the aggregate (8-16 mm)	Crushed
Garding of 0.125/8 mm	Straight

Table 3.1: The input to calculate the void space in the aggregate

For aggregate with 60/40, where 60% is the aggregate between 0-8 mm and 40% is the aggregate between 8-16 mm. This gives a void space of 29.76%. For aggregate with 70/30, give a void space of 30.99%. For aggregate, 72/28 provides a void space of 31.35%. This is used in the calculation of the workability function.

With the equations specified in section 2.1.2 and the void space specified above there have been performed an analysis of the data from Rheology of concrete with crushed aggregate and the data used in the master thesis of Adamski and Grefstad. The results are presented in the Appendix F. The workability function in Figure F.3 fits the measured data well. The workability function for F.2, F.4, F.10 and F.12 have a partly good fit. Some of the values in F.2 have a good fit, but the two values do not align with the workability function. The other figures shows that there is a horizontal displacement of the workability curve according to the observed values.

3.2 Results from own experiments

The experiments performed for this master’s thesis were performed in the Department of Structural Engineering Laboratory at NTNU.

3.2.1 Matrix

Table 3.2 presents the matrix mixes tested. There were tests on 11 different matrix mixes, where three matrix mixes were retested to confirm the validity of the measurements.

Table 3.2: Matrix mixes and results from own experiments

Mix	w/c	sp/c	fi/c	Solid volume fraction	Flow resistance	Mini slump flow
B55 M40 - 1	0.4	1.2	0.3049	0.525	0.85	380
B55 M40 - 2	0.4	1.2	0.2664	0.521	0.79	380
B55 M40 - 3	0.4	1.2	0.2243	0.515	0.8	390
B55 M40 - 4	0.4	1.2	0.2664	0.521	0.78	345
B55 M40 - 5	0.4	0.5	0.2659	0.522	0.92	165
B55 M40 - 6	0.4	0.9	0.2662	0.521	0.82	280
B55 M40 - 7	0.4	1.5	0.2666	0.520	0.75	375
B55 M40 - 8	0.4	1.7	0.2667	0.519	0.77	420
B35 M60 - 1	0.6	0.3	0.3865	0.470	0.52	247
B35 M60 - 2	0.6	0.3	0.3386	0.476	0.44	263
B35 M60 - 3	0.6	0.3	0.2978	0.460	0.43	280

To test the results presented in section 3.1.1, a test with varying sp/c was performed. Figure 3.3 illustrates the same effect as Figure 3.1 that the flow resistance ratio depends on the sp/c and that an increasing sp/c decreases the flow resistance ratio.

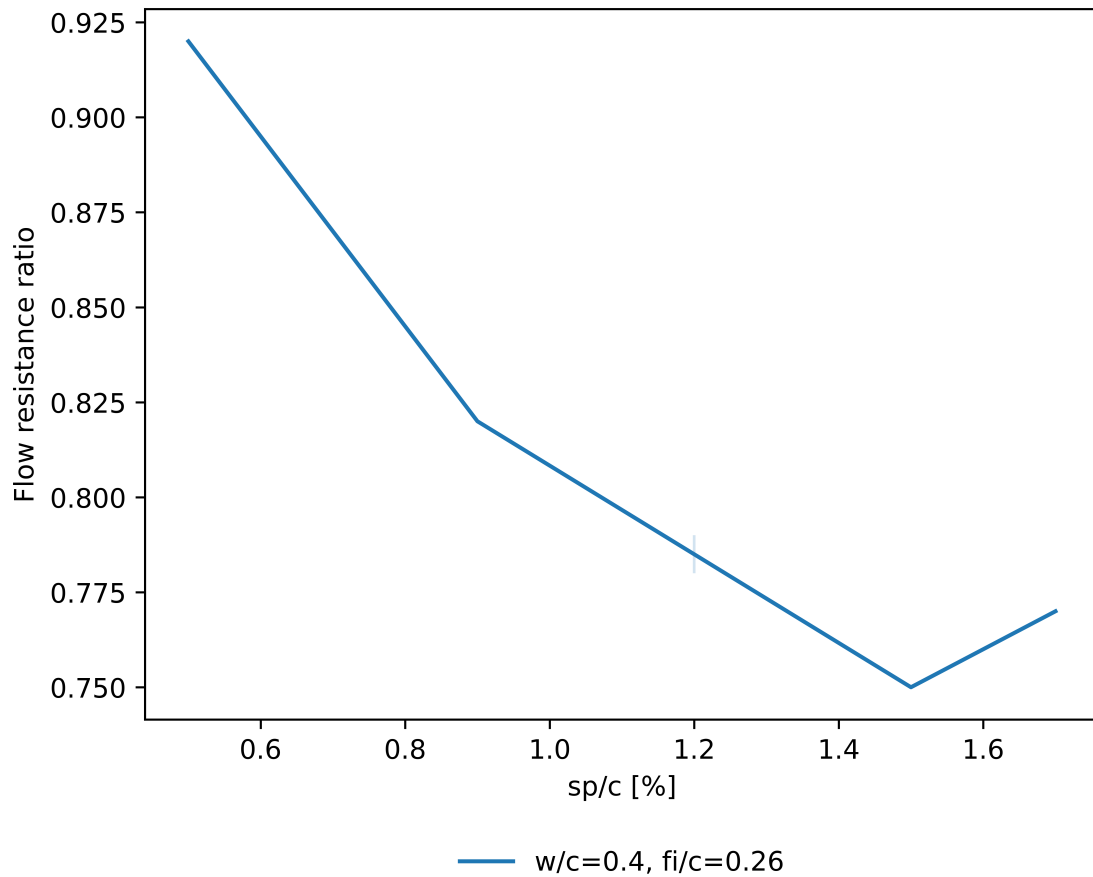


Figure 3.3: The sp/c effect on flow resistance ratio from the experiments explained in section 2.3.

As Figure 3.3 illustrates, there is a jump at the end, this error can be due to errors in the mixing of the matrix or the performance of the FlowCyl.

3.2.2 Concrete

The concrete mixes from the experiments presented in section 2.3, there are 12 concrete mixes that are tested, and they are presented in Table 3.3.

Table 3.3: The recipes for the 20 liter concrete mixes

Mix	Cement	Water	Matrix volume	Aggregate	sp/c	Slump	Slump flow
B55 M40 - 1	7.022	2.961	300	38.525	0.012	151	340
B55 M40 - 2	7.736	3.232	325	37.108	0.012	230	640
B55 M40 - 3	8.45	3.503	350	35.692	0.012	270	720
B55 M40 - 4	7.736	3.232	325	37.108	0.012	245	632
B55 M40 - 5	7.7	3.1	325	37.108	0.005	115	210
B55 M40 - 6	7.7	3.1	325	37.108	0.009	223	450
B55 M40 - 7	7.73	3.212	325	37.108	0.015	205	690
B55 M40 - 8	7.726	3.1	325	37.108	0.017	228	678
B35 M60 - 1	5.539	2.735	300	38.316	0.003	7	200
B35 M60 - 2	6.103	3.079	325	37.871	0.003	35	215
B35 M60 - 3	6.666	3.451	350	36.425	0.003	176	365
B35 M60 - 4	6.666	3.451	350	36.425	0.003	162	328

The workability function is presented in the figures below, where the mixes with the constant sp/c for each figure. In Figures 3.4 and 3.5, the values for the experiment and the belonging workability function are plotted. The workability function for each plot will be slightly different due to different flow resistance ratios, as Table 3.3 describes.

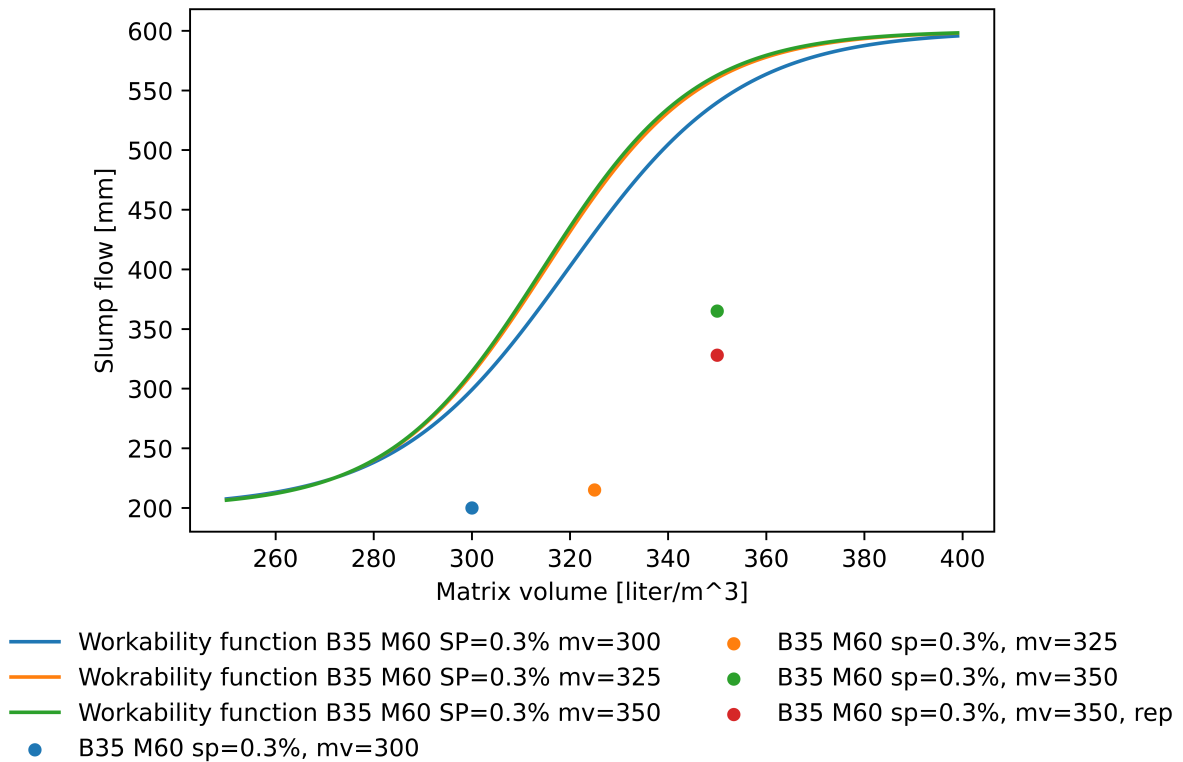


Figure 3.4: The observed values and the different workability function for the mixes with B35 M60 with $sp/c=0.3\%$.

The figure illustrates that the fit for the workability function is not very good. Figure 3.4 illustrates a significant deviation between the observed points and the belonging workability function.

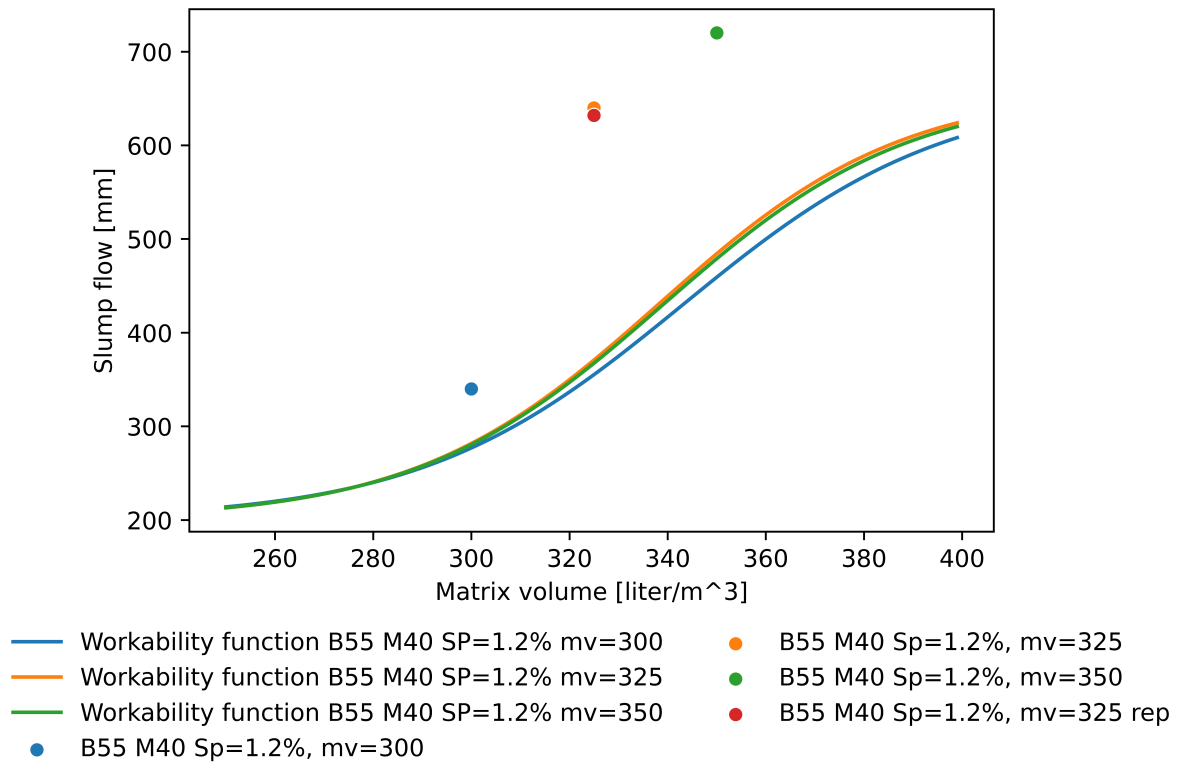


Figure 3.5: The observed values and the different workability function for the mixes, B55 M40 with $sp/c=1.2\%$.

Figure 3.5 illustrates that the fit of the workability function to the observed point is not very good. In Figure 3.5, the observed points are above the workability function, but in Figure 3.4, the observed values are below the workability function. Considering the differences in the workability function, there are three main changes, it is w/c , matrix quality, and sp/c between the experiments.

As illustrated by Figures 3.4 and 3.4, there is not easy to estimate the flow of the concrete. Figure 3.4 where the data from the lab is below the workability function, and Figure 3.5 where the data is higher than the workability function.

Chapter 4

Analysis

This section analyses the flow resistance ratio and the workability function. First, the flow resistance ratio is calculated with equation 2.13 and compared with the observed points. To adjust the coefficient for the flow resistance ratio, the coefficient for sp/c is changed. Second, the workability function is attempted to be improved. As illustrated by the models illustrated by the Figures in 3.1.2 and 3.2.2 differences in the fit of the workability function. To create a model better fitting for the porpoise, machine learning will be used to adjust the offset variable of the workability function to the best fit for the given variables. The offset will be trained against the variables in the data and checked against the data in the experiments performed for this master thesis. Also, there will be performed an analysis, to see if insecurities in the void space are affecting the workability function.

4.1 Analyzing the matrix

The analyses of the fit of equation 2.13 on the existing data and the results from the FlowCyl measurements performed.

4.1.1 Calculated flow resistance ratio data existing data

The Equation 2.13 takes in 9 coefficients, where the coefficients are presented in Table 4.1.

To use the equation to calculate the flow resistance ratio, the VSSA needs to be calculated. Calculation of VSSA is calculated on the bases of the values in [23] Table 2. The VSSA

is based on the filler used and the cement used described by Equation 2.14.

To compare the different values for the constant, presented in section 2.1.5, all values are compared with the data given in [5].

The constants created by Skare et al. [24] were calculated and simulated with the measured values of the FlowCyl. The average deviation between the calculation performed and the Skare et al. constants are 0.4098. In the specialization project of Sydtangen et al. [27], they tried to adjust the constant, which calculates the flow resistance, and it seems like during this study there where performed a mistake, so this function was revised again. See table for the revised function Table 4.1 but looked only at one variable and did not consider how the adjustment changed the other variables. The variable that where adjusted for was the amount of SP. The adjusted constants created by Sydtangen et al. had an error from the measured variables with above 0.5854 on average.

Table 4.1: Adjusted constants to equation 2.13 and average error

	k_1	k_2	k_3	k_4	k_5	k_6	k_7	k_8	k_9	Average error
Skare et al.	0.42	2.72	1.47	0.06	0.31	1.41	0.31	2.15	0.58	0.4098
Adamski and Grefstad	0.38	1.07	1.44	0.07	0.13	0.17	-0.1	1.6	0.226	0.2392
Adjusted values	0.42	1.07	1.44	60	0.13	0.17	-0.1	1.6	0.58	0.5854
Adjusted values 2.0	0.42	1.07	1.44	6.0	0.13	0.17	-0.1	1.6	0.58	0.0588

The average difference between the calculated flow resistance ratio and the measured flow resistance ratio is presented in Table 4.1. As the table illustrates, the best fit for the flow resistance ratio is the adjusted value 2.0. The variables used to calculate the flow resistance ratio and the calculated flow resistance ratio are presented in Appendix C.1. The Adjusted constants 2.0 with varying sp/c are presented in Figure 4.1:

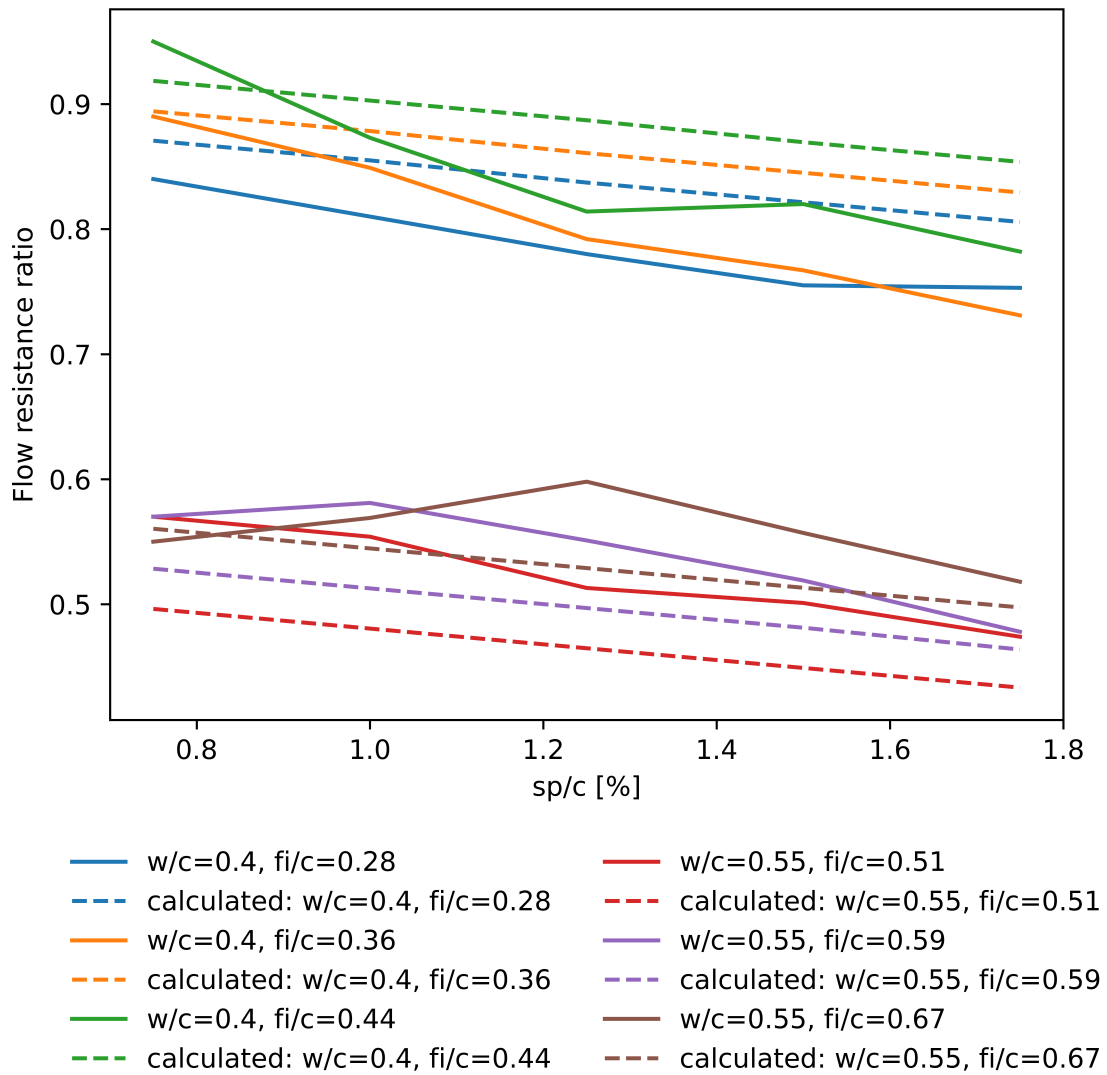


Figure 4.1: The flow resistance for the values from Skare with the calculated value for flow resistance with the coefficients for Adjusted constants 2.0 in Table 4.1.

Figure 4.1 illustrates the observed values with the continuous line and the calculated values with the dotted line. As illustrated by Figure 4.1, there is a connection between the flow resistance ratio and the increasing sp/c . When the sp/c increases, the flow resistance decreases. The model illustrates a decrease in the λ_Q of 0.06 when the sp/c increases with 1%. The variation in flow resistance ratio due to sp/c is bigger, which can vary between 0.087 and 0.20. So the model is not capturing the entire reduction in flow resistance ratio due to sp/c .

Calculated flow resistance in own experiments

The calculated flow resistance is presented in Appendix E.1. There is detailed information about the variables used to calculate the flow resistance and the calculated flow resistance ratios for each observation. A summary of the deviation between the observed values and the calculated values for the different constants is presented in Table 4.2

Table 4.2: Calculated average and the error which is the difference between the measured value and the calculated value. The flow resistance is calculated by using equations in section 2.1.5

Constants used	Calculated average flow resistance	Average error
Skare et al.	0.325	0.391
Adamski and Grefstad	0.521	0.195
Adjusted constants	0.181	0.534
Adjusted constants 2.0	0.707	0.086

The results from these experiments are in the same range as those in Table 4.1, with the Adjusted Constants 2.0 having the smallest error. This time the average error is 0.086, which is a good fit. The fit is illustrated in Figure 4.2:

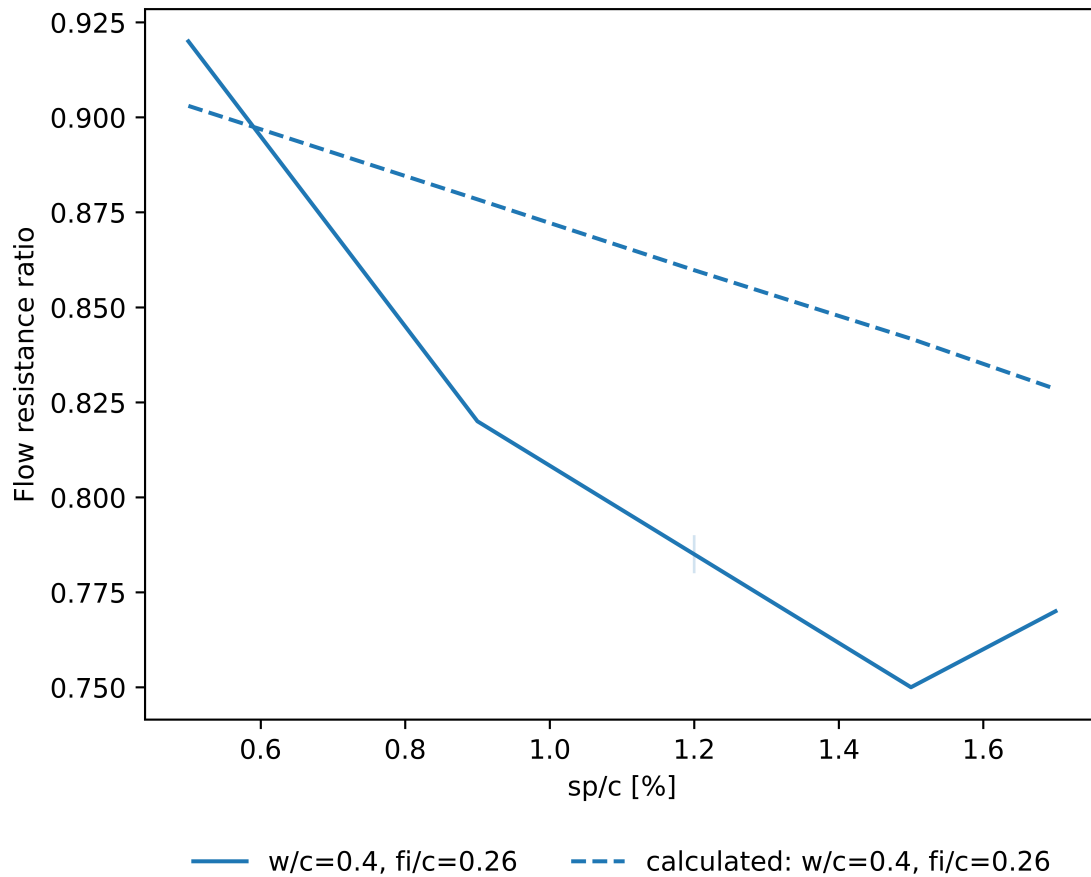


Figure 4.2: The flow resistance for the own experiments with the calculated value for flow resistance with the coefficients for Adjusted constants 2.0 in Table 4.2.

Figure 4.2 illustrates the observed values with the continuous line and the calculated values with the dotted line. Also, this figure illustrates that the sp/c has a larger effect on λ_Q compared with the observed observations.

4.2 Modification of the offset in the workability function

The target for modifying the workability function will be optimizing the offset function, which will be done by linear optimization as described in 2.4.1. The data used to perform the training of the linear optimization results is the data found in previous works, which are presented in section 2.2, and the results from the existing workability function are presented in section 3.1.2.

4.2.1 The training data

After using the training data and running the 20 000 iterations for each value. There are in total performed three different techniques to find the minimum error:

1. Free training with linear minimization
2. Linear minimization with a constant
3. Linear minimization with a checkpoint and constant

The errors are given in absolute value and are the difference between the observed points and the workability curve with the adjusted offset variable. It is important to keep in mind that the error is dependent on the number of variables, so the error between flow resistance ratios is not possible to compare.

Free training with linear minimization

The equations received from the machine learning are presented in Table 4.3. This is the standard linear minimization which is straightforward without any other changes. The figure for these values is presented in Appendix G.

Table 4.3: The equation found with machine learning without restrictions and the error which is the deviation between the workability curve and observed values.

λ_Q	Equations	Error
0.29	$1.6163 + 0.0032\lambda_Q$	29.52
0.33	$-0.1742 - 0.0021\lambda_Q$	40.53
0.38	$-0.9203 + 0.0009\lambda_Q$	98.16
0.45	$0.4782 - 0.0676\lambda_Q$	91.14
0.49	$-0.7633 + 0.0030\lambda_Q$	77.84
0.51	$0.5126 - 0.0009\lambda_Q$	20.22
0.55	$-1.9263 - 0.0768\lambda_Q$	31.78
0.67	$0.4385 - 0.0865\lambda_Q$	29.61
0.68	$-0.8847 - 0.0609\lambda_Q$	26.26

As presented by the table, the equations vary in the intercept and the slope, which is given by λ_Q . In other words, the effect of the flow resistance ratio varies. For the flow resistance ratio of 0.29, the equation is $1.6163 + 0.0032 \cdot \lambda_Q$, but on the other hand, we have the flow resistance ratio of 0.55, which have an equation $-1.9263 - 0.0768 \cdot \lambda_Q$. The

deviation between these two variables is significant, which illustrates the complexity of the offset variable.

Linear minimization with a constant interception

To reduce the complexity of all the different variations, the intercept is held constant at 1.5, the lowest value possible for the offset presented in section 2.1.2. This makes it easier to compare the values to each other since the only variation is the slope of the equation, and also easier to compare it with the original Equation 2.5. Table 4.4 has a constant value of 1.5.

Table 4.4: The equation found with linear optimization with restrictions of the intercept, and the error which is the deviation between the workability curve and observed values.

λ_Q	Equations	Error
0.29	$1.5 + 0.0035\lambda_Q$	35.28
0.33	$1.5 - 0.0073\lambda_Q$	21.12
0.38	$1.5 - 0.0066\lambda_Q$	95.92
0.45	$1.5 - 0.0601\lambda_Q$	49.07
0.49	$1.5 + 0.0043\lambda_Q$	76.54
0.51	$1.5 + 0.0068\lambda_Q$	19.34
0.55	$1.5 - 0.0031\lambda_Q$	31.34
0.67	$1.5 - 0.0056\lambda_Q$	44.18
0.68	$1.5 - 0.0001\lambda_Q$	25.30

The equation presented in Table 4.4 has a varying slope level. Three are positive, and 6 are negative. In theory, all the variables should be positive, and increasing λ_Q should give an increased offset, but these equations illustrates that this is not the case. The equations given in Table 4.4 are closer to the observed value for most of the flow resistances than Table 4.3. This is possible to see by that the error is smaller, but it is illustrated by figures in Appendix G.

Linear minimization with checkpoint and constant interception

To minimize the error and improve the equations further, it is used checkpoints which saves the best error found during the process of machine learning. The checkpoint gave the results given in Table 4.5:

Table 4.5: The equation found with machine learning with restricted interception and checkpoints and the error which is the deviation between the workability curve and observed values.

λ_Q	Equations	Error
0.29	$2.5714 - 0.0007\lambda_Q$	29.03
0.33	$1.5 + 0.0047\lambda_Q$	20.92
0.38	$1.5 - 0.0004\lambda_Q$	95.06
0.45	$1.5 + 0.0180\lambda_Q$	56.96
0.49	$1.5 - 0.0028\lambda_Q$	76.51
0.51	$1.5 + 0.0010\lambda_Q$	16.70
0.55	$1.5 + 0.0030\lambda_Q$	31.05
0.67	$1.5 - 0.0047\lambda_Q$	44.06
0.68	$1.5 - 0.0033\lambda_Q$	25.29

The method resulted in only small improvements of the error. The error was significantly reduced for the flow resistance of 0.29 and 0.51, but at the same time, the error had a significant increase for the flow resistances of 0.45.

A significant change is the flow resistance ratio which was tried to hold the intercept equal to 1.5 for $\lambda_Q = 0.29$, but it was not possible to perform within limits. Hence, the linear optimization changed the parameter for the intercept. For this reason, it is reasonable to believe that the value for interception for the flow resistance ratio of 0.29 in Tables 4.3 and 4.4 should have been higher. Four flow resistance ratios have a positive slope, where two of them are new compared with Table 4.4. The variables which changed the sign of the slope are the flow resistance ratio of 0.29, 0.33, 0.45, 0.49, and 0.51. 0.29 have increased the intercept of the equation significantly, so it is logical that the slope sign is changed, even though the fit could have been increased. 0.33 and 0.55 change from a negative slope to a positive sign. $\lambda_Q = 0.45$ has increased the error when using the checkpoint from 49.07 to 56.96, a significant increase in the error. The changes in the sign are likely to be due to this. 0.49 have a minor change in the error, but it also has a minor change in the slope, which is on 0.0071.

Due to the small improvement in using the more advanced method with checkpoints, it is better to use the easier method without checkpoints to work from. This is simply the process of working ahead.

General equation to fit all the flow resistance ratio

As illustrated above, there are large differences for the different values so it is hard to find one equation to fit all the different flow resistance ratios. There are performed two different equations for one common equation, one with free intercept and one with a decided overlap of 1.5.

Table 4.6: Using one equation, one for the free machine learning and one with restricted intercept with the belonging error.

λ_Q ratio	Free equation	Free equation error	Restricted equation	Restricted error
0.29	$0.2397 + 0.0028 \cdot \lambda_Q$	93.56	$1.5 - 0.0056 \cdot \lambda_Q$	82.77
0.33	$0.2397 + 0.0028 \cdot \lambda_Q$	86.86	$1.5 - 0.0056 \cdot \lambda_Q$	183.45
0.38	$0.2397 + 0.0028 \cdot \lambda_Q$	101.89	$1.5 - 0.0056 \cdot \lambda_Q$	102.86
0.45	$0.2397 + 0.0028 \cdot \lambda_Q$	158.11	$1.5 - 0.0056 \cdot \lambda_Q$	142.30
0.49	$0.2397 + 0.0028 \cdot \lambda_Q$	112.29	$1.5 - 0.0056 \cdot \lambda_Q$	96.40
0.51	$0.2397 + 0.0028 \cdot \lambda_Q$	33.54	$1.5 - 0.0056 \cdot \lambda_Q$	110.72
0.55	$0.2397 + 0.0028 \cdot \lambda_Q$	38.81	$1.5 - 0.0056 \cdot \lambda_Q$	116.00
0.67	$0.2397 + 0.0028 \cdot \lambda_Q$	54.49	$1.5 - 0.0056 \cdot \lambda_Q$	95.97
0.68	$0.2397 + 0.0028 \cdot \lambda_Q$	43.42	$1.5 - 0.0056 \cdot \lambda_Q$	26.58

The two equations which are common for all the observations are given in:

$$offset = 0.2397 + 0.0028 \cdot \lambda_Q \tag{4.1}$$

$$offset = 1.5 - 0.0056 \cdot \lambda_Q \tag{4.2}$$

With the one common equation, the error for each λ_Q should increase due to not having an individual best-fit function, as presented in the previous tables. The sum of the average errors for the free model is 722.98, and the restricted model is 956.07. The free model, which is Equation 4.1 gives a lower sum of the average error than the restricted model, which is Equation 4.2. So the fit for the free model is significantly better. For most of the flow resistance ratios, there is a large increase in the error for the restricted equation. The ones with a significant decrease are 0.29, 0.45, 0.49, and 0.68, but these values are not weighted up with the increase in the other flow resistance ratios. Due to this, the free equation is compared with the comparing data below.

4.2.2 Comparing data

Equation 4.1 is used to calculate the workability function for the mixtures in E.2. To see if it is possible to calculate a more precise workability function by using the equation presented in Table 4.6.

Table 4.7: Using the data from the experiments, the calculated error using the original offset from Equation 2.5 and the optimized equation with free machine learning from Equation 4.1 is presented.

Flow resistance	Error for the original offset	Error for the optimized offset
0.805	345.53	230.39
0.463	294.86	361.47
0.92	112.19	178.87
0.82	108.45	34.23
0.75	272.76	164.8
0.77	267.58	161.14

As illustrated by Table 4.7 and the figures in Appendix G.2, the fit is better for the equations of the matrix quality M40 but worse for the M60. It is difficult to have a linear function that adapts to both the higher and lower values for the matrix quality when at the same time containing values that make sense from the literature. The fit is increased for the flow resistance ratios, equal to 0.805, 0.82, 0.75, and 0.77. But the error increases for the other flow resistance ratios. In total, the error for the original offset variable is 1285.00, and for the optimized is 1012.63, which is a significant improvement of the error. This is a reduction of 21.8% in the error. The fit for some of the points with the M40 matrix quality is good, this is for the matrix volume of 300 in Figure 4.3 and the value for Figure 4.4 have a good fit. These two observations have SP-dosage of 1.2% and 0.9%, respectively.

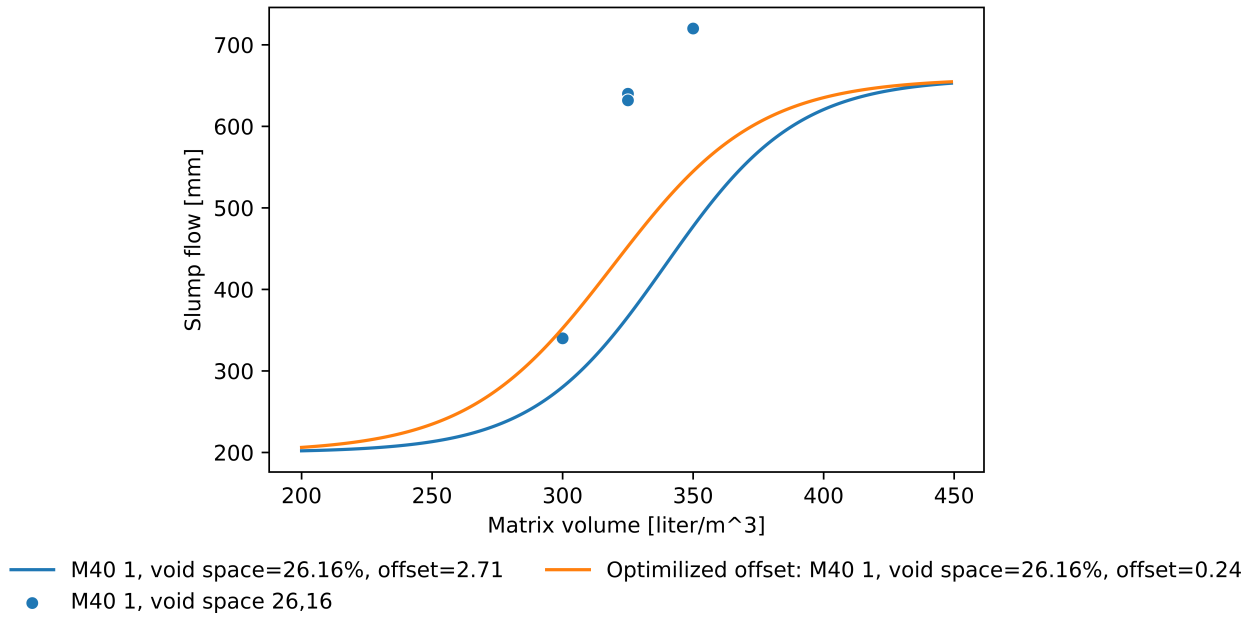


Figure 4.3: B55 M40 1, with void space 26.16%, $\lambda_Q = 0.805$, $sp/c = 1.2\%$ and offset is given by the legends. The same figure is illustrated in Appendix G and is named Figure G.13

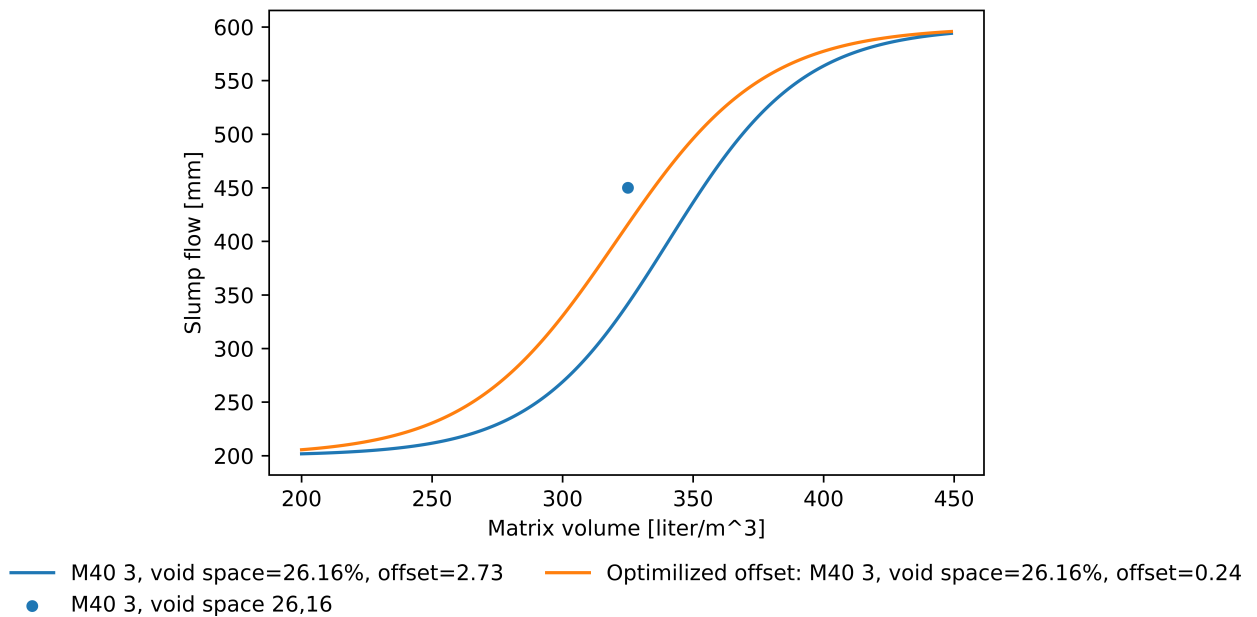


Figure 4.4: B55 M40 3, with void space 26.16%, $\lambda_Q = 0.$, $sp/c = 0.9\%$ and the offset is given by the legends. The same figure is illustrated in Appendix G and is named Figure G.13

4.3 Modifying the void space

As presented in section 2.1.6, the measured void space can vary by up to 7% depending on which measurement method is used to find the void space of the data used in the data

analysis, but also the void space in which is calculated in the experiments. Due to this effect, it is interesting to see if changing the void space of the analysis will reduce the error observed between the workability function and the observed variables. The void space is changed with 3.5% both up and down to see if this will increase the fit of the workability function since this value is in the middle of the average deviation for EN 1097-3 to the lowest height measuring error. The void space changes by adding or subtracting the change from the observed void space.

4.3.1 Increase the void space by 3.5%

By increasing the void space by 3.5%, the curve is shifted against the right side, illustrated by the figures in the Appendix H. Here there is plotted the existing workability function, with the optimized curve and a reference curve which is the original workability function without any changes.

Table 4.8: Using the data from the experiments with a 3.4% increase in void space, the calculated error using the original offset from equation 2.5 and the optimized equation with free machine learning from Table 4.6

Flow resistance ratio	Error for the original offset	Error for the optimized offset
0.805	500.02	398.98
0.463	94.32	223.68
0.92	38.65	93.16
0.82	198.37	136.20
0.75	415.32	321.45
0.77	404.45	313.07

The sum of the error for the standard equation of offset is 1600.65, at the same time, the standard error for the error of the optimized equation is 1378.26. As presented in Table 4.8, the error from the observed values has increased drastically from the error in Table 4.7 for the original offset and optimized offset. The sum of the average error has increased significantly for both the original offset and the optimized offset, but most for the initial offset. There is worth noting that the original equation for the offset is doing best for the M60 concrete, which has a flow resistance of 0.463 which is logical because this value had the lowest slump for the given matrix volumes. From the original offset equation, the error is reduced from 178.49 without 43.48 with the shift, which is a significant improvement. This is illustrated in Figure 4.5. At the same time, the table presents that the reduction

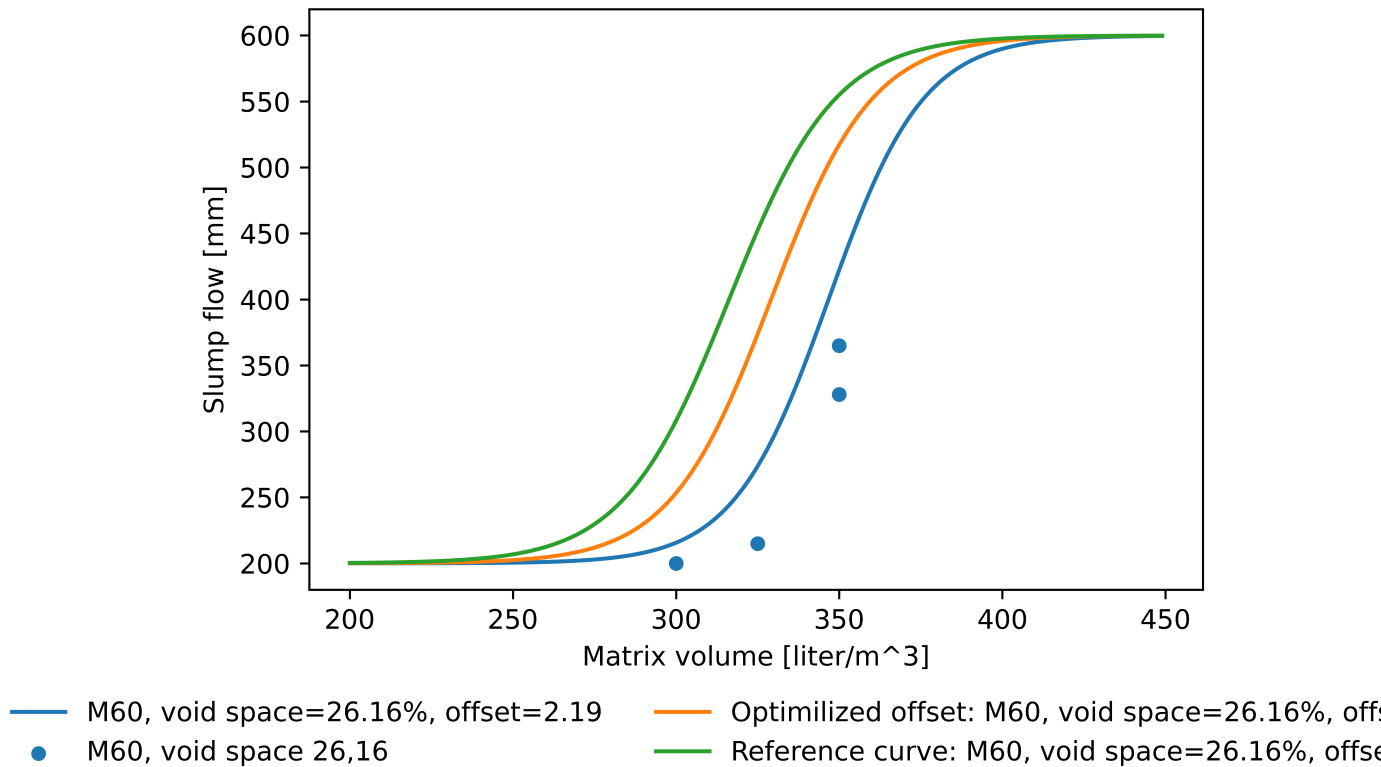


Figure 4.5: B35 M60 mixes from own experiments with $sp/c=0.3\%$ and average λ_Q . The figure is also illustrated in Appendix H.1 in Figure H.6

in error is only for 0.463 and 0.92 in flow resistance ratios. The rest of the flow resistance ratios have increased errors.

4.3.2 Reduce the void space by 3.5%

By reducing the void space by 3.5%, the curve is shifted against the left side. The errors are presented in Table 4.9.

Table 4.9: Using the data from the experiments with a 3.4% reduction in void space, the calculated error using the original offset from equation 2.5 and the optimized equation with free machine learning from Table 4.6

Flow resistance ratio	Error for the original offset	Error for the optimized offset
0.805	205.81	161.70
0.463	392.83	317.37
0.92	196.33	244.84
0.82	11.00	36.70
0.75	127.68	65.86
0.77	125.42	62.26

The sum of the average error for the original offset is 943.17, and for the optimized error, it is 875.70. There is essential to keep in mind that there are more variables of the B55 M40 than B35 M60, and since B55 M40 are above the workability function, reducing the void space is increasing the total error. Therefore, the total error cannot compare the increase in void space given in section 4.3.1 and the values presented in this section. It is possible to compare the error for each flow resistance ratio.

The error for the flow resistance ratio of 0.805, 0.82, 0.75, and 0.77 are reduced, and the values are also lower than those presented in Table 4.7 for the original offset. At the same time, the values for the flow resistance ratio of 0.463, 0.92, and 0.82 increased significantly. This, due to a shift to the left, increases the values for the given matrix volume for the workability curve is increasing, and therefore the error increases.

Chapter 5

Discussion

In this section, the findings and analyses from Chapter 3 and Chapter 4 are discussed. First, the calculation of the flow resistance ratio and the influence of solid content to cement content ratio (sp/c) on the calculated flow resistance are discussed. Next, the workability function is examined, including the conducted optimization test, as well as the limitations observed in the data and the utilized model. Finally, potential directions for future research are presented.

5.1 Calculating the flow resistance ratio

The Equation 2.13 has, as described earlier, been the object for multiple revisions, but the coefficients proposed have not been able to capture the deviations in the data which are used in this thesis. The constant for Adjusted constants 2.0 means that a 1% increase in sp/c reduces the flow resistance ratio by 0.06, which is illustrated by the calculated lines in Figures 4.1 and 4.1. sp/c have a smaller effect on the flow resistance ratio compared with the observed values, but the error is significantly improved from the previous coefficients. It is hard to increase the sp/c without reducing the fit of the model due to increasing sp/c will reduce the first value of λ_Q and, therefore, also reduce the fit, especially for the values for $w/c=0.55$ in Figure 4.1. The coefficients in Adjusted Values 2.0 create the best fit of the observed values for the data collected from Skare and the values from the experiments.

5.2 The workability function

An equation for the offset that only depends on one equation is hard to model by one variable. As illustrated in Appendix G.1, there is possible to find equations that fit well for the different, but it is hard to find one equation that fits all variables. This is due to imperfections in the concrete, in addition, the fluidity of the concrete is dependent on a large number of variables. In other words, modeling concrete is complicated, which reduces the chances of creating a workability function that fits observed values well with such a simple model.

5.2.1 The optimized workability function with machine learning

The optimized equation for the training data reduces the error, which is logical because each equation is optimized for the current data. The common optimized equation over all the training data significantly increases the error compared with the individually adapted equation. At the same time, it reduces the original offset, which has a sum of an average error of 1285, to 1012.63 for the optimized offset.

5.2.2 Modified the void space

Changing the void space will move the curve in one direction, like changing the offset. A reduction in the void space reduces the starting point of the slope of the workability curve. This gives a reduced error for the observations above the void space. An increase in the void space is delaying the start of the slope. This provides a reduction in the error for the observations that are below the workability curve. This means that a change in the void space can not be utilized to fit both the values over the workability curve and below the curve. This change is, therefore, not something that can give a conclusion on whether or not changing the void space is creating a better workability function.

5.3 Limitations

Limitations in the experiments and the methods used are presented in this section.

5.3.1 Data collected

Concrete is a unique material, and there is a high number of factors that affects the slump flow of the concrete. The data used in this master thesis have different sources, increasing the possibility that the methods or materials differ. The difference here can cause the results to change. Furthermore, these experiments contain numerous variables that are attempted to be controlled, although there is a possibility that some of these variables may not have been successfully controlled.

5.3.2 Coefficients for the flow resistance ratio

The coefficients for Adjusted values 2.0 are based on the values from Skare et al. [24] and from Adamski and Grefstad [1] and chosen to get the best fit to the observed values. sp/c is the only variable not based on these previous studies, but this one is changed to get the best possible fit using eye measurements.

5.3.3 Linear optimization of offset

Several limitations exist in the machine learning model used to perform the analysis. The results depended on the model's learning rate and that the intercept and slope of the offset are between -2 and 6. Another limitation of machine learning is the assumption that the offset variable is linear and dependent on flow resistance. These three assumptions increase the speed of the machine learning process but may also reduce how the offset variable captures the complexity of the model. In the case of the equation for $\lambda_Q = 0.29$ and 0.45 , where the machine learning hits local minima, which it did not manage to overcome. This is easy to see during the model's training since it does not continue minimizing the smallest error but falls back to more significant errors. This could also be the case for other equations, but it is difficult to observe when the errors are smaller. The same issue might also be the case for the one common offset equation, but it is harder to discover the error due to a high number of iterations.

The data should have more observations to get a more accurate variable for the offset. A higher number of observations would be able to isolate more of the randomness in the variables. The comparing data set should also be larger to remove randomness in these

variables.

5.3.4 Workability function

The workability function is a simulation of the slump flow of the concrete. To create the simulation, there are four input variables, matrix volume, void space, flow resistance ratio, and SP-dosage. There is illustrated in section 2.1.5 and later in section 3.1.1 and 3.2.1 that the matrix has a lot of inputs variables. It might there be a simplification to say that the flow properties depend only on these four inputs. But never the less, this simple function is not likely to be able to have a reasonable replication of the flow properties of such a complex material as concrete for all cases.

5.4 Further work

Possible research can be based on the list below, which are questions that have occurred during working on this thesis that has not been further investigated.

- Look at the offset being dependent on other variables. Or if it has a more advanced mathematical expression.
- Study a larger data set used in this master thesis should have been larger to get more general results.
- See that the experiments performed for this master thesis have a higher slump value than the workability curve allows. This has to be investigated whether or not the limit for n is correct or not.
- Equation to calculate the flow resistance ratio. It may be necessary to see other coefficients to get a more accurate calculation.
- Perform the workability function with machine learning techniques where all the variables can be optimized to fit the observed data, and the observed values are used to generate simulations of the data which can be trained.

Chapter 6

Conclusion

The purpose of this master's thesis was to investigate the impact of sp/c on the flow resistance ratio and improve the workability function. The illustration for the sp/c effect shows that the impact of sp/c on flow resistance is between 0.086 and 0.20. Meanwhile, the equation is not giving such high effects. The coefficient Adjusted values 2.0 are an improvement, which only has an average error of 0.0588 and 0.086 for the values from Skare and the experiments, respectively. There still needs more research to capture the impact of the sp/c variation and keep the error as low as possible.

The workability function with the optimized offset reduces the error compared with the original offset. The equations that are individually adapted to have a significant reduction in the offset illustrate that offset is a good equation to adjust the workability function to the observed values. The sum of the average error for each flow resistance ratio is reduced from 1285 for the original offset to 1012.63 for the optimized offset. This is an improvement of 21.8%. The error is still significant, so the fit of the offset is possible to improve. However, changes still have to be performed to get one general offset equation that replicates the observed values well.

References

- [1] Adrian Adamski and Andreas Erlien Grefstad. *Partikkel-Matriks modellering av fersk betong med hensyn til ønsket betongflyt*. Trondheim: NTNU, 2022.
- [2] *Årdal sandtak / NorStone*. URL: <https://www.norstone.no/no/ardal> (visited on 03/21/2023).
- [3] P. F. G. Banfill. “Additivity effects in the rheology of fresh concrete containing water-reducing admixtures”. In: *Construction and Building Materials* 25.6 (June 1, 2011), pp. 2955–2960. ISSN: 0950-0618. DOI: 10.1016/j.conbuildmat.2010.12.001. URL: <https://www.sciencedirect.com/science/article/pii/S0950061810006781> (visited on 10/31/2022).
- [4] Rolands Cepuritis. “Development of chruised sand for concrete production with micro-proportioning”. Doctoral theses. Trondheim: Norwegian University of Science and Technology, Feb. 2016.
- [5] Rolands Cepuritis et al. “Analysing limitations of the FlowCyl as a one-point viscometer test for cement paste”. In: *Construction and Building Materials* 218 (Sept. 10, 2019), pp. 333–340. ISSN: 0950-0618. DOI: 10.1016/j.conbuildmat.2019.05.127. URL: <https://www.sciencedirect.com/science/article/pii/S0950061819312966> (visited on 10/24/2022).
- [6] *ChatGPT*. URL: <https://chat.openai.com> (visited on 06/07/2023).
- [7] Colin R. Gagg. “Cement and concrete as an engineering material: An historic appraisal and case study analysis”. In: *Engineering Failure Analysis* 40 (May 1, 2014), pp. 114–140. ISSN: 1350-6307. DOI: 10.1016/j.engfailanal.2014.02.004. URL: <https://www.sciencedirect.com/science/article/pii/S1350630714000387> (visited on 06/03/2023).
- [8] Prashant Gupta. *Regularization in Machine Learning*. Medium. Nov. 16, 2017. URL: <https://towardsdatascience.com/regularization-in-machine-learning-76441ddcf99a> (visited on 05/31/2023).
- [9] Lars Egil Helseth. *viskositet*. In: *Store norske leksikon*. Jan. 25, 2023. URL: <https://snl.no/viskositet> (visited on 03/29/2023).

- [10] Sagar Imambi, Kolla Bhanu Prakash, and G. R. Kanagachidambaresan. “PyTorch”. In: *Programming with TensorFlow: Solution for Edge Computing Applications*. Ed. by Kolla Bhanu Prakash and G. R. Kanagachidambaresan. EAI/Springer Innovations in Communication and Computing. Cham: Springer International Publishing, 2021, pp. 87–104. ISBN: 978-3-030-57077-4. DOI: 10.1007/978-3-030-57077-4_10. URL: https://doi.org/10.1007/978-3-030-57077-4_10 (visited on 05/22/2023).
- [11] S. Jacobsen et al. *Concrete Technology*. 5th ed. Trondheim: NTNU, 2023.
- [12] M. JOHN Lever. “15 - Mass transport processes in artificial organs”. In: *Biomaterials, Artificial Organs and Tissue Engineering*. Ed. by Larry L. Hench and Julian R. Jones. Woodhead Publishing Series in Biomaterials. Woodhead Publishing, Jan. 1, 2005, pp. 153–166. ISBN: 978-1-85573-737-2. DOI: 10.1533/9781845690861.3.153. URL: <https://www.sciencedirect.com/science/article/pii/B9781855737372500158> (visited on 03/17/2023).
- [13] Mapei. “Produktdatablad SX-23”. In: (). (Visited on 03/17/2023).
- [14] Tor Arne Martius-Hammer, Ola Skjølsvold, and Rolands Cepuritis. *Rheology of concrete with crushed aggregate*. Trondheim: SINTEF, Oct. 11, 2021. (Visited on 02/03/2023).
- [15] Tor Arne Martius-Hammer, Ola Skjølsvold, and Rolands Cepuritis. *Rheology of mortars with manufactured sand*. Trondheim: SINTEF, Oct. 29, 2020. (Visited on 02/03/2023).
- [16] P. C. F. Møller, A. Fall, and D. Bonn. “Origin of apparent viscosity in yield stress fluids below yielding”. In: *Europhysics Letters* 87.3 (Aug. 2009), p. 38004. ISSN: 0295-5075. DOI: 10.1209/0295-5075/87/38004. URL: <https://dx.doi.org/10.1209/0295-5075/87/38004> (visited on 10/24/2022).
- [17] Ernst Mørtzell. *Modellering av delmaterialenes betydning for betongens konsistens*. Trondheim: Department of Structural Engineering, NTNU, Feb. 1996.
- [18] *Produktdatablad Standardsement FA*. Oct. 2022. URL: https://www.norcem.no/sites/default/files/2022-09/Produktdatablad_StandardFA_ensidig_oktober2022.pdf (visited on 03/16/2023).

- [19] Gopinath Rebala, Ajay Ravi, and Sanjay Churiwala. “Machine Learning Definition and Basics”. In: *An Introduction to Machine Learning*. Ed. by Gopinath Rebala, Ajay Ravi, and Sanjay Churiwala. Cham: Springer International Publishing, 2019, pp. 1–17. ISBN: 978-3-030-15729-6. DOI: 10.1007/978-3-030-15729-6_1. URL: https://doi.org/10.1007/978-3-030-15729-6_1 (visited on 05/31/2023).
- [20] Oxford Reference. *Bingham fluid*. Oxford Reference. DOI: 10.1093/oi/authority.20110803095506560. URL: <https://> (visited on 02/13/2023).
- [21] N. Roussel. “A Theoretical Frame to Study Stability of Fresh Concrete”. In: *Materials and Structures* 39.1 (Jan. 1, 2006), pp. 81–91. ISSN: 1871-6873. DOI: 10.1617/s11527-005-9036-1. URL: <https://doi.org/10.1617/s11527-005-9036-1> (visited on 10/25/2022).
- [22] N. Roussel, C. Stefani, and R. Leroy. “From mini-cone test to Abrams cone test: measurement of cement-based materials yield stress using slump tests”. In: *Cement and Concrete Research* 35.5 (May 1, 2005), pp. 817–822. ISSN: 0008-8846. DOI: 10.1016/j.cemconres.2004.07.032. URL: <https://www.sciencedirect.com/science/article/pii/S0008884604003333> (visited on 09/23/2022).
- [23] Elisabeth Leite Skare. “Prediction of rheological properties of filler modified cement paste from constituent properties, flow measurements and modelling”. Doctoral theses. Trondheim: Norwegian University of Science and Technology, Feb. 2022.
- [24] Elisabeth Leite Skare et al. “Application of an Improved Empirical Model for Rheology Prediction of Cement Pastes Modified with Filler from Manufactured Sand”. In: *Nordic Concrete Research* 65.2 (Dec. 1, 2021), pp. 1–18. DOI: 10.2478/ncr-2021-0005. URL: <https://sciendo.com/it/article/10.2478/ncr-2021-0005> (visited on 11/16/2022).
- [25] Norsk Standard. *NS-EN 12350-2:2019*. 2019. URL: <https://www.standard.no/no/Nettbutikk/produktkatalogen/Produktpresentasjon/?ProductID=1106511> (visited on 02/07/2023).
- [26] Norsk Standard. *NS-EN 12350-7:2019*. 2019. URL: <https://www.standard.no/no/Nettbutikk/produktkatalogen/Produktpresentasjon/?ProductID=1106516> (visited on 02/08/2023).

- [27] Magnus Sydtangen, Stefan Jacobsen, and Rolands Cepuritis. *The effect of superplasticizer on flow resistance in concrete*. Dec. 19, 2022. (Visited on 12/19/2022).
- [28] Zhijun Tan, Susan A. Bernal, and John L. Provis. “Reproducible mini-slump test procedure for measuring the yield stress of cementitious pastes”. In: *Materials and Structures* 50.6 (Oct. 19, 2017), p. 235. ISSN: 1871-6873. DOI: 10.1617/s11527-017-1103-x. URL: <https://doi.org/10.1617/s11527-017-1103-x> (visited on 05/25/2023).
- [29] G. H. Tattersall and P. F. G. Banfill. *The Rheology of Fresh Concrete*. Pitman Publishing, 1983.
- [30] Velde. Velde. Apr. 2023. URL: <https://www.veldeas.no/fvd> (visited on 04/13/2023).
- [31] Olafur Haraldsson Wallevik and Jon Elvar Wallevik. “Rheology as a tool in concrete science: The use of rheographs and workability boxes”. In: *Cement and Concrete Research. Conferences Special: Cement Hydration Kinetics and Modeling, Quebec City, 2009 & CONMOD10, Lausanne, 2010* 41.12 (Dec. 1, 2011), pp. 1279–1288. ISSN: 0008-8846. DOI: 10.1016/j.cemconres.2011.01.009. URL: <https://www.sciencedirect.com/science/article/pii/S000888461100010X> (visited on 10/24/2022).

Appendix

Chapter A

Manual of laboratory tests

A.1 FlowCyl

The mixing procedure is presented in table A.1:

Table A.1: FlowCyl mixing procedure

Mixing step no.	Time line		Action
	Total time [min]	Length of action [min]	
Pre mixing			
1	-3	2	All of the dry materials are mixed in a standard Hobart mixer with a "flat blade" at speed nr 1 (Low speed, 140 rpm)
2	-1	1	Water and admixtures are mixed in the yellow container with a rotating movement.
Wet mixing			
3	0	0.5	The dry materials are poured over in the yellow container. A funnel and a spatula are used to reduce the chance of spilled materials.
4	2.5	2	Start mixing the dry and the wet materials with a "drill mixer" with speed nr 2 (high speed = 1850 rpm).
5	4.5	2	Rest
6	6.5	2	Mixing at speed nr 1 (low speed = 400 rpm).
7	8.5	1.5	The pasta are filled over in a 3 liter plastic container.
8	12-15	-	Rheometer and FlowCyl test are performed, and thereafter the mini slump test.

Chapter B

Aggregate size distribution

The aggregate size distribution are presented in the data sheet from Norstone:

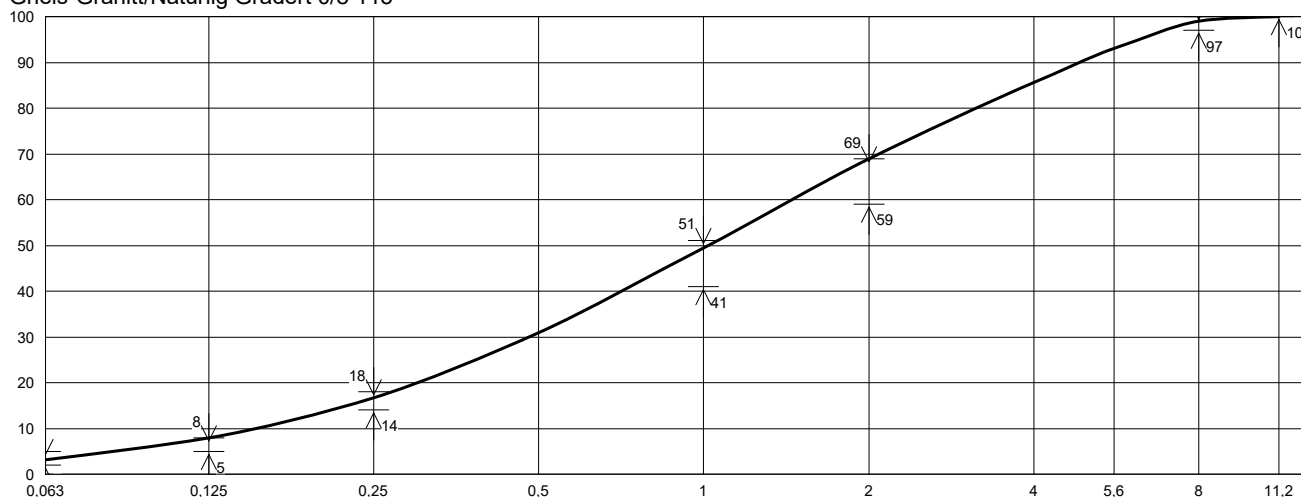
Dato: 21.02.2022 **Kunde:** NTNU
Materiale: 0/8 mm System 2+ **Havn:**
Varenr: 101718-115 **Båt:**
Følgeseddel nr:

Test NS-EN 933-1 Laboratorium NorStone Årdal
 Identifikasjon av prøven 0/8 mm 115 Operatør Sæbø
 Dato mottatt/uttatt 21.02.2022 Dato utført 21.02.2022
 Metod (angi) Vasking og sikting Standard NS-EN 12620
 Tørrsikting Sertifikat: 1111-CPD-0007
 Produksjonssted NorStone Årdal

Total tørr masse $M_1 =$ 483,7 g
 Tørr masse etter vasking $M_2 =$ g
 Tørr masse av Finstoff fjernet ved vasking $M_1 - M_2 =$ g
 Vanninnhold (%) NS 1097-5 =

Sikteåpning (mm)	Masse tilbakehold (g)	Prosentandel (%)	Akkumulert Prosentandel (%)	Gjennomgang		
				Idealkurve (%)	Min (%)	Max (%)
11,2			100,0	100,0	100,0	
8	4,5	0,9	99,1	99,0	97,0	100,0
5,6	29,4	6,1	93,0	90,0		
4	35,9	7,4	85,5	80,0		
2	80,0	16,6	69,0	64,0	59,0	69,0
1	94,7	19,6	49,4	46,0	41,0	51,0
0,5	89,3	18,5	30,9	28,0		
0,25	68,6	14,2	16,7	16,0	14,0	18,0
0,125	42,0	8,7	8,0	7,0	5,0	8,0
0,063	23,1	4,8	3,2	3,0	2,0	5,0
< 0,063	15,5	3,2				
Sum	483,0	100,0	0,1	< 1% Prosentats materiale tapt		

Gneis-Granitt/Naturlig Gradert 0/8 115



21.02.2022

Dato

Gro Sæbø

Signatur

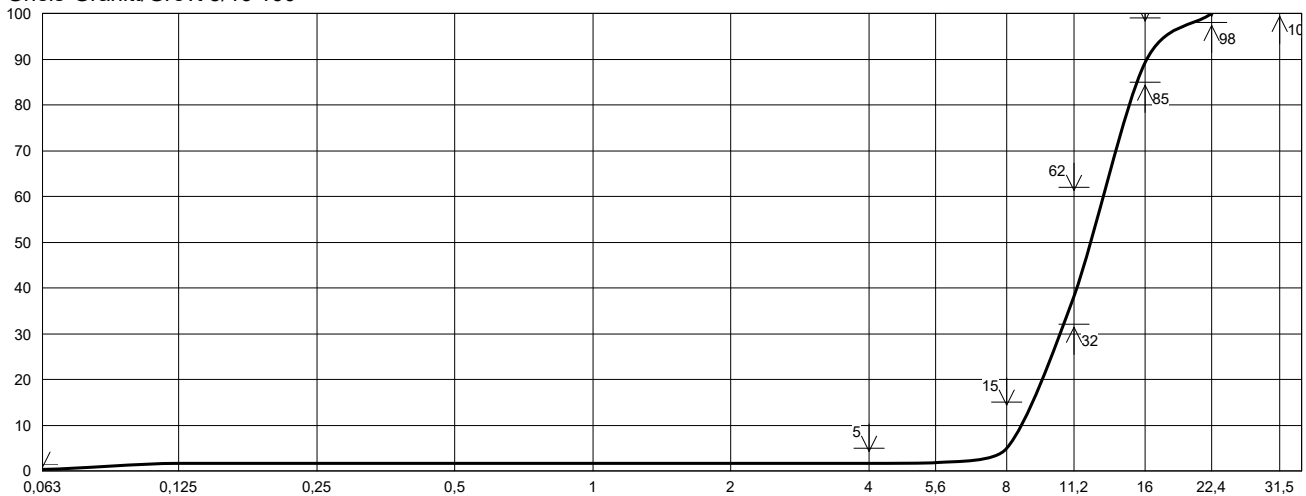
Dato: 21.02.2022 **Kunde:** NTNU
Materiale: 8/16 mm System 2+ **Havn:**
Varenr: 101711-160 **Båt:**
Følgeseddel nr:

Test NS-EN 933-1 Laboratorium NorStone Årdal
 Identifikasjon av prøven 8/16 mm 160 Operatør Sæbø
 Dato mottatt/uttatt 18.02.2022 Dato utført 18.02.2022
 Metod (angi) Vasking og sikting Standard NS-EN 12620
 Tørrsikting Sertifikat: 1111-CPD-0007
 Produksjonssted NorStone Årdal

Total tørr masse $M_1 =$ 1988,9 g
 Tørr masse etter vasking $M_2 =$ g
 Tørr masse av Finstoff fjernet ved vasking $M_1 - M_2 =$ g
 Vanninnhold (%) NS 1097-5 = 1,4

Sikteåpning (mm)	Masse tilbakehold (g)	Prosentandel (%)	Akkumulert Prosentandel (%)	Gjennomgang		
				Idealkurve (%)	Min (%)	Max (%)
31,5					100,0	
22,4			100,0	100,0	98,0	100,0
16	212,6	10,7	89,3	90,8	85,0	99,0
11,2	1015,9	51,1	38,2	46,9	32,0	62,0
8	662,0	33,3	4,9	8,9		15,0
5,6	61,6	3,1	1,8	2,7		
4	3,4	0,2	1,6	2,3		5,0
2	0,0	0,0	1,6	2,0		
1	0,0	0,0	1,6	1,7		
0,5	0,0	0,0	1,6	1,3		
0,25	0,0	0,0	1,6	0,9		
0,125	0,0	0,0	1,6	0,6		
0,063	27,2	1,4	0,3	0,4		1,5
< 0,063	5,4	0,3				
Sum	1988,1	100,0	0,0	< 1% Prosentats materiale tapt		

Gneis-Granitt/Grovt 8/16 160



21.02.2022	Gro Sæbø
Dato	Signatur

Chapter C

Matrix calculations

Table C.1: The variables used to calculate the flow resistance ratio are presented in this table. The calculated flow resistance ratios are presented to the right in the table.

mix	w/c	sp/c	fi/c	Solid volume fraction	Flow resistance ratio	Calculated VSSA	Skare constants	Adamski&Grefstad constants	Adjusted constants	Adjusted constants 2.0
A-11	0.4	0.75	0.36	0.531	0.89	375	0.502	0.678	0.473	0.894
A-12	0.4	0.75	0.44	0.545	0.95	375	0.504	0.677	0.497	0.919
A-13	0.55	0.75	0.51	0.477	0.57	321	0.066	0.255	0.075	0.496
A-14	0.55	0.75	0.59	0.49	0.57	322	0.077	0.261	0.107	0.528
A-15	0.55	0.75	0.67	0.502	0.55	323	0.089	0.268	0.139	0.56
A-16	0.7	0.75	0.68	0.444	0.35	285	-0.249	-0.079	-0.22	0.201
A-17	0.7	0.75	0.76	0.456	0.38	287	-0.232	-0.069	-0.184	0.238
A-18	0.7	0.75	0.82	0.464	0.49	288	-0.219	-0.061	-0.157	0.264
B-1	0.4	1	0.28	0.516	0.81	375	0.503	0.679	0.293	0.855
B-2	0.4	1	0.36	0.531	0.849	375	0.502	0.677	0.317	0.878
B-3	0.4	1	0.44	0.545	0.873	375	0.503	0.677	0.341	0.903
B-13	0.55	1	0.51	0.477	0.554	321	0.066	0.254	-0.081	0.481
B-14	0.55	1	0.59	0.49	0.581	322	0.077	0.261	-0.049	0.513

Table C.1 continued from previous page

mix	w/c	sp/c	fi/c	Solid volume fraction	Flow resistance ratio	Calculated VSSA	Skare constants	Adamski&Grefstad constants	Adjusted constants	Adjusted constants 2.0
B-15	0.55	1	0.67	0.502	0.569	323	0.089	0.268	-0.017	0.545
B-4	0.4	1.25	0.28	0.515	0.78	375	0.503	0.677	0.135	0.837
B-5	0.4	1.25	0.36	0.53	0.792	374	0.501	0.676	0.159	0.861
B-6	0.4	1.25	0.44	0.545	0.814	375	0.503	0.677	0.185	0.887
B-16	0.55	1.25	0.51	0.477	0.513	321	0.066	0.254	-0.237	0.465
B-17	0.55	1.25	0.59	0.49	0.551	322	0.076	0.261	-0.205	0.497
B-18	0.55	1.25	0.67	0.502	0.598	323	0.089	0.267	-0.173	0.529
B-7	0.4	1.5	0.28	0.515	0.755	375	0.502	0.677	-0.021	0.821
B-8	0.4	1.5	0.36	0.53	0.767	374	0.501	0.675	0.003	0.845
B-9	0.4	1.5	0.44	0.544	0.82	374	0.503	0.675	0.027	0.869
B-19	0.55	1.5	0.51	0.477	0.501	321	0.065	0.254	-0.393	0.449
B-20	0.55	1.5	0.59	0.49	0.519	322	0.076	0.26	-0.361	0.481
B-21	0.55	1.5	0.67	0.502	0.557	323	0.088	0.267	-0.329	0.513
B-10	0.4	1.75	0.28	0.515	0.753	375	0.502	0.676	-0.177	0.806
B-11	0.4	1.75	0.36	0.53	0.731	374	0.501	0.675	-0.154	0.829
B-12	0.4	1.75	0.44	0.544	0.782	374	0.502	0.674	-0.129	0.854
B-22	0.55	1.75	0.51	0.477	0.474	321	0.065	0.253	-0.549	0.433
B-23	0.55	1.75	0.59	0.489	0.478	321	0.076	0.259	-0.519	0.464
B-24	0.55	1.75	0.67	0.502	0.518	323	0.088	0.267	-0.485	0.497
A-1	0.4	0.75	0.28	0.516	0.89	393	0.577	0.746	0.523	0.944
A-2	0.4	0.75	0.36	0.531	0.92	397	0.594	0.761	0.564	0.986
A-3	0.4	0.75	0.44	0.545	0.96	401	0.612	0.775	0.606	1.027
A-4	0.55	0.75	0.51	0.477	0.58	346	0.171	0.35	0.18	0.601

Table C.1 continued from previous page

mix	w/c	sp/c	fi/c	Solid volume fraction	Flow resistance ratio	Calculated VSSA	Skare constants	Adamski&Grefstad constants	Adjusted constants	Adjusted constants 2.0
A-5	0.55	0.75	0.59	0.49	0.59	350	0.195	0.368	0.226	0.647
A-6	0.55	0.75	0.67	0.502	0.65	354	0.22	0.386	0.27	0.691
A-7	0.7	0.75	0.68	0.444	0.39	313	-0.132	0.026	-0.103	0.318
A-8	0.7	0.75	0.76	0.456	0.41	317	-0.104	0.047	-0.055	0.366
A-9	0.7	0.75	0.82	0.464	0.43	320	-0.083	0.062	-0.021	0.4
A-19	0.4	0.75	0.28	0.516	0.93	416	0.675	0.834	0.621	1.042
A-20	0.4	0.75	0.36	0.531	0.99	426	0.715	0.871	0.686	1.107
A-21	0.4	0.75	0.44	0.545	1	435	0.756	0.906	0.75	1.171
A-22	0.55	0.75	0.51	0.477	0.72	379	0.311	0.476	0.319	0.74
A-23	0.55	0.75	0.59	0.49	0.77	388	0.353	0.511	0.383	0.804
A-24	0.55	0.75	0.57	0.502	0.83	398	0.351	0.531	0.401	0.823
A-25	0.7	0.75	0.68	0.444	0.52	350	0.023	0.167	0.052	0.473
A-26	0.7	0.75	0.76	0.456	0.58	358	0.066	0.201	0.115	0.536
A-27	0.7	0.75	0.82	0.464	0.6	363	0.098	0.225	0.16	0.581

Chapter D

Concrete from data set

Table D.1: The table is the data from other reports. The void space which are calculated are marked with a star (*).

Mix	Silica		Water	Aggregate	Matrix		Flow	Matrix	Void
	Cement	fume			volume	Slump			
3200K2	365.3	0	196	1917	365	660	0.29	Feiring M60 1	27.19*
3200K1	374.9	0	202	1893.2	375	660	0.29	Feiring M60 1	27.19*
3200K4	337	0	182	1984.6	345	500	0.29	Feiring M60 1	27.19*
3200K5	326.7	0	175	2016.1	335	350	0.29	Feiring M60 1	27.19*
3200K3REF	350.1	0	189	1953.2	355	610	0.29	Feiring M60 1	27.19*
4700K3REF	432.4	18	178	1871.3	355	450	0.45	Feiring M40 1	29.4*
4700K2	450.8	20.1	186	1826.3	385	540	0.45	Feiring M40 1	29.4*
4700K1	462	20.5	191	1799.3	395	580	0.45	Feiring M40 1	29.4*
4700K6	476.7	18	195	1780	400	600	0.45	Feiring M40 1	29.4*
4700K5	488.5	19	201	1748.2	405	685	0.45	Feiring M40 1	29.4*
A22	452.5	19	192.9	1667.2	385	640	0.68	Velde M40	28.9*
A23	436.9	17	185.9	1700.3	375	660	0.68	Velde M40	28.9*
A24	424.7	17.1	181	1725.9	365	600	0.68	Velde M40	28.9*
A25	416.6	17	174.9	1747.2	355	570	0.68	Velde M40	28.9*
A26	394.8	16.9	166.5	1788.7	345	460	0.68	Velde M40	28.9*
A27	378.6	15.9	161.2	1818.2	335	470	0.68	Velde M40	28.9*
A12	350.5	0	188.8	1791.5	370	730	0.49	Velde M60	27.38*

Table D.1: The table is the data from other reports. The void space which are calculated are marked with a star (*).

Mix	Silica			Aggregate	Matrix		Flow	Matrix	Void
	Cement	fume	Water		volume	Slump			
A13	339.7	0	180.9	1713.3	360	710	0.49	0.0135	27.38*
A14	328.7	0	176.4	1843.7	350	635	0.49	0.0137	27.38*
A14	325.7	0	173.7	1855.8	350	640	0.49	0.0135	27.38*
A15	315.7	0	167.2	1881.1	340	470	0.49	0.0136	27.38*
A16	300.5	0	160.4	2155.3	330	300	0.49	0.0136	27.38*
A17	295	0	153.1	1948	320	270	0.49	0.0133	27.38*
Årdal open 1	432.5	0	233.5	1407	473	0	0	0.0125	0
Årdal open 2	450.8	0	243.4	1253.7	493	0	0	0.0124	0
Årdal open 3	469	0	253.3	1300	513	0	0	0.0126	0
Årdal open 4	487.3	0	253.3	1247	533	0	0	0.0125	0
Årdal open 5	505.6	0	273	1193.5	553	0	0	0.0125	0
Lørenskog open 1	479.1	0	258.7	1352	524	0	0	0.0125	0
Lørenskog open 2	497.4	0	268.6	1295	544	0	0	0.0125	0
Lørenskog open 3	515.7	0	278.5	1238.2	564	0	0	0.0124	0
Lørenskog open 4	534	0	288.3	1181.4	584	0	0	0.0125	0
Lørenskog open 5	552.2	0	298.2	1125	604	0	0	0.0125	0
Lørenskog VSI open 1	469	0	253.3	1383.1	513	0	0	0.0126	0

Table D.1: The table is the data from other reports. The void space which are calculated are marked with a star (*).

Mix	Silica		Water	Aggregate	Matrix volume	Slump flow	Flow resistance ratio	sp/b	Matrix quality	Void space
	Cement	fume								
Lørenskog VSI open 2	487.4	0	263.2	1326	533	0	0	0.0125		0
Lørenskog VSI open 3	505.6	0	273	1270	553	0	0	0.0125		0
Lørenskog VSI open 4	523.9	0	292.8	1213	573	0	0	0.0124		0
Lørenskog VSI open 5	542.2	0	243.9	1156	593	0	0	0.0103		0
Velde open 1	451.7	0	243.9	1326	494	0	0	0.0124		0
Velde open 2	470	0	253.8	1273	514	0	0	0.0126		0
Velde open 3	488.2	0	263.7	1221	534	0	0	0.0125		0
Velde open 4	506.5	0	273.5	1169	554	0	0	0.0124		0
Velde open 5	524.8	0	283.4	1116	574	0	0	0.0126		0
Årdal dense 1	366.6	0	198	1599	401	0	0	0.0125		0
Årdal dense 2	394.1	0	212.8	1519.2	431	0	0	0.0124		0
Årdal dense 3	407.8	0	220.2	1479	446	0	0	0.0125		0
Årdal dense 4	421.5	0	227.6	1439	461	0	0	0.0126		0
Årdal dense 5	448.9	0	242.4	1359	491	0	0	0.0125		0
Lørenskog dense 1	402.3	0	217.2	1590	440	0	0	0.0124		0
Lørenskog dense 2	429.7	0	232.1	1505	470	0	0	0.0126		0
Lørenskog dense 3	457.2	0	246.9	1420	500	0	0	0.0125		0

Table D.1: The table is the data from other reports. The void space which are calculated are marked with a star (*).

Mix	Silica			Aggregate	Matrix		Flow		Matrix	Void
	Cement	fume	Water		volume	Slump	resistance ratio	sp/b		
Lørenskog dense 4	484.6	0	261.7	1334.8	530	0	0	0.0126		0
Lørenskog VSI dense 1	391.3	0	211.3	1624.5	428	0	0	0.0125		0
Lørenskog VSI dense 2	418.8	0	226.1	1539	458	0	0	0.0124		0
Lørenskog VSI dense 3	432.5	0	233.5	1497	473	0	0	0.0125		0
Lørenskog VSI dense 4	446.2	0	240.9	1454	488	0	0	0.0126		0
Lørenskog VSI dense 5	473.6	0	255.8	1369	518	0	0	0.0125		0
Velde dense 1	371.2	0	200.5	1556	406	0	0	0.0124		0
Velde dense 2	389.5	0	210.3	1504	426	0	0	0.0126		0
Velde dense 3	407.8	0	220.2	1452	446	0	0	0.0125		0
Velde dense 4	426.1	0	230.1	1399	466	0	0	0.0124		0
Velde dense 5	444.4	0	240	1347	486	0	0	0.0126		0
Test 1	327.9	0	177.1	1989.6	330	200	0.4264	0.007	Feiring M60 2	0
Test 2	370.6	0	200.1	1882.3	365	533	0.4264	0.007	Feiring M60 2	0
Test 3	372.2	0	201	1878.4	365	595	0.4264	0.007	Feiring M60 2	0
Test 4	355.3	0	191.9	1920.7	345	580	0.4264	0.007	Feiring M60 2	0
Test 5	355.3	0	192	1920.7	345	200	0.4264	0.005	Feiring M60 2	0
Test 6	458.5	0	183.4	1845.1	370	530	0.6351	0.011	Feiring M40 2	0

Table D.1: The table is the data from other reports. The void space which are calculated are marked with a star (*).

Mix	Silica		Water	Aggregate	Matrix		Flow	sp/b	Matrix	Void
	Cement	fume			volume	Slump				
Test 7	454.8	0	181.9	1795.3	370	520	0.6351	0.011	Feiring M40 2	0
Rheology 1	219.7	0.0	120.8	0	330	385	0.55	0.0273	M60 SCC	31.4*
Rheology 2	349.5	0.0	192.2	0	350	480	0.55	0.0273	M60 SCC	34*
Rheology 3	652.8	0.0	261.1	0	360	410	0.67	0.0375	M40 1	34*
Rheology 4	634.6	0.0	253.9	0	350	355	0.67	0.0375	M40 1	31.4*
Rheology 5	320.9	0.0	176.5	0	330	410	0.55	0.0273	M60 SCC	29.76*
Rheology 6	340.3	0.0	187.2	0	350	500	0.55	0.0273	M60 SCC	30.99*
Rheology 7	652.8	0.0	261.1	0	360	390	0.67	0.0375	M40 1	30.99*
Rheology 8	616.5	0.0	246.6	0	340	350	0.67	0.0375	M40 1	29.76*
Rheology 9	670.9	0.0	268.4	0	370	435	0.67	0.0375	M40 1	30.99*
Rheology 10	634.6	0.0	253.9	0	350	355	0.67	0.0375	M40 1	29.76*
Rheology 11	689.0	0.0	275.6	0	380	435	0.67	0.0375	M40 1	30.99*
Rheology 12	652.8	0.0	261.1	0	360	425	0.67	0.0375	M40 1	29.76*
Rheology 13	707.2	0.0	282.9	0	390	505	0.67	0.0375	M40 1	30.99*
Rheology 14	670.9	0.0	268.4	0	370	425	0.67	0.0375	M40 1	29.76*
Rheology 20	351.8	14.7	193.5	0	360	670	0.33	0.0291	M60 1	30.99*
Rheology 21	342.0	14.3	188.1	0	350	645	0.33	0.0291	M60 1	30.99*

Table D.1: The table is the data from other reports. The void space which are calculated are marked with a star (*).

Mix	Silica		Water	Aggregate	Matrix		Flow	Matrix	Void
	Cement	fume			volume	Slump			
Rheology 22	332.3	13.8	182.7	0	340	620	0.33	M60 1	30.99*
Rheology 23	322.5	13.4	177.4	0	330	540	0.33	M60 1	30.99*
Rheology 24	312.7	13.0	172.0	0	320	445	0.33	M60 1	30.99*
Rheology 25	687.1	28.6	274.9	0	380	665	0.51	M40 2	29.76*
Rheology 26	669.1	27.9	267.6	0	370	640	0.51	M40 2	29.76*
Rheology 27	651.0	27.1	260.4	0	360	630	0.51	M40 2	29.76*
Rheology 28	632.9	26.4	253.2	0	350	555	0.51	M40 2	29.76*
Rheology 29	614.8	25.6	245.9	0	340	500	0.51	M40 2	29.76*
Rheology 30	687.1	28.6	274.9	0	380	655	0.51	M40 2	29.76*
Rheology 31	669.1	27.9	267.6	0	370	655	0.51	M40 2	29.76*
Rheology 32	651.0	27.1	260.4	0	360	650	0.51	M40 2	29.76*
Rheology 33	632.9	26.4	253.2	0	350	615	0.51	M40 2	29.76*
Rheology 34	614.8	25.6	245.9	0	340	520	0.51	M40 2	29.76*
Rheology 35	338.5	14.1	186.2	0	370	645	0.38	M60 2	30.99*
Rheology 36	329.3	13.7	181.1	0	360	565	0.38	M60 2	30.99*
Rheology 37	320.2	13.3	176.1	0	350	490	0.38	M60 2	30.99*
Rheology 38	311.0	13.0	171.1	0	340	690	0.38	M60 2	30.99*

Table D.1: The table is the data from other reports. The void space which are calculated are marked with a star (*).

Mix	Cement	Silica fume	Water	Aggregate	Matrix volume	Slump flow	Flow resistance ratio	sp/b	Matrix quality	Void space
Rheology 39	301.9	12.6	166.0	0	330	450	0.38	0.0273	M60 2	30.99*

Chapter E

The mixes and results from the experiments

E.1 Matrix mixes and calculations

Table E.1: The flow resistance mix and calculated flow resistance values.

mix	w/c	sp/c	fi/c	Solid volume fraction	Flow resistance ratio	Calculated VSSA	Skare constants	Adamski&Grefstad constants	Adjusted constants	Skare constants 2.0	Adjusted constants 2.0
B55 M40-1	0.4	1.2	0.30	0.525	0.85	378	0.525	0.694	0.205	16.699	0.879
B55 M40-2	0.4	1.2	0.27	0.521	0.79	378	0.513	0.688	0.186	16.456	0.860
B55 M40-3	0.4	1.2	0.22	0.515	0.8	378	0.500	0.682	0.165	16.176	0.839
B55 M40-4	0.4	1.2	0.27	0.521	0.78	378	0.513	0.688	0.186	16.456	0.860
B55 M40-5	0.4	0.5	0.27	0.522	0.92	379	0.510	0.688	0.622	16.460	0.903
B55 M40-6	0.4	0.9	0.27	0.521	0.82	378	0.512	0.688	0.373	16.458	0.878
B55 M40-7	0.4	1.5	0.27	0.520	0.75	378	0.515	0.689	-0.001	16.462	0.842
B55 M40-8	0.4	1.7	0.27	0.519	0.77	378	0.515	0.688	-0.126	16.426	0.828
B35 M60-1	0.6	0.3	0.39	0.470	0.52	301	-0.156	0.081	0.151	2.341	0.320
B35 M60-2	0.6	0.3	0.34	0.476	0.44	305	-0.185	0.077	0.132	2.273	0.301
B35 M60-3	0.6	0.3	0.30	0.460	0.43	299	-0.189	0.062	0.100	2.165	0.269

E.1.1 Pictures for the slump flow of the matrix



Figure E.1: Matrix for B35 M60 MV300 sp/c=0.3%



Figure E.2: Matrix for B35 M60 MV325 sp/c=0.3%



Figure E.3: Matrix for B35 M60 MV350 sp/c=0.3%

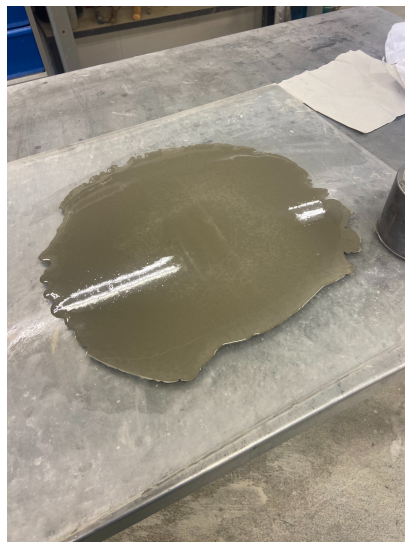


Figure E.4: Matrix for B55 M40 MV300 sp/c=1.2%

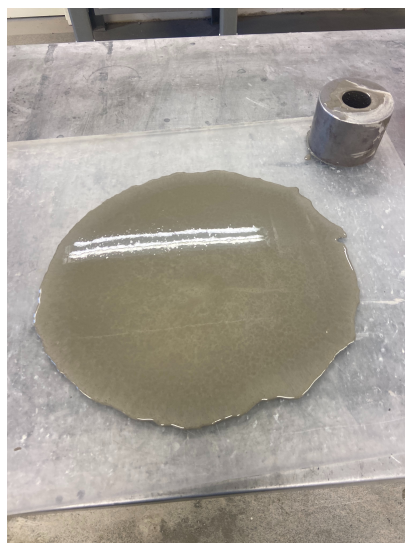


Figure E.5: Matrix for B55 M40 MV325 sp/c=1.2%



Figure E.6: Matrix for B55 M40 MV350 sp/c=1.2%



Figure E.7: Matrix for B55 M40 MV325 sp/c=0.5%

Pictures of the matrix of B55 M40 MV325 sp/c=0.9% was forgotten to perform.

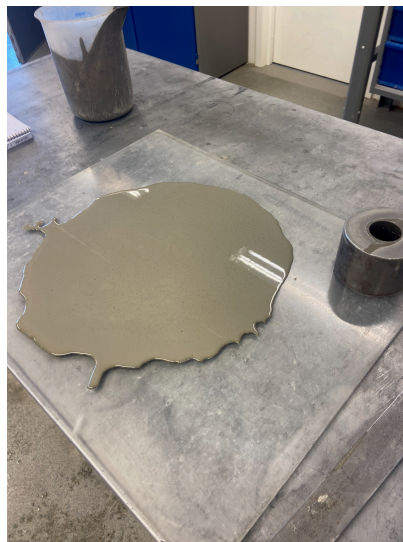


Figure E.8: Matrix for B55 M40 MV325 sp/c=1.5%

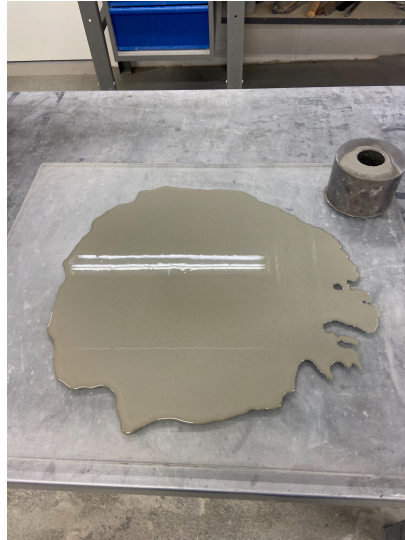


Figure E.9: Matrix for B55 M40 MV325 sp/c=1.7%



Figure E.10: Matrix for B35 M60 MV325 sp/c=0.3%

Pictures of the matrix of B55 M40 MV325 sp/c=1.2% was forgotten to perform.



Figure E.11: Matrix for B55 M40 MV325 sp/c=1.7%

E.2 Concrete mixes

The composition of the concrete recipient performed in the laboratory for this master thesis is presented in table E.2.

Table E.2: The concrete recipe with slump flow

Concrete mixes	Strength class	Durability class	Matrix volume	w/c	sp/c	sand/stone	Slump flow
B55 M40 - 300 - 1.2	B55	M40	300	0.4	1.2%	60/40	340
B55 M40 - 325 - 1.2	B55	M40	325	0.4	1.2%	60/40	640
B55 M40 - 350 - 1.2	B55	M40	350	0.4	1.2%	60/40	720
B55 M40 - 325- 1.2 (2)	B55	M40	325	0.4	1.2%	60/40	632
B55 M40 - 325 - 0.5	B55	M40	325	0.4	0.5%	60/40	210
B55 M40 - 325 - 0.9	B55	M40	325	0.4	0.9%	60/40	450
B55 M40 - 325 1.5	B55	M40	325	0.4	1.5%	60/40	690
B55 M40 - 325 - 1.75	B55	M40	325	0.4	1.75%	60/40	678
B35 M60 - 300 - 0.3	B35	M60	300	0.6	0.3%	60/40	200
B35 M60 - 325 - 0.3	B35	M60	325	0.6	0.3%	60/40	215
B35 M60 - 350 - 0.3	B35	M60	350	0.6	0.3%	60/40	365
B35 M60 - 350 - 0.3 (2)	B35	M60	350	0.6	0.3%	60/40	328

E.3 Pictures of the slump flow of the concrete mixes



Figure E.12: B35 M60 MV300 sp/c=0.3%



Figure E.13: B35 M60 MV325 sp/c=0.3%

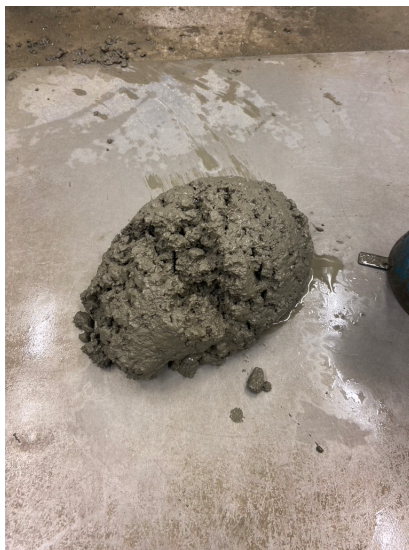


Figure E.14: B35 M60 MV350 sp/c=0.3%



Figure E.15: B55 MV300 sp/c=1.2%



Figure E.16: B55 M40 MV325 sp/c=1.2%



Figure E.17: B55 M40 MV350 sp/c=1.2%



Figure E.18: B55 M40 MV325 sp/c=0.5%



Figure E.19: B55 M40 MV325 sp/c=0.9%



Figure E.20: B55 M40 MV325 sp/c=1.5%



Figure E.21: B55 M40 MV325 sp/c=1.7%



Figure E.22: B35 M60 MV350 sp/c=0.3% repetition



Figure E.23: B55 M40 MV325 sp/c=1.2% repetition

Chapter F

Workability function with original offset

The plots calculated from the analysed data are presented here:

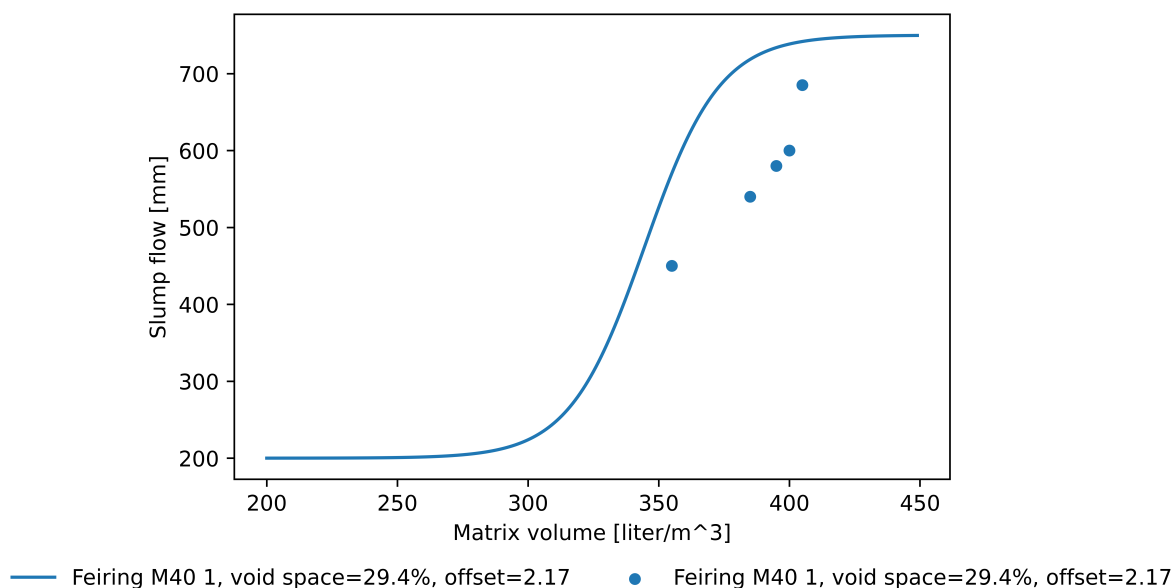
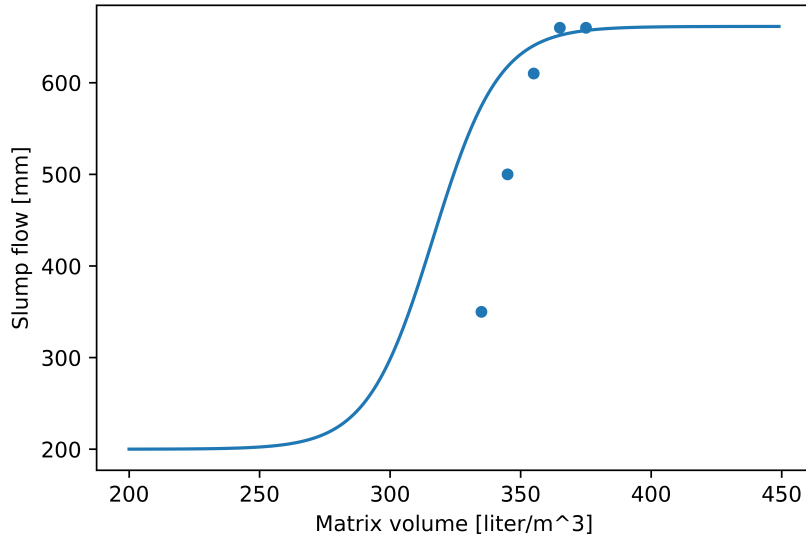
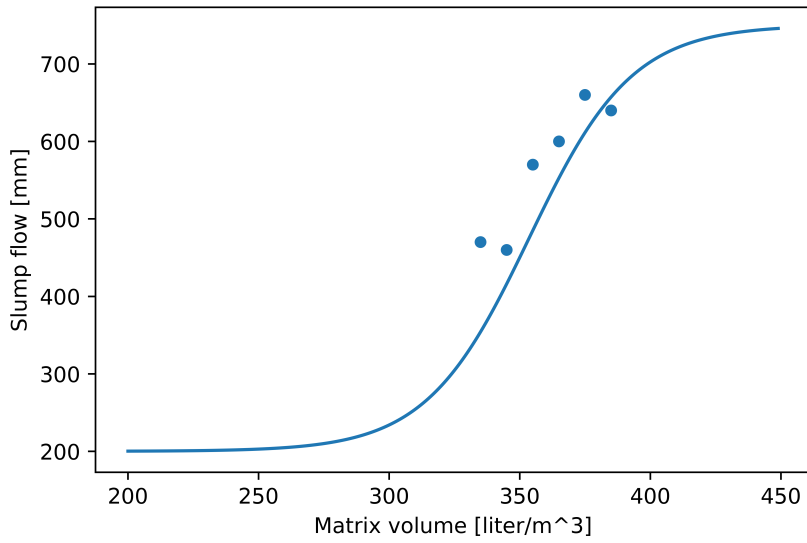


Figure F.1: Feiring M40 from [1] have $\lambda_Q = 0.45$, $H = 29.4\%$, $sp/c = 1.94\%$, and $offset = 2.23$.



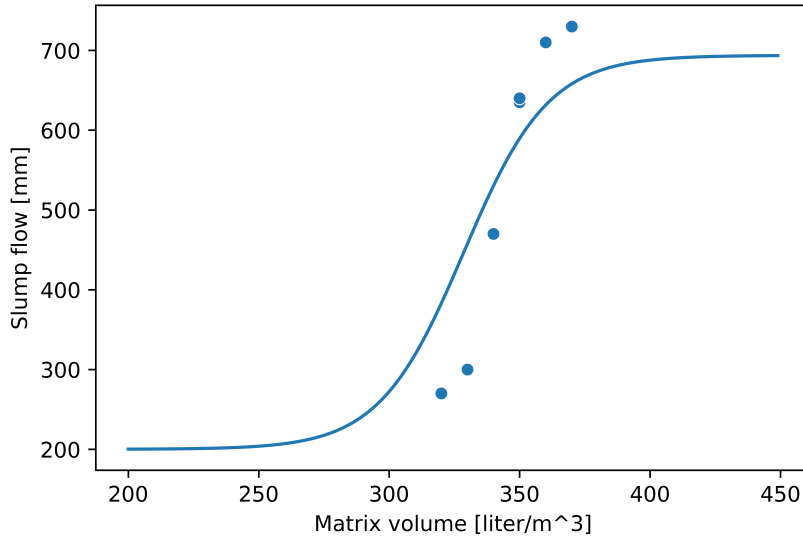
— Feiring M60 1, void space=27.19%, offset=1.94 • Feiring M60 1, void space=27.19%, offset=1.94

Figure F.2: Feiring M60 from [1] have $\lambda_Q = 0.29$, $H = 27.19\%$, $sp/c = 1.22\%$, and $offset = 1.94$.



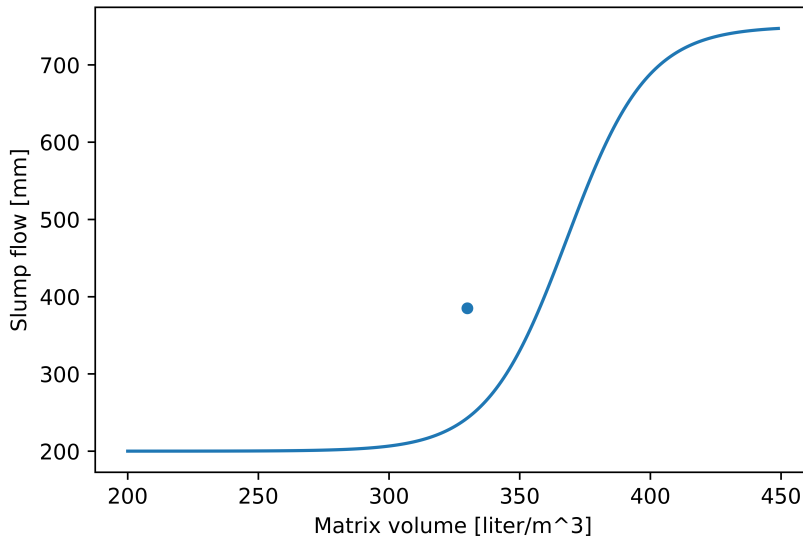
— Velde M40, void space=28.9%, offset=2.52 • Velde M40, void space=28.9%, offset=2.52

Figure F.3: Velde M40 from [1] have $\lambda_Q = 0.68$, $H = 28.9\%$, $sp/c = 1.65\%$, and $offset = 2.52$.



— Velde M60, void space=27.38%, offset=2.23 • Velde M60, void space=27.38%, offset=2.23

Figure F.4: Velde M60 from [1] have $\lambda_Q = 0.49$, $H = 27.38\%$, $sp/c = 1.35\%$, and $offset = 2.23$.



— M60 SCC, void space=31.4%, offset=2.33 • M60 SCC, void space=31.4%, offset=2.33

Figure F.5: M60 SCC mix from the Sintef Rheology report have $\lambda_Q = 0.55$, $H = 31.4\%$, $sp/c = 2.72\%$, and $offset = 2.33$.

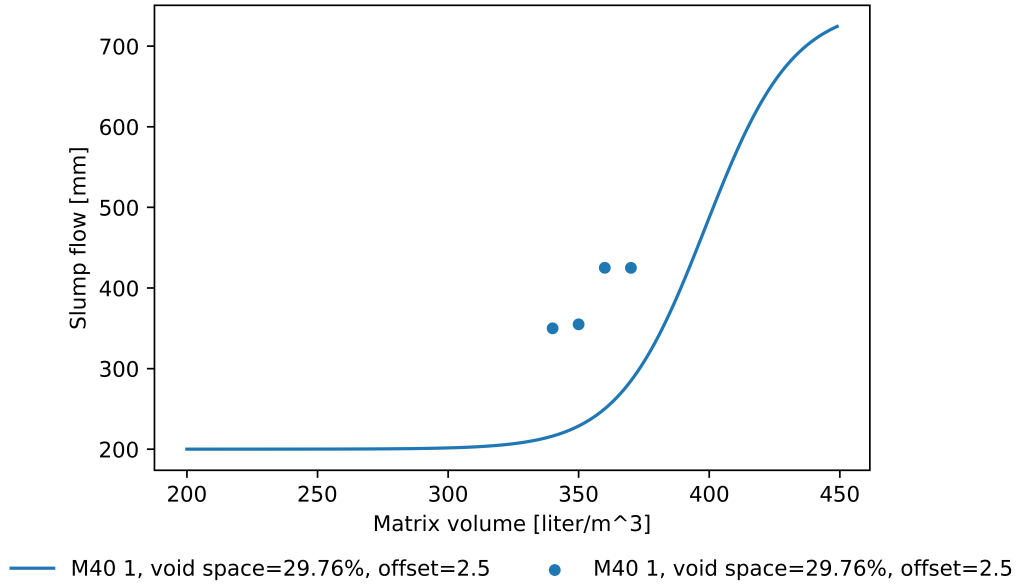


Figure F.6: The first M40 mix from the Sintef Rheology report have $\lambda_Q = 0.67$, $H = 31.4\%$, $sp/c = 3.75\%$, and $offset = 2.5$.

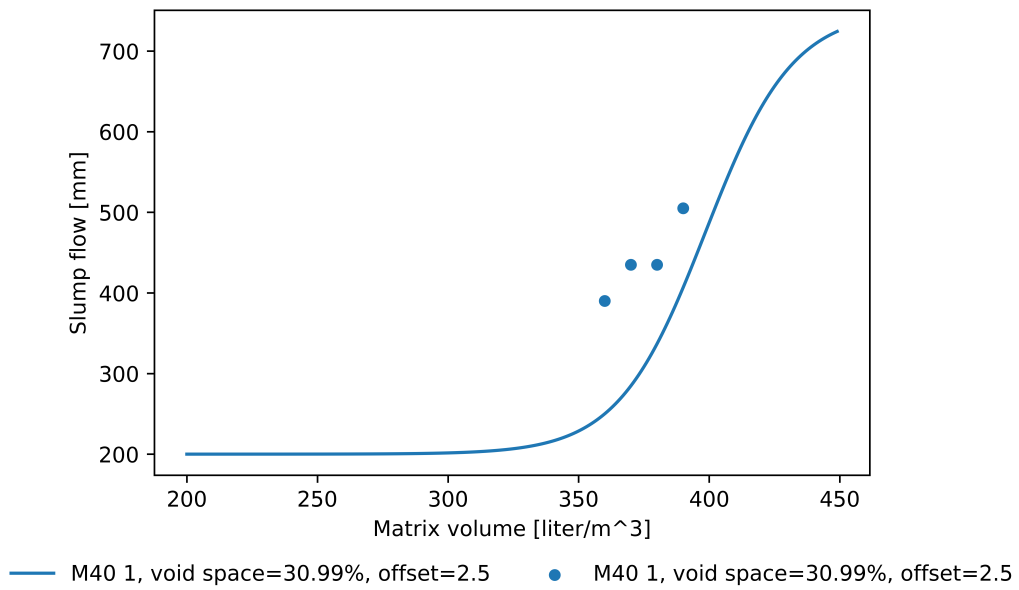


Figure F.7: The first M40 mix from the Sintef Rheology report have $\lambda_Q = 0.67$, $H = 31.4\%$, $sp/c = 3.75\%$, and $offset = 2.5$.

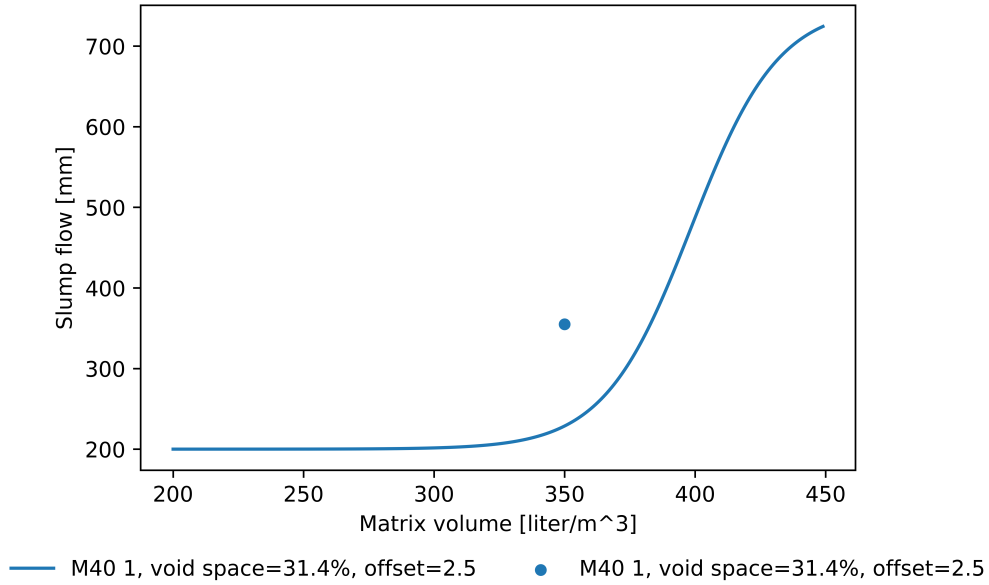


Figure F.8: The first M40 mix from the Sintef Rheology report have $\lambda_Q = 0.67$, $H = 31.4\%$, $sp/c = 3.75\%$, and $offset = 2.5$.

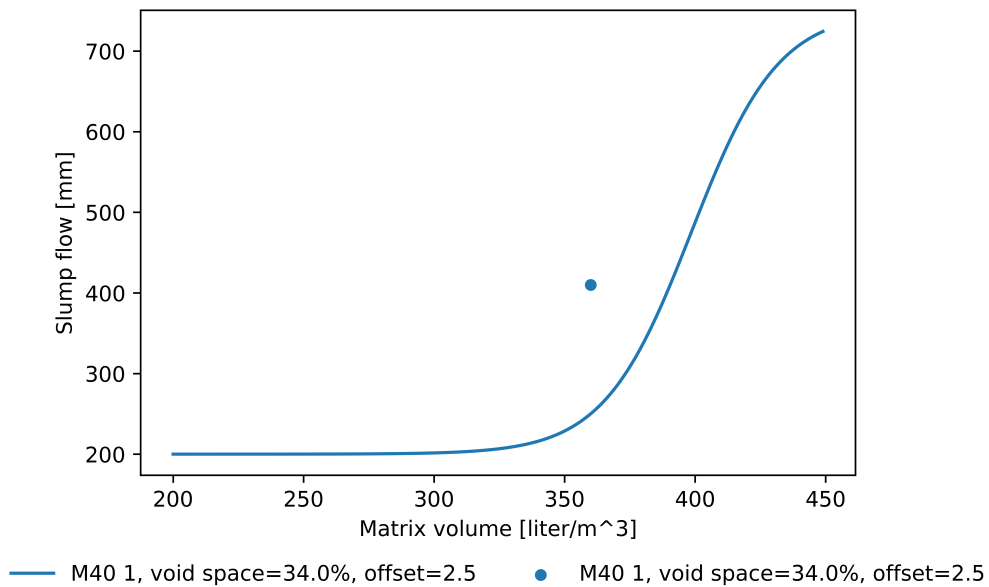


Figure F.9: The first M40 mix from the Sintef Rheology report have $\lambda_Q = 0.67$, $H = 31.4\%$, $sp/c = 3.75\%$, and $offset = 2.5$.

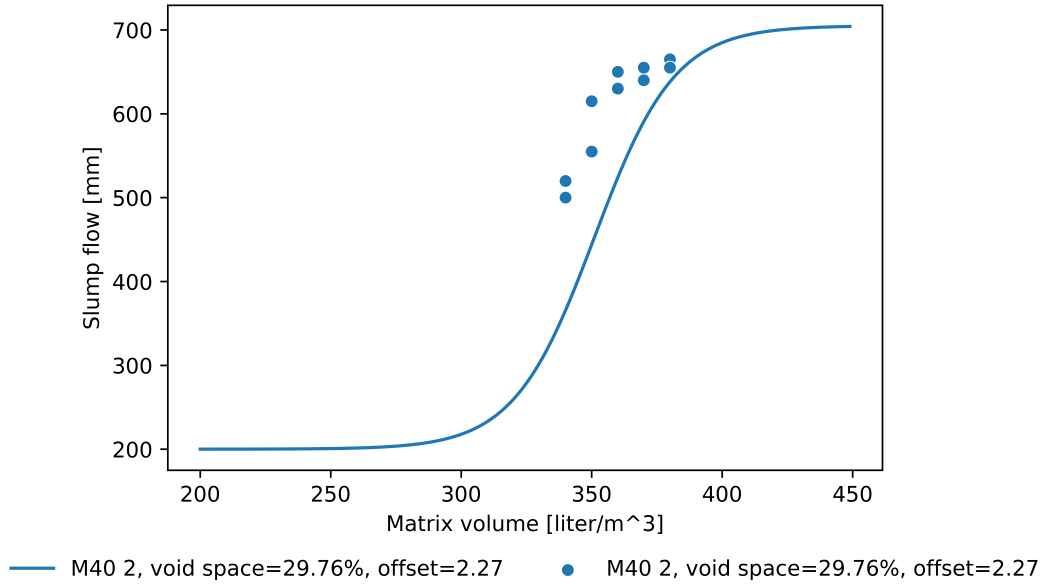


Figure F.10: The second M40 mix from the Sintef Rheology report have $\lambda_Q = 0.51$, $H = 29.76\%$, $sp/c = 3.38\%$, and $offset = 2.27$.

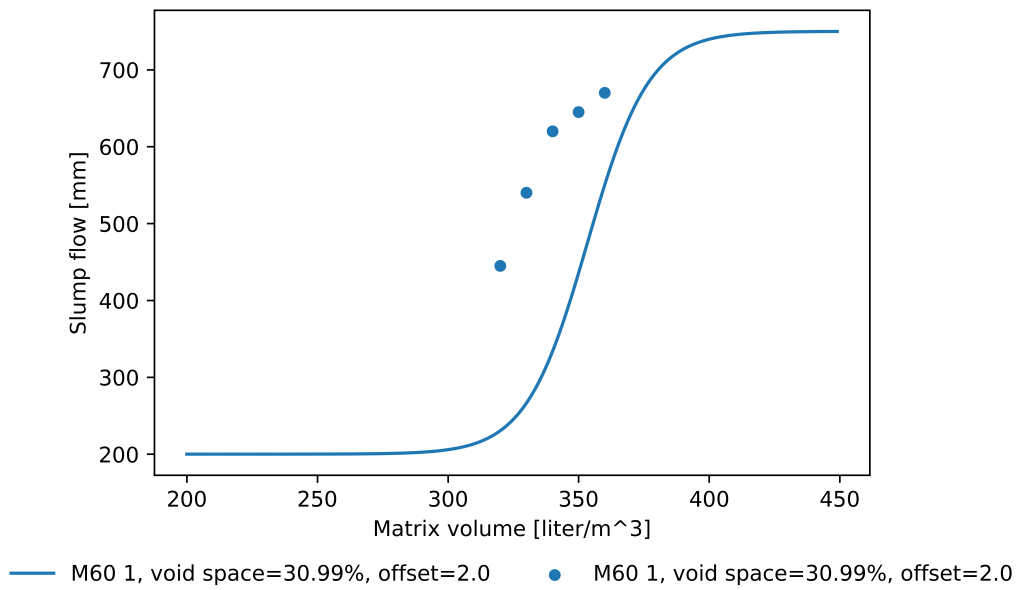


Figure F.11: The first M60 mix from the Sintef Rheology report have $\lambda_Q = 0.33$, $H = 30.99\%$, $sp/c = 2.90\%$, and $offset = 2.0$.

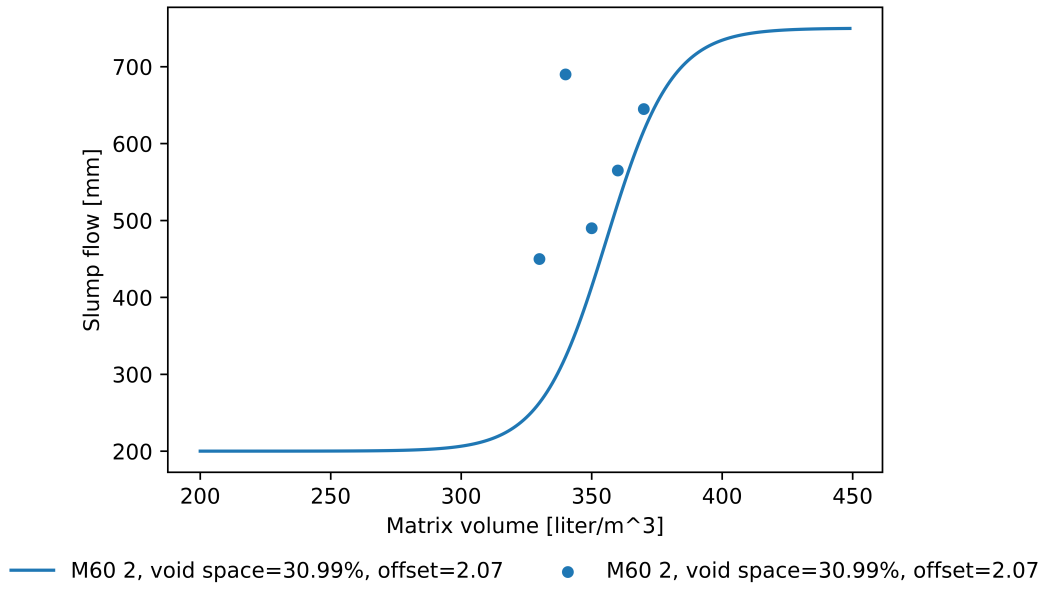


Figure F.12: The second M60 mix from the Sintef Rheology report have $\lambda_Q = 0.38$, $H = 30.99\%$, $sp/c = 2.73\%$, and $offset = 2.07$.

Chapter G

Workability function with offset from linear optimization

The following appendix presents the outcomes derived from machine learning-based optimization of offsets for three distinct scenarios: free training, restricted training, and a single equation approach.

G.1 Linear optimization training

Each figure in this section contains a reference curve which is the original offset function, observed values, linear equation presented in Table 4.3, linear equation with restricted interception presented in Table 4.4 and the common equation without restriction in the intercept presented in Table 4.6.

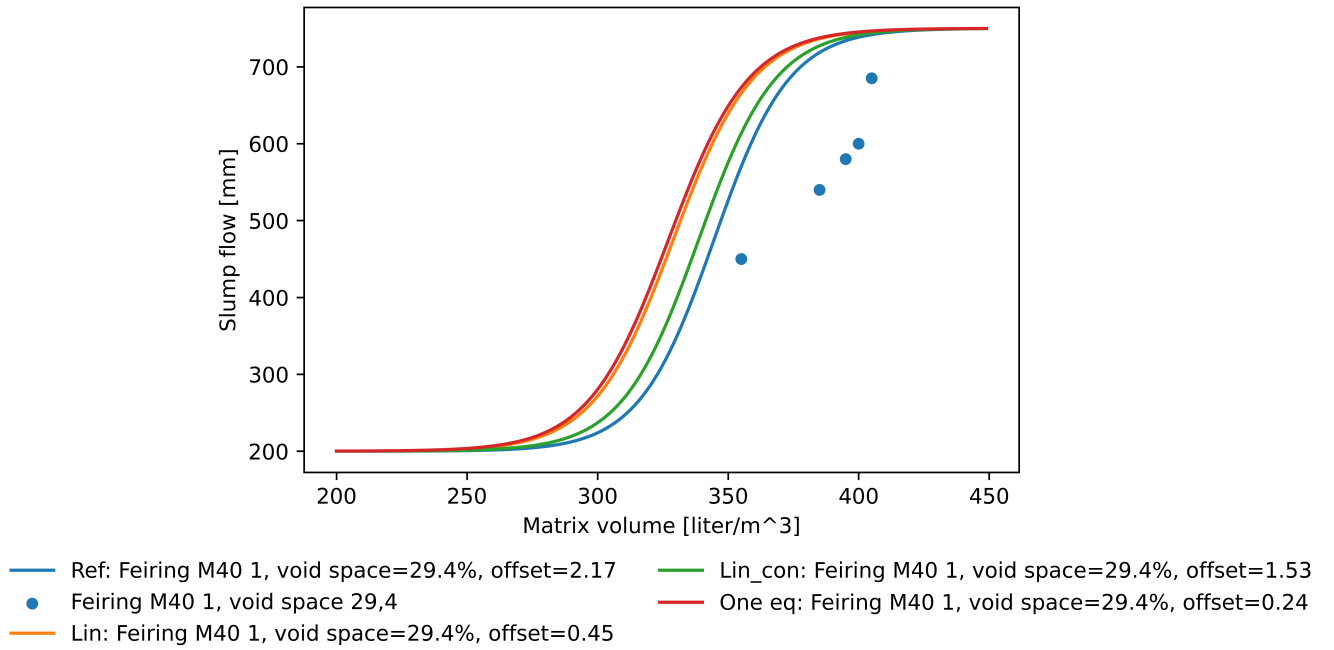


Figure G.1: Feiring M40 from [1] have $\lambda_Q = 0.45$ and $H = 29.4\%$, $sp/c = 1.94\%$, and offset is given by the legends.

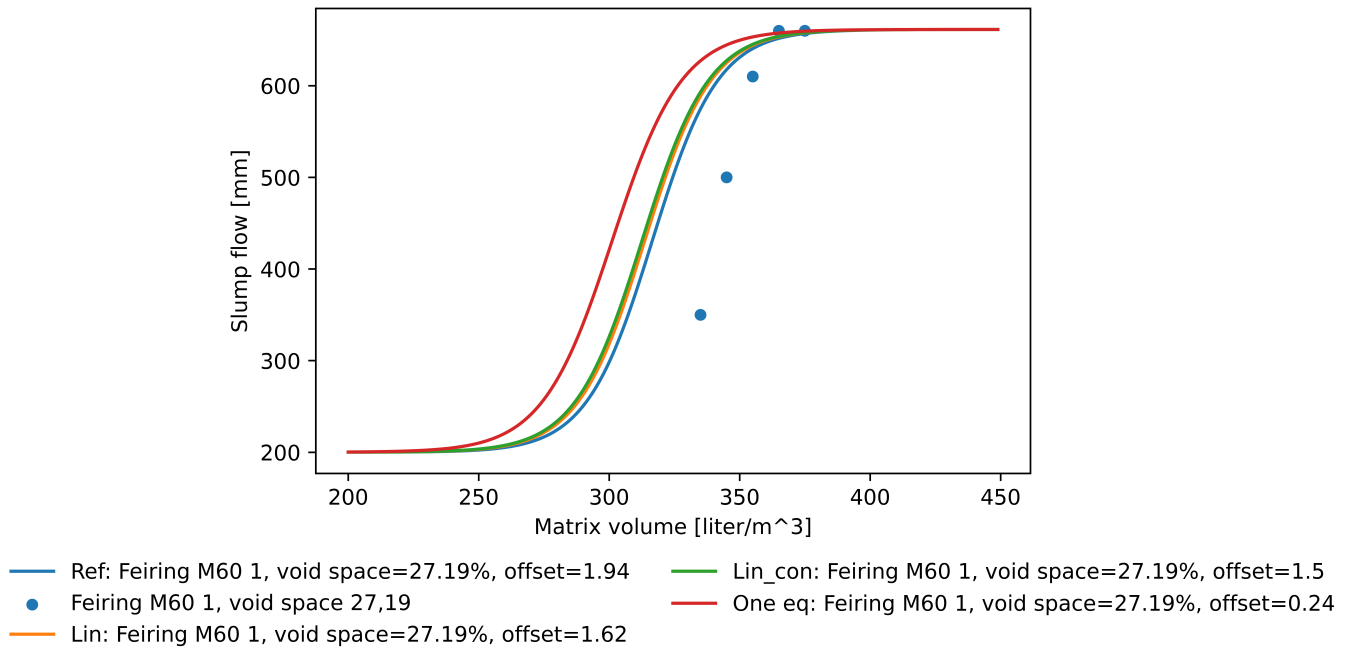


Figure G.2: Feiring M60 from [1] have $\lambda_Q = 0.29$, $H = 27.19\%$, $sp/c = 1.22\%$, and offset is given by the legends.

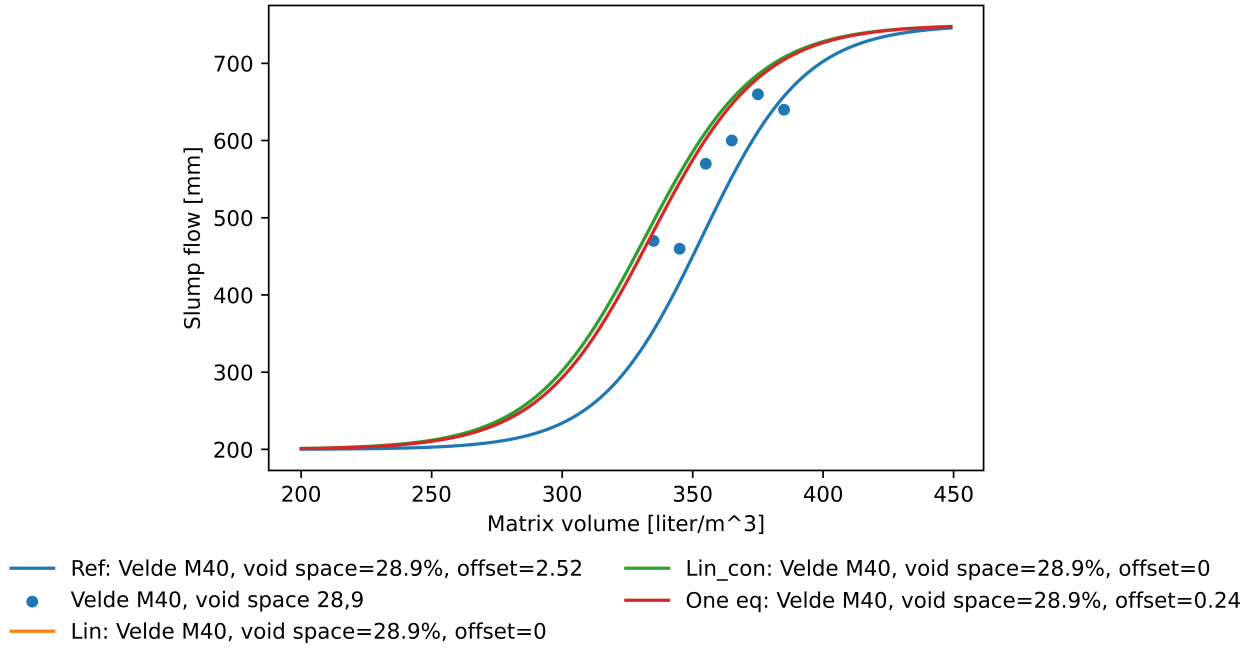


Figure G.3: Velde M40 from [1] have $\lambda_Q = 0.68$, $H = 28.9\%$, $sp/c = 1.65\%$, and offset is given by the legends.

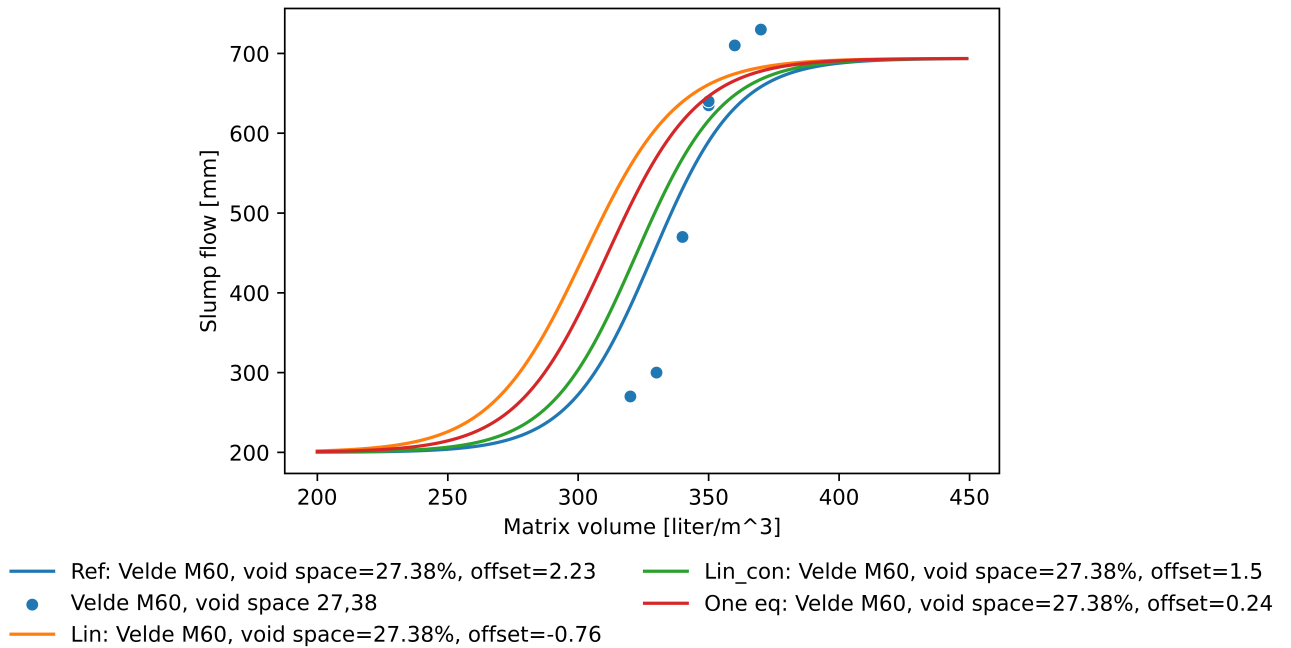


Figure G.4: Velde M60 from [1] have $\lambda_Q = 0.49$, $H = 27.38\%$, $sp/c = 1.35\%$, and offset is given by the legends.

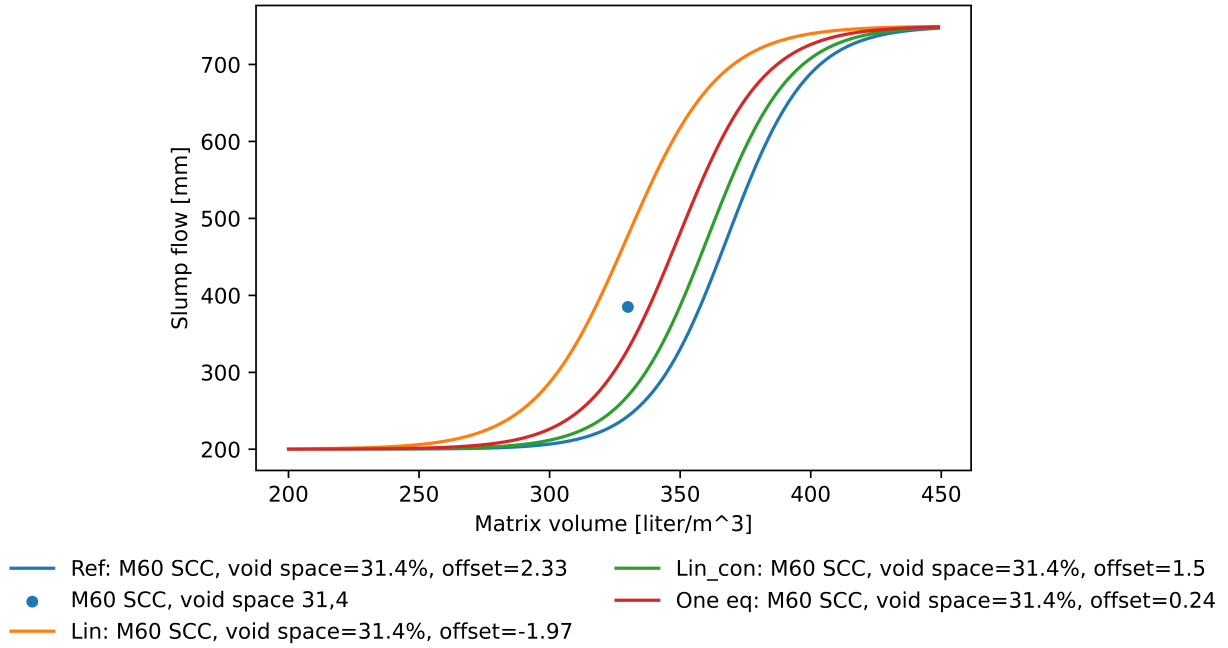


Figure G.5: M60 SCC mix from the Sintef Rheology report have $\lambda_Q = 0.55$, $H = 31.4\%$, $sp/c = 2.72\%$, and offset is given by the legends.

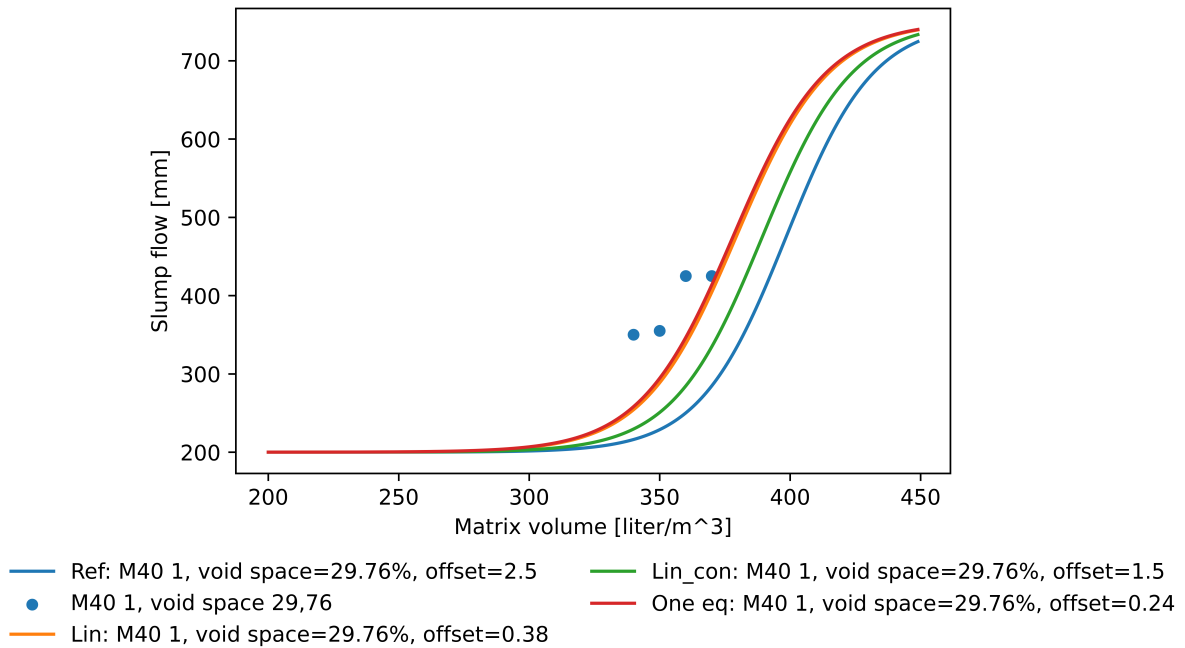


Figure G.6: The first M40 mix from the Sintef Rheology report have $\lambda_Q = 0.67$, $H = 31.4\%$, $sp/c = 3.75\%$, and offset is given by the legends.

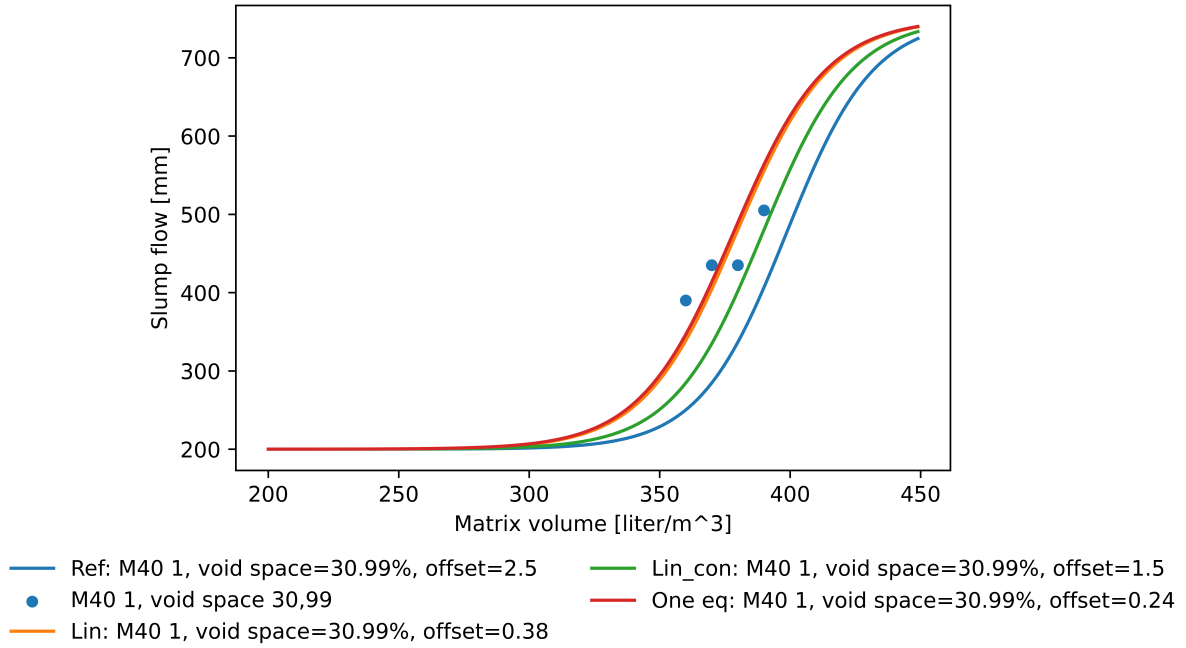


Figure G.7: The first M40 mix from the Sintef Rheology report have $\lambda_Q = 0.67$, $H = 31.4\%$, $sp/c = 3.75\%$, and offset is given by the legends.

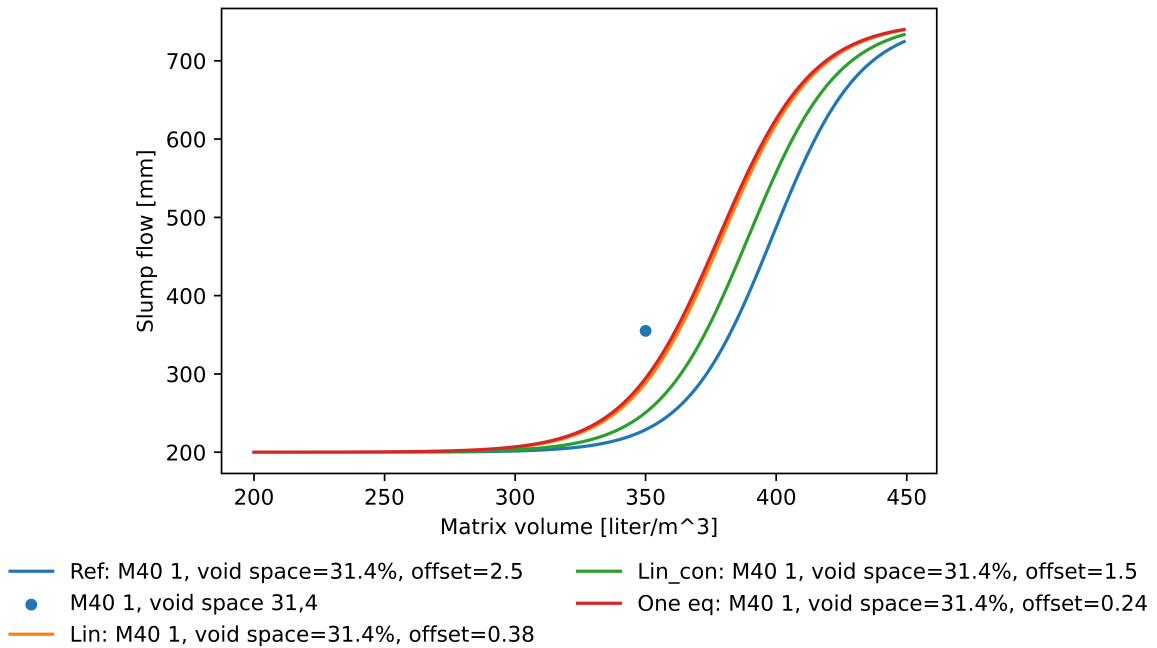


Figure G.8: The first M40 mix from the Sintef Rheology report have $\lambda_Q = 0.67$, $H = 31.4\%$, $sp/c = 3.75\%$, and offset is given by the legends.

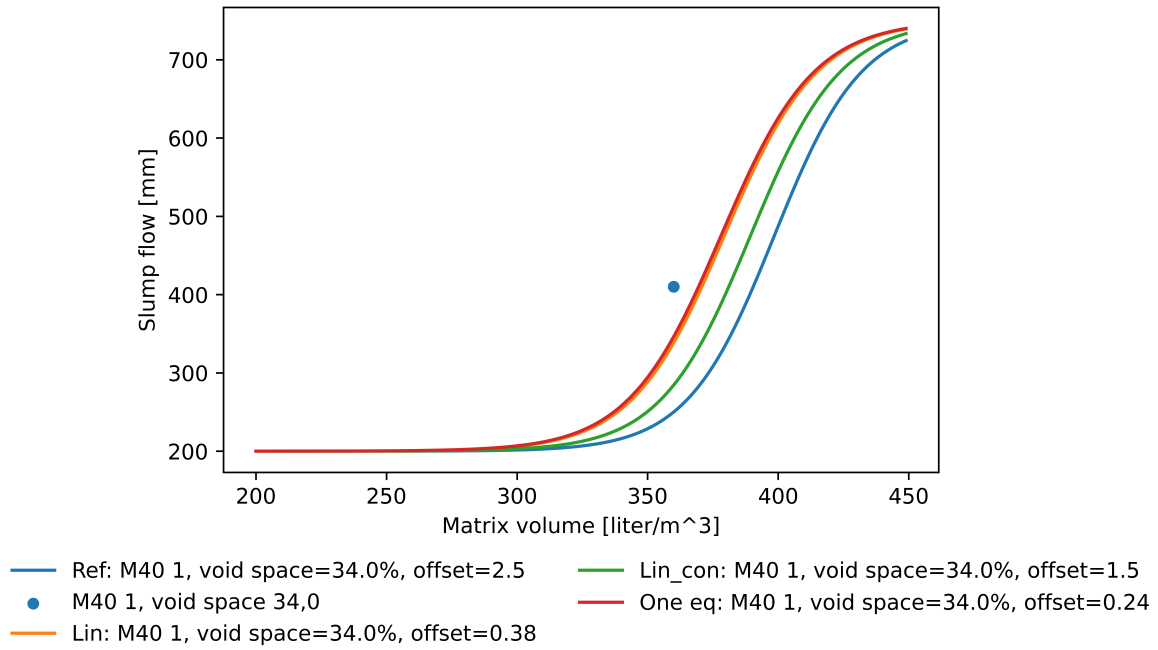


Figure G.9: The first M40 mix from the Sintef Rheology report have $\lambda_Q = 0.67$, $H = 31.4\%$, $sp/c = 3.75\%$, and offset is given by the legends.

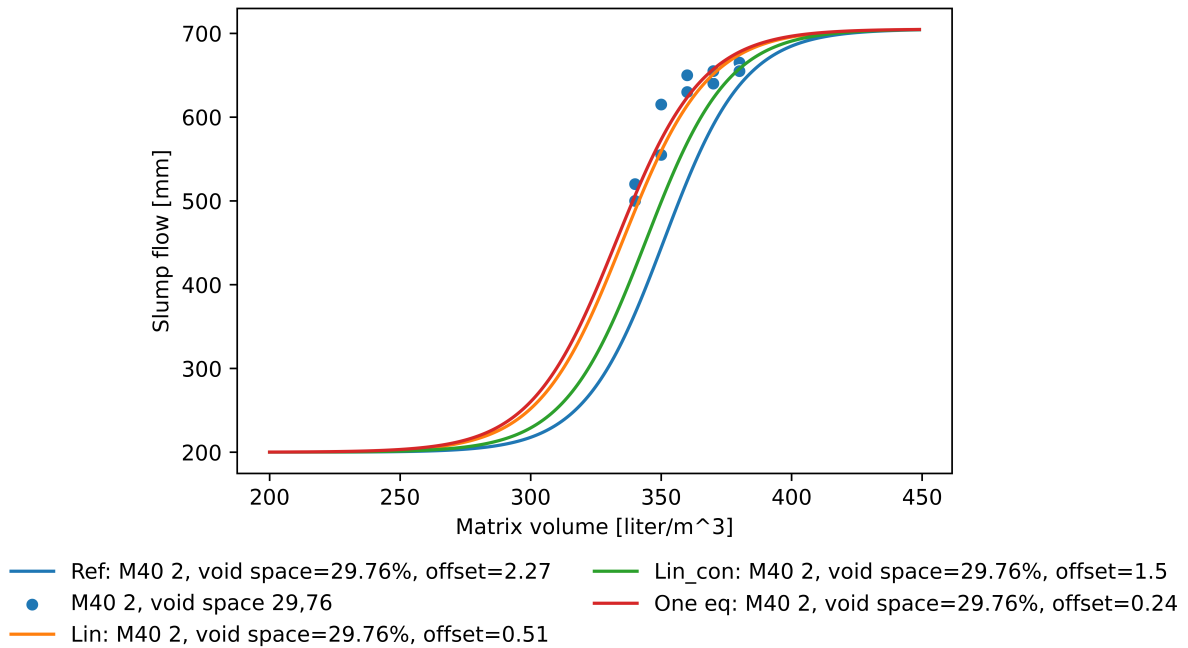


Figure G.10: The second M40 mix from the Sintef Rheology report have $\lambda_Q = 0.51$, $H = 29.76\%$, $sp/c = 3.38\%$, and offset is given by the legends.

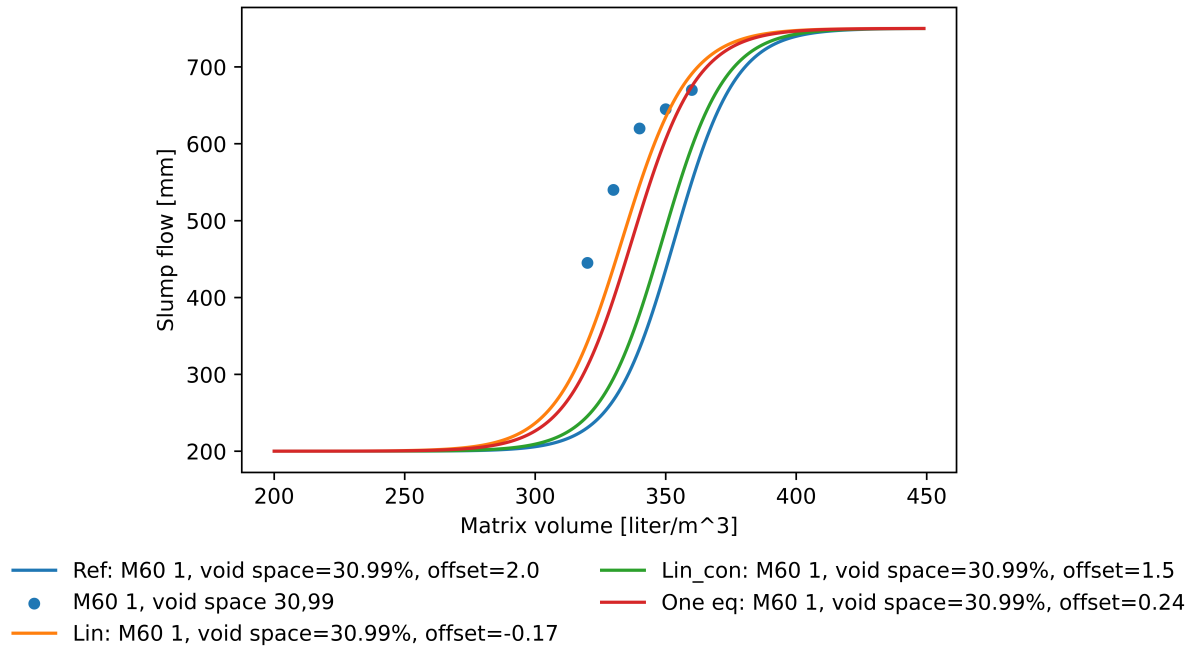


Figure G.11: The first M60 mix from the Sintef Rheology report have $\lambda_Q = 0.33$, $H = 30.99\%$, $sp/c = 2.29\%$, and offset is given by the legends.

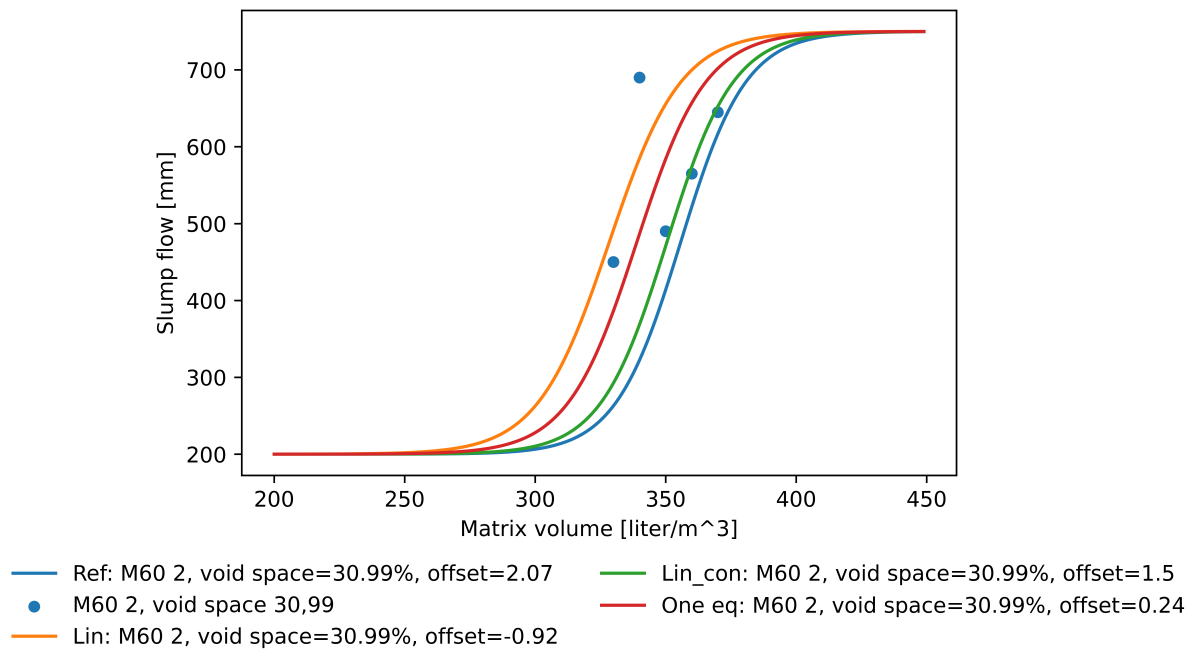


Figure G.12: The second M60 mix from the Sintef Rheology report have $\lambda_Q = 0.38$, $H = 30.99\%$, $sp/c = 2.72\%$, and offset is given by the legends.

G.2 Comparing data

All figures in this section contain a reference curve, which is the blue curve. The blue scatter plots is the observe red valued and the optimized offset illustrated as the orange curve is the equation without restriction from Table 4.6. The void space for these plots are all equal to 26.16%.

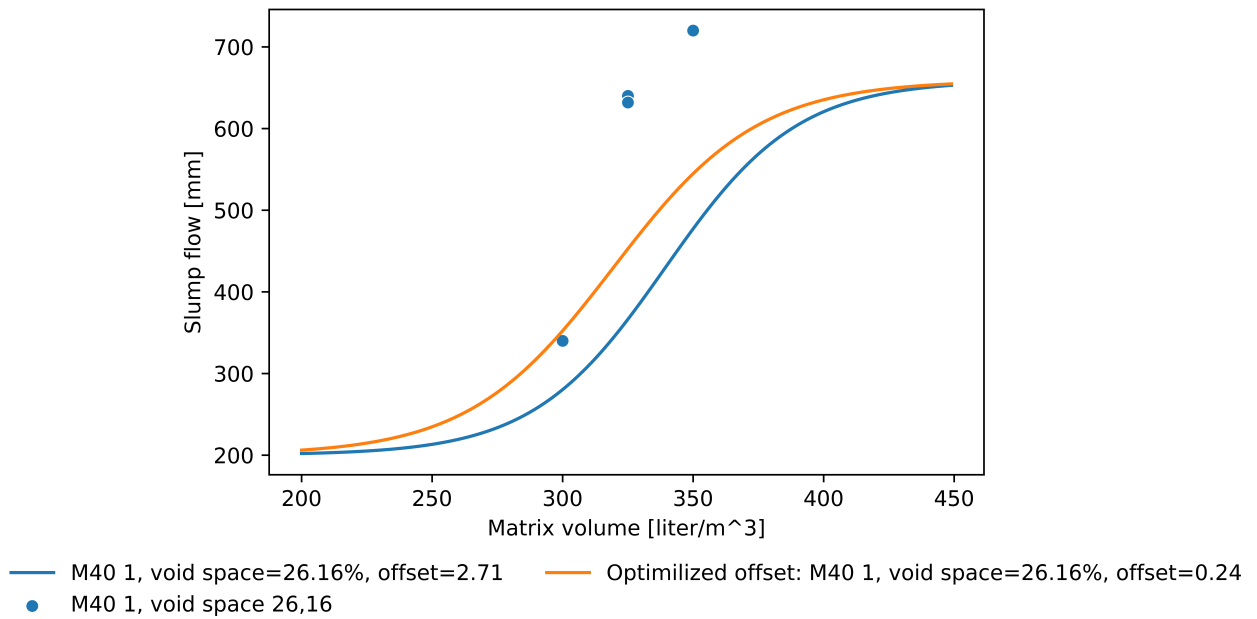


Figure G.13: B55 M40 with mixes one to four, from the experiments with $sp/c=1.2\%$ and the average $\lambda_Q = 0.805$, the offset are given in the legends. This figure is also illustrated in Chapter 4, which is Figure 4.3.

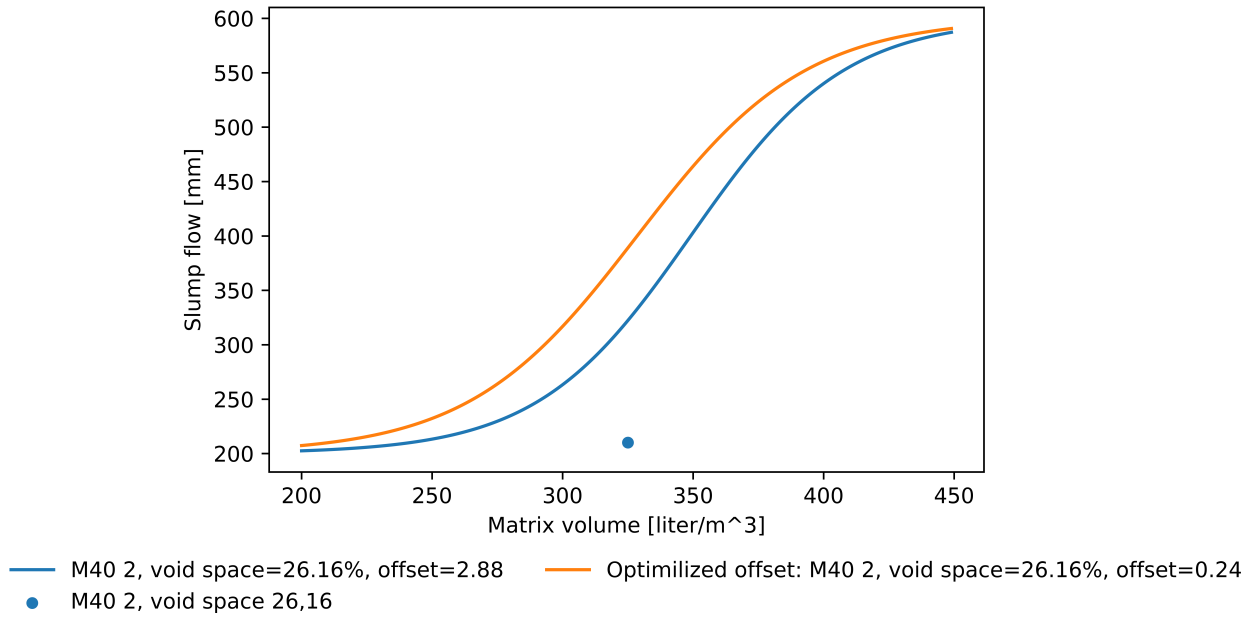


Figure G.14: B55 M40- 5 mix from the experiments with $sp/c=0.5\%$ and $\lambda_Q = 0.92$, the offset are given in the legends.

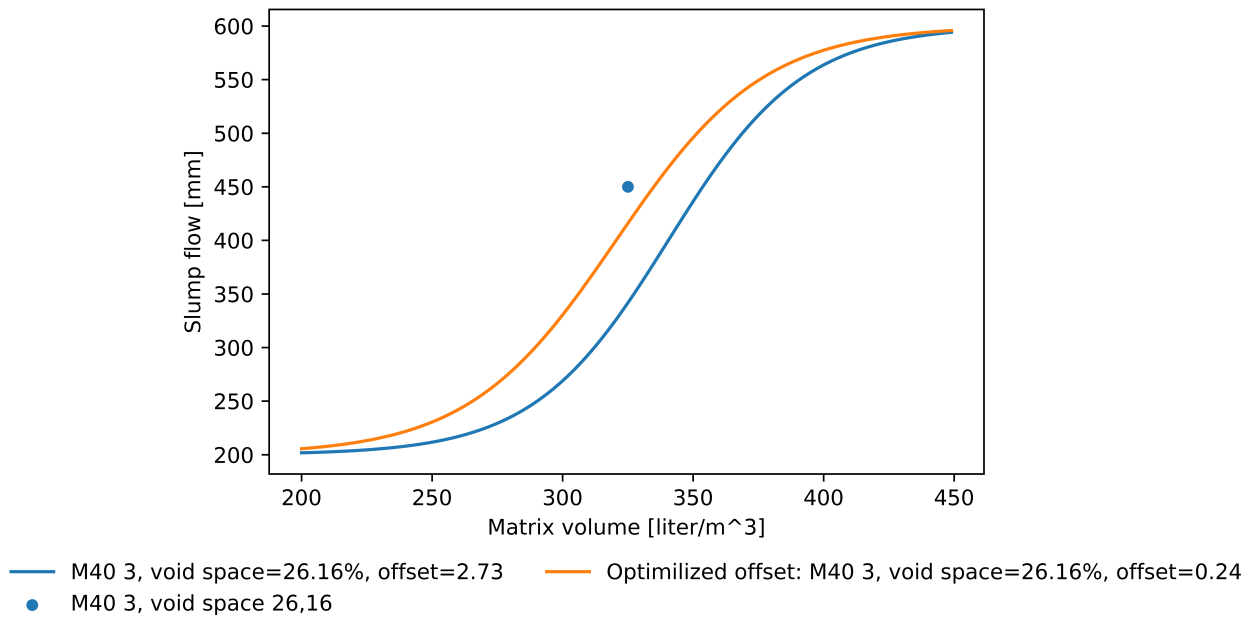


Figure G.15: B55 M40 - 6 from the experiments with $sp/c=0.9\%$ and $\lambda_Q = 0.82$, the offset are given in the legends. This figure is also illustrated in Chapter 4, which is Figure 4.4.

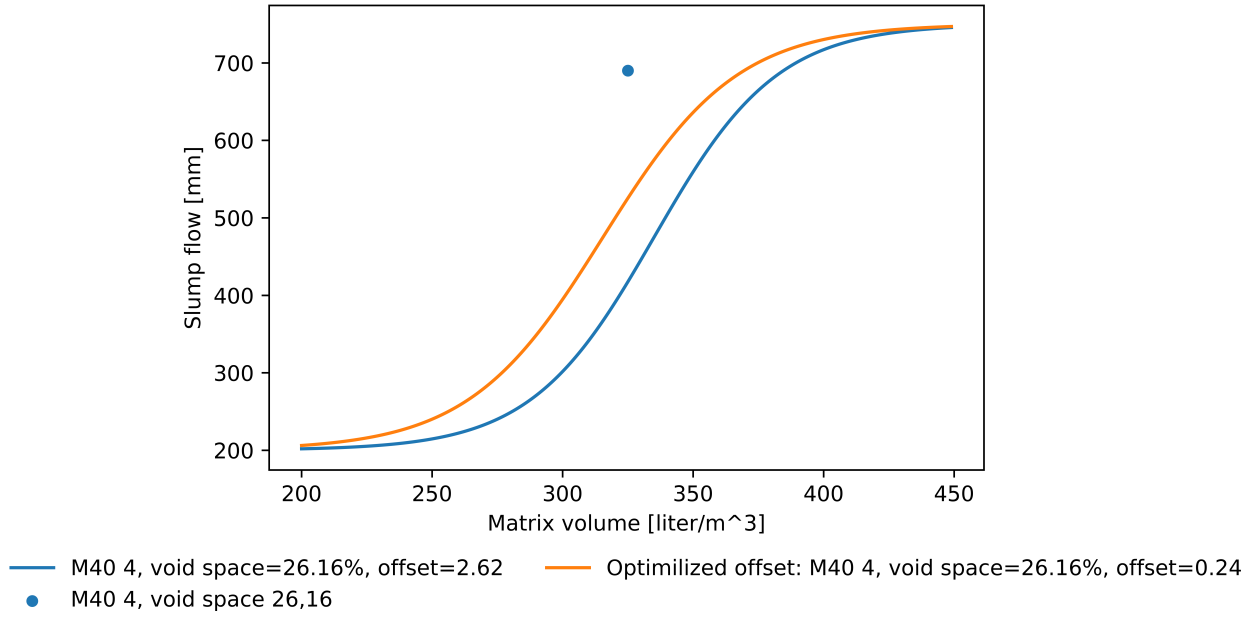


Figure G.16: B55 M40 - 7 from the experiments with $sp/c=1.5\%$ and $\lambda_Q = 0.75$, the offset are given in the legends.

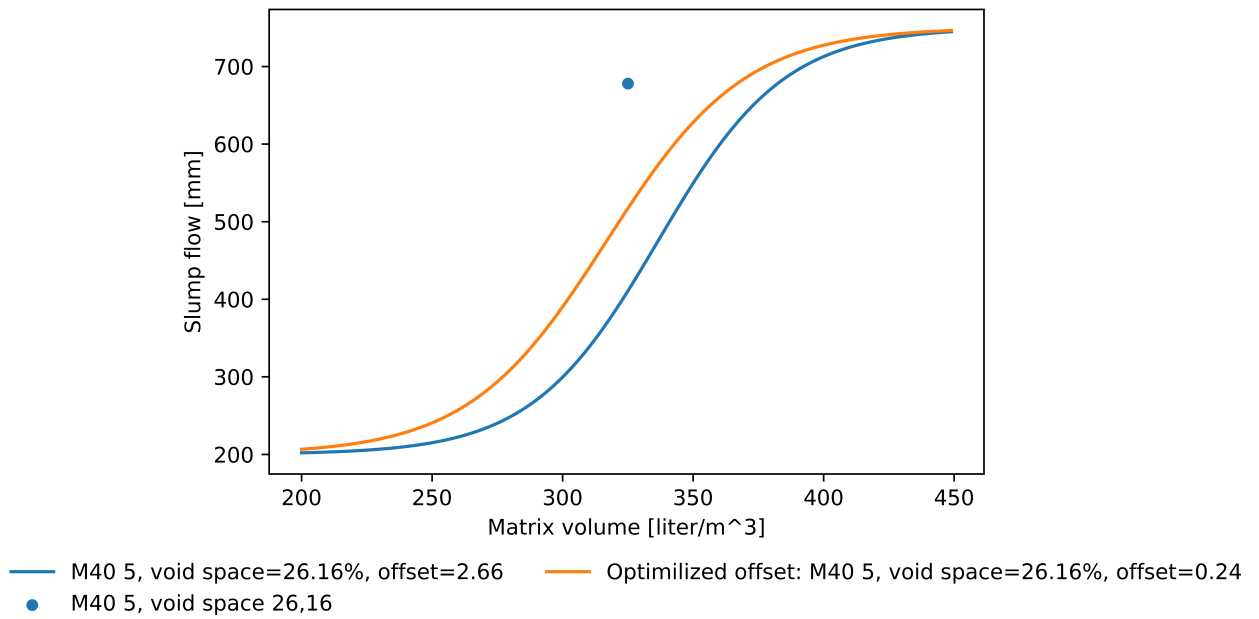


Figure G.17: B55 M40 - 8 from the experiments with $sp/c=1.7\%$ and $\lambda_Q = 0.77$, the offset are given in the legends.

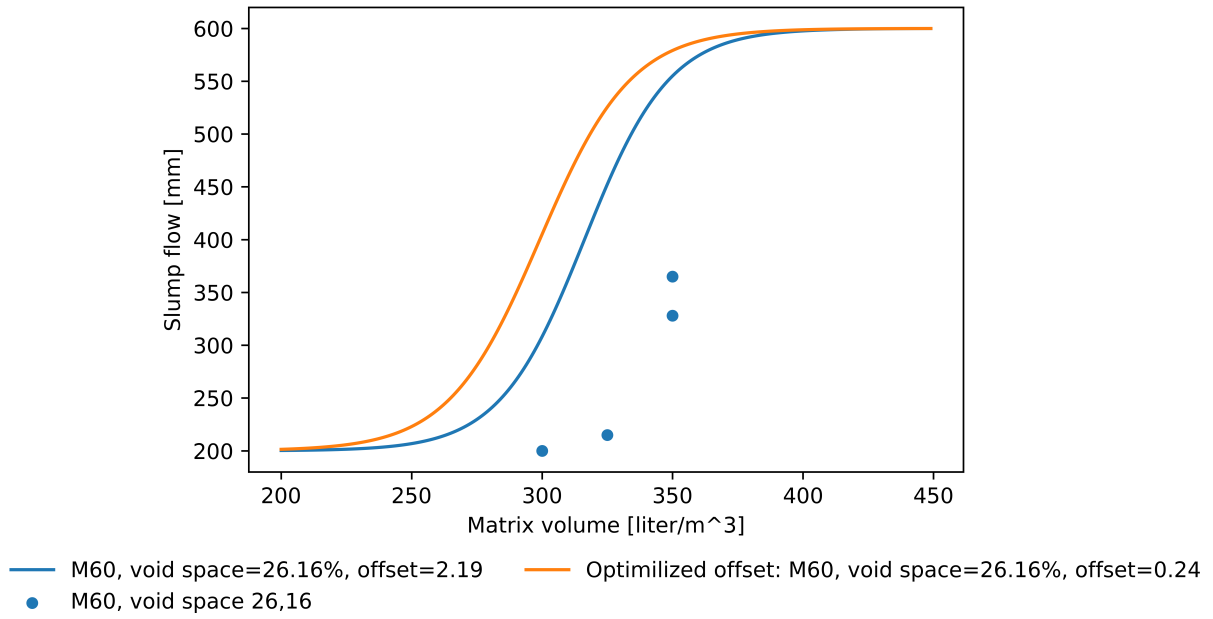


Figure G.18: B35 M60 mixes from one to three from experiments with $sp/c=0.3\%$ and average $\lambda_Q = 0.463$, the offset are given in the legends.

Chapter H

Workability function with changed void space

H.1 Increased void space

The figures in this section contains a blue curve with the original offset equation presented in equation 2.5 and an increase in the void space by 3.4%, and a orange curve with the optimized offset variable for one equation without any restrictions presented in Table 4.6 with an increase in the void space by 3.4%. In addition the blue scatter plot is the observed values, and the green curve is the original offset variable without any changes in the void space.

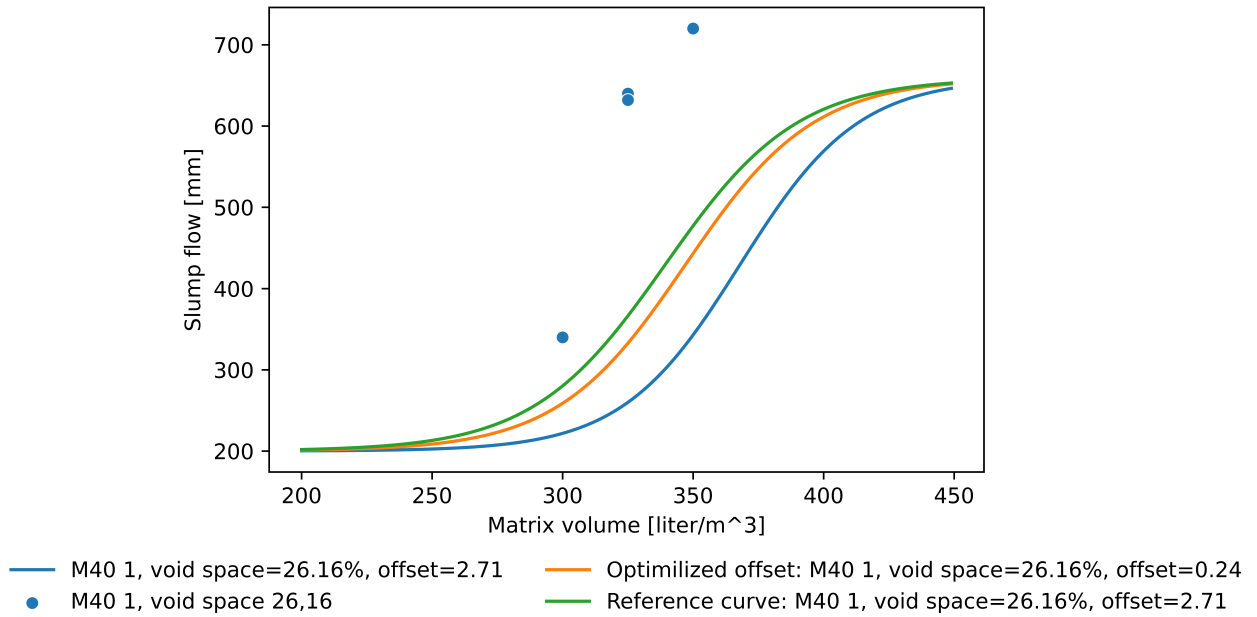


Figure H.1: B55 M40 with mixes one to four, from the experiments with $sp/c=1.2\%$ and the average $\lambda_Q = 0.805$.

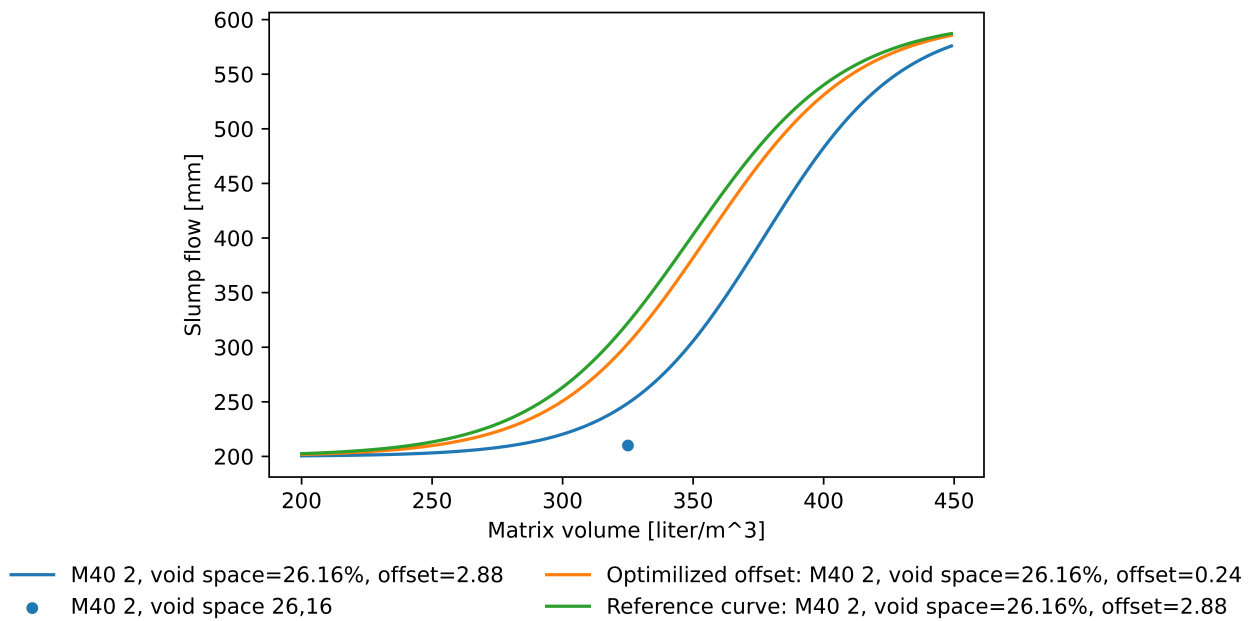


Figure H.2: B55 M40- 5 mix from the experiments with $sp/c=0.5\%$ and $\lambda_Q = 0.92$.

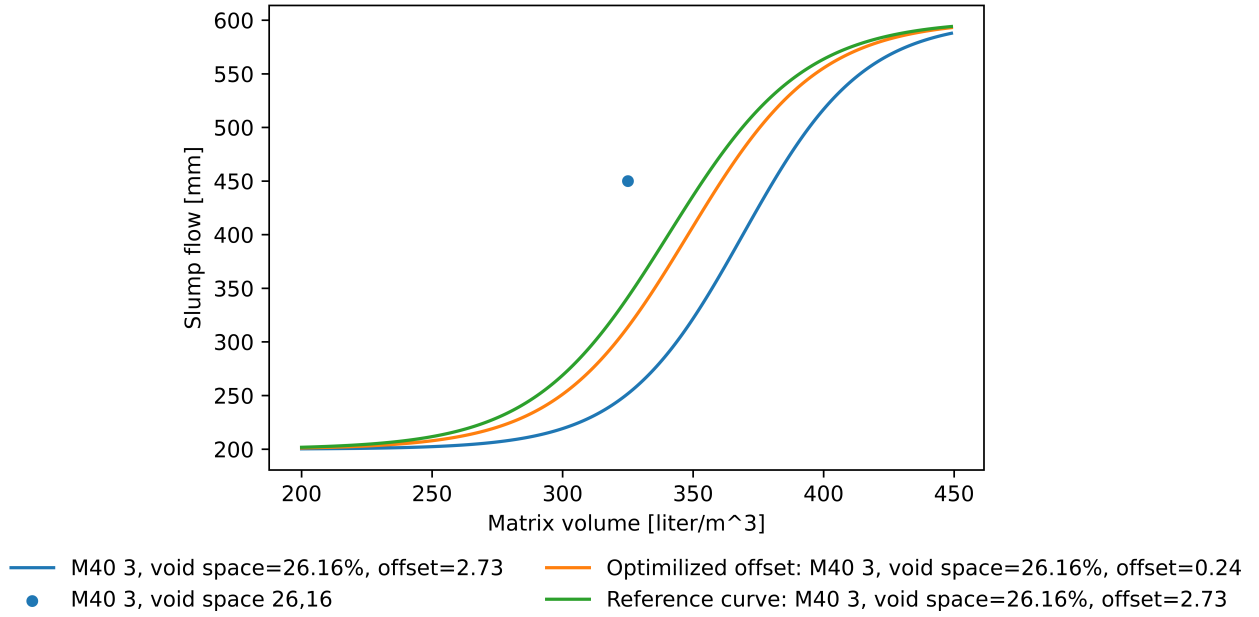


Figure H.3: B55 M40 - 6 from the experiments with $sp/c=0.9\%$ and $\lambda_Q = 0.82$.

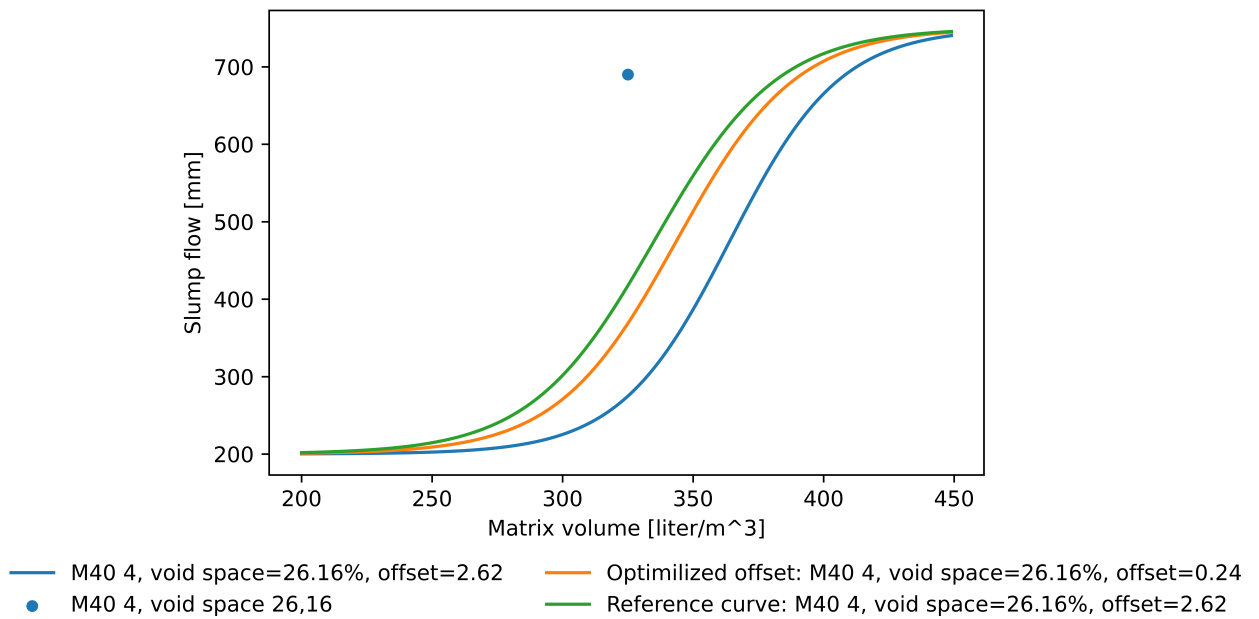


Figure H.4: B55 M40 - 7 from the experiments with $sp/c=1.5\%$ and $\lambda_Q = 0.75$.

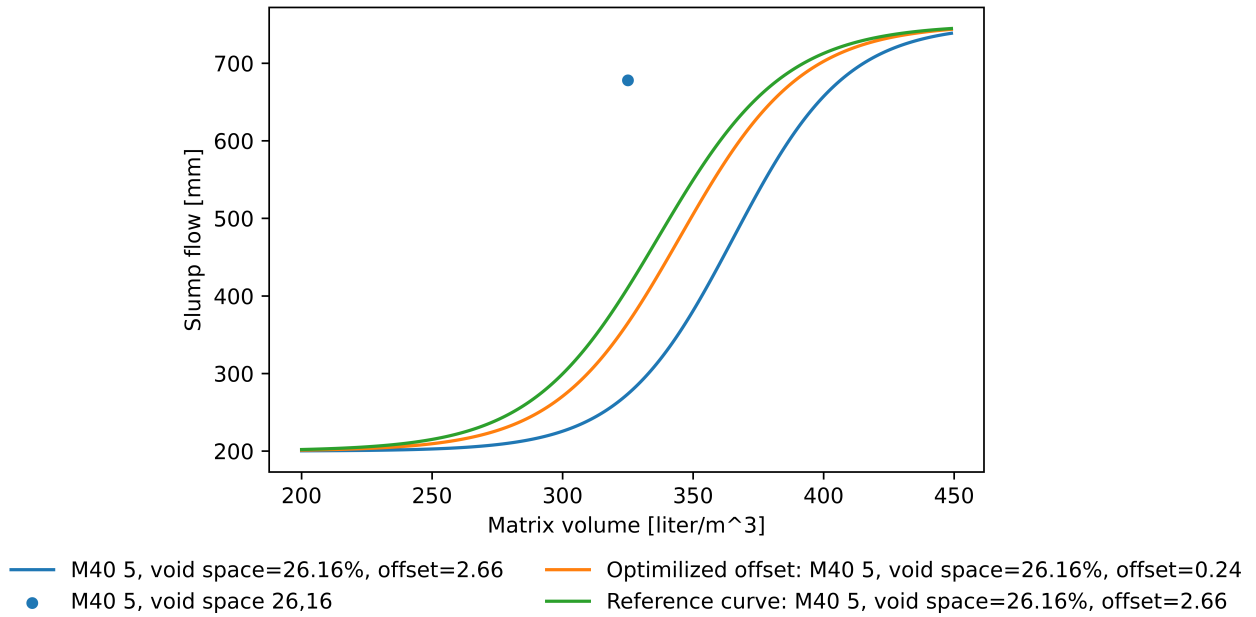


Figure H.5: B55 M40 - 8 from the experiments with $sp/c=1.7\%$ and $\lambda_Q = 0.77$.

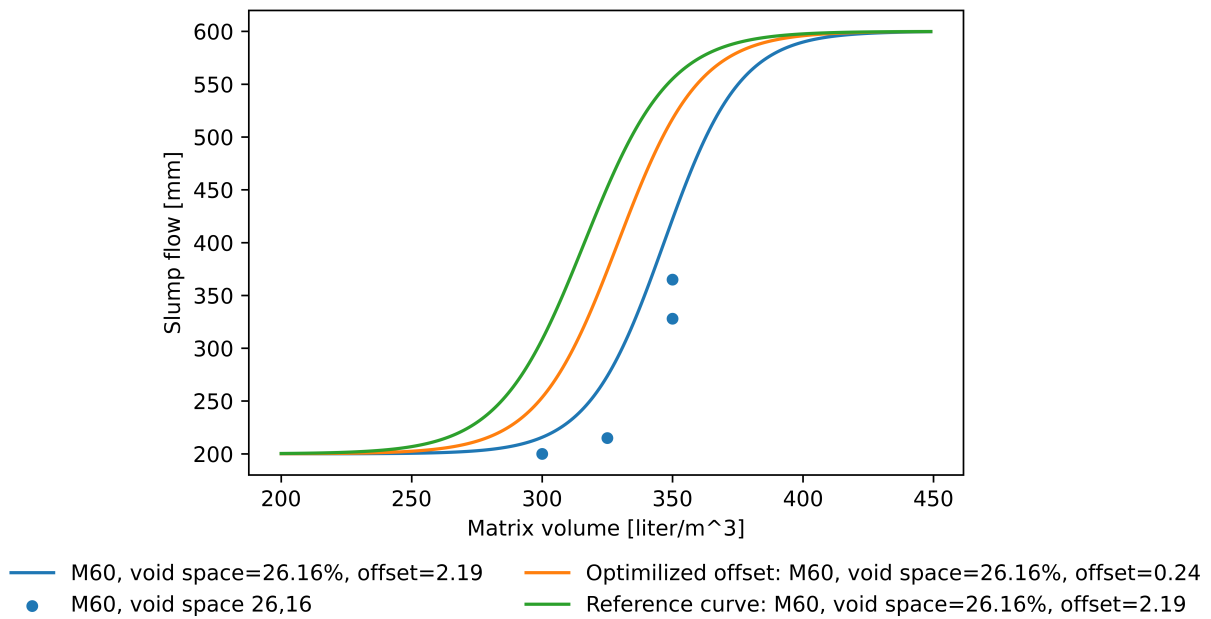


Figure H.6: B35 M60 mixes from one to three from experiments with $sp/c=0.3\%$ and average $\lambda_Q = 0.463$. The figure is also illustrated in Chapter 4 in Figure 4.5

H.2 Reduced void space

The figures in this section contains a blue curve with the original offset equation presented in equation 2.5 and an reduction in the void space by 3.4%, and a orange curve with the

optimized offset variable for one equation without any restrictions presented in Table 4.6 with an reduction in the void space by 3.4%. In addition the blue scatter plot is the observed values, and the green curve is the original offset variable without any changes in the void space.

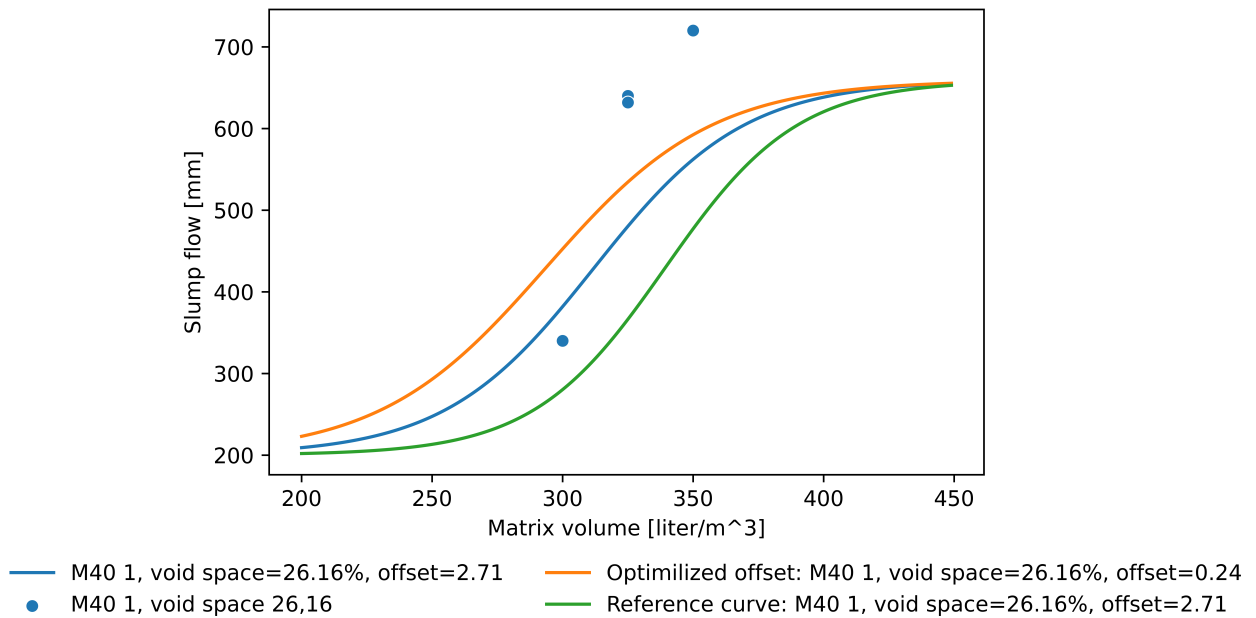


Figure H.7: B55 M40 with mixes one to four, from the experiments with $sp/c=1.2\%$ and the average $\lambda_Q = 0.805$.

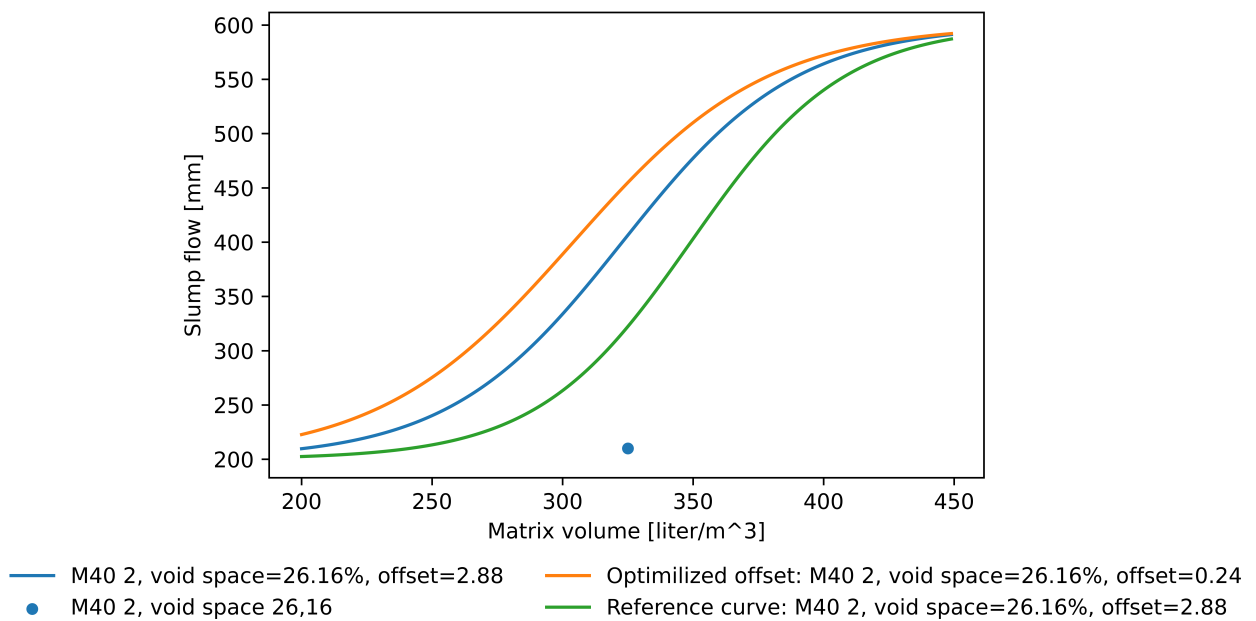


Figure H.8: B55 M40- 5 mix from the experiments with $sp/c=0.5\%$ and $\lambda_Q = 0.92$.

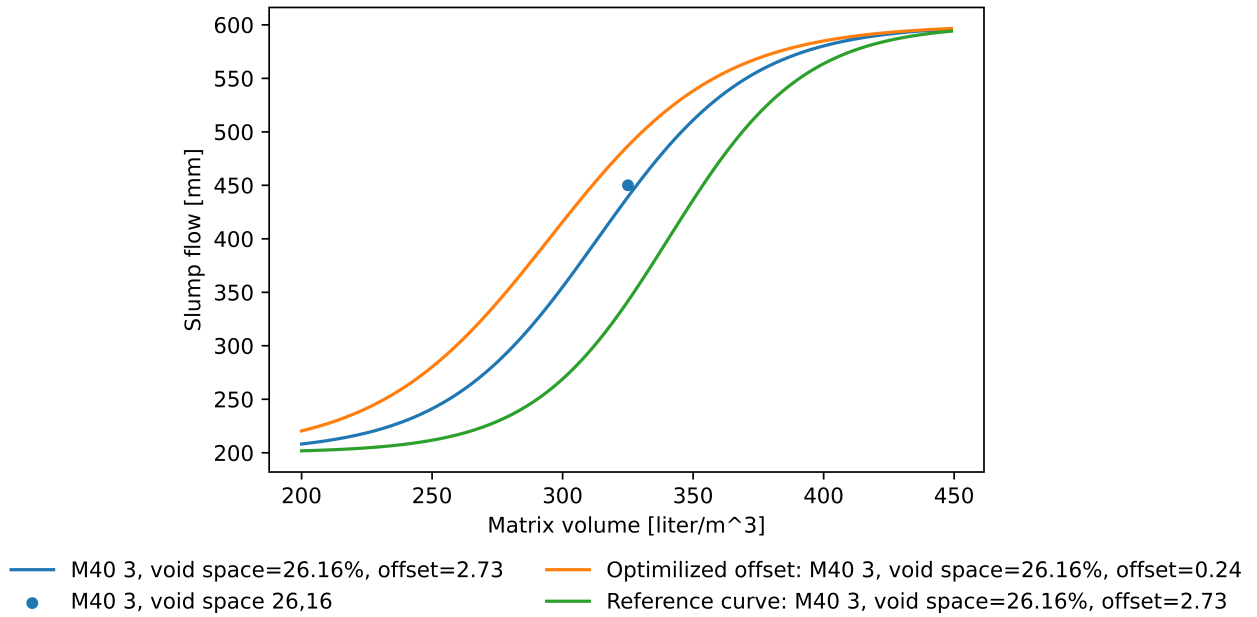


Figure H.9: B55 M40 - 6 from the experiments with $sp/c=0.9\%$ and $\lambda_Q = 0.82$.

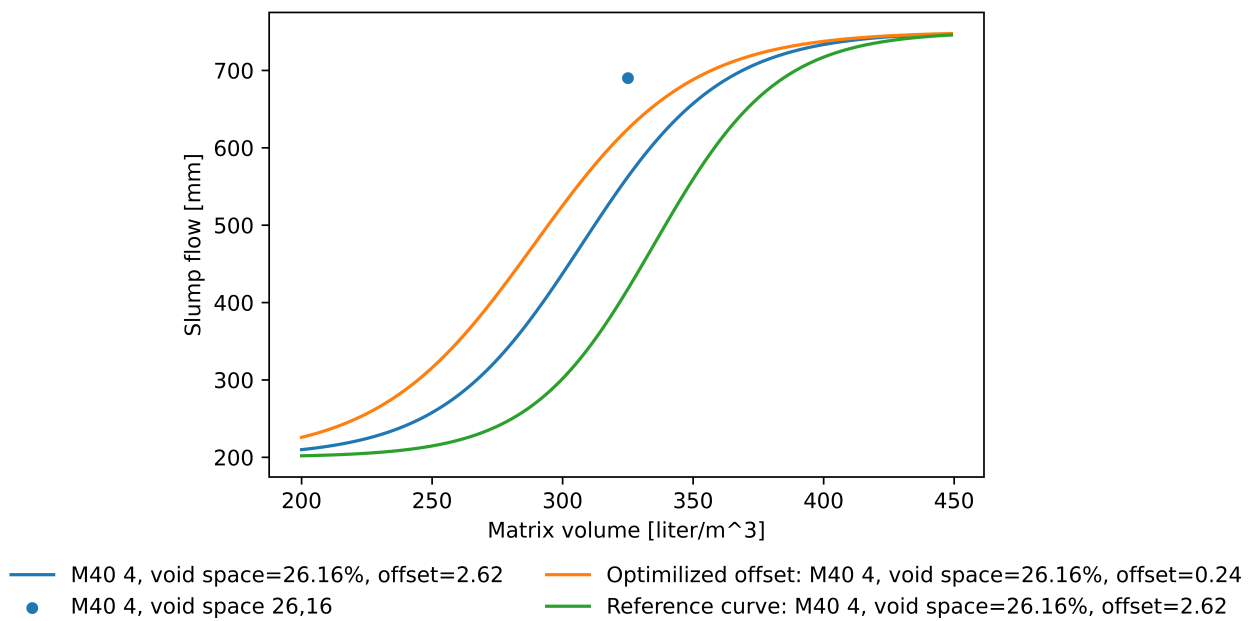


Figure H.10: B55 M40 - 7 from the experiments with $sp/c=1.5\%$ and $\lambda_Q = 0.75$.

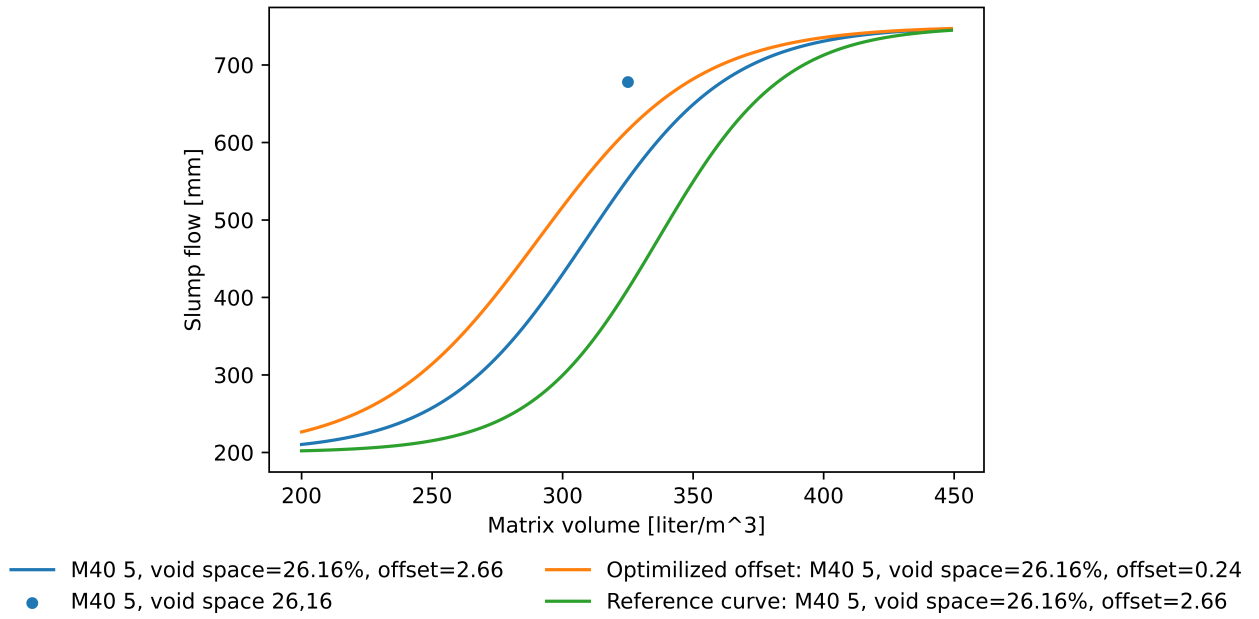


Figure H.11: B55 M40 - 8 from the experiments with $sp/c=1.7\%$ and $\lambda_Q = 0.77$.

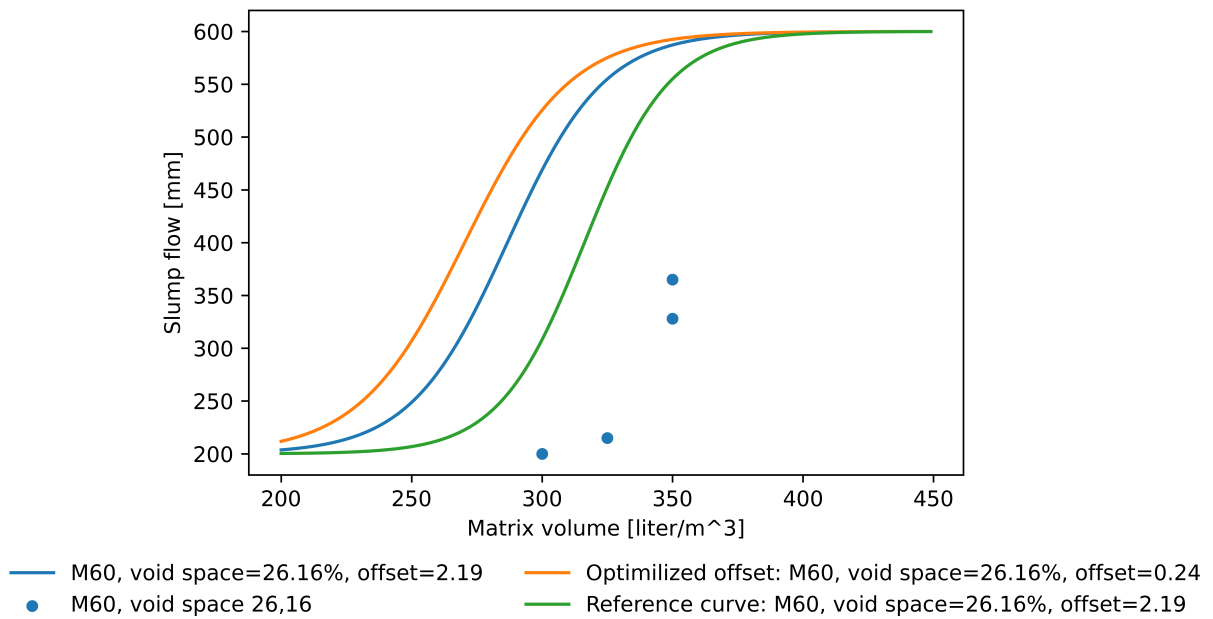


Figure H.12: B35 M60 mixes from one to three from experiments with $sp/c=0.3\%$ and average $\lambda_Q = 0.463$



 **NTNU**

Norwegian University of
Science and Technology